AN ACOUSTIC EMISSION AND ACOUSTO-ULTRASONIC ANALYSIS OF IMPACT DAMAGED COMPOSITE PRESSURE VESSELS

D.O. 122

Prepared by

James L. Walker
Center for Automation and Robotics
University of Alabama in Huntsville
Huntsville, AL 35899
(205)-895-6578*207

Principle Investigator

Gary L. Workman
Center for Automation and Robotics
University of Alabama in Huntsville
Huntsville, AL 35899
(205)-895-6578*240

Submitted to

Samuel Russell
EH13
National Aeronautics and Space Administration
Marshall Space Flight Center, AL 35812
(205)-544-4411

May, 1996

TABLE OF CONTENTS

ABSTRACT

The research presented herein summarizes the development of acoustic emission (AE) and acousto-ultrasonic (AU) techniques for the nondestructive evaluation of filament wound composite pressure vessels. Vessels fabricated from both graphite and Kevlar fibers with an epoxy matrix were examined prior to hydroburst using AU and during hydroburst using AE. A dead weight drop apparatus featuring both blunt and sharp impactor tips was utilized to produce a single known energy "damage" level in each of the vessels so that the degree to which the effects of impact damage could be measured. The damage levels ranged from barely visible to obvious fiber breakage, matrix cracking and delamination.

Independent neural network burst pressure prediction models were developed from a sample of each fiber/resin material system. Here, the cumulative AE amplitude distribution data collected from low level proof tests (25% of the expected burst for undamaged vessels) were used to measure the effects of the impact on the residual burst pressure of the vessels. The results of the AE/neural network model for the inert propellant filled graphite/epoxy vessels "IM7/3501-6, IM7/977-2 and IM7/8553-45" demonstrated that burst pressures can be predicted from low level AE proof test data, yielding an average error of 5.0 %. The trained network for the filled IM7/977-2 class vessels was also able to predict the expected burst pressure of taller, unfilled, vessels (three times longer hoop region length) constructed of the same material and using the same manufacturing technique, with an average error of 4.9 %. Burst pressure prediction models were also generated for both inert propellant filled and un-filled Kevlar/epoxy "Kevlar 49/ DPL862" vessels. Here, burst pressures were predicted with an average error of 5.4% and 5.6% for the un-filled and filled vessels respectively.

An acousto-ultrasonic robotic evaluation system (AURES) was developed for mapping the effects of damage on filament wound pressure vessels prior to hydroproof testing. The AURES injects a single broadband ultrasonic pulse into each vessel at preprogrammed positions and records the effects of the interaction of that pulse on the material volume with a broadband receiver. A stress wave factor in the form of the energy associated with the 750 to 1000 kHz and 1000 to 1250 kHz frequency bands were used to map the potential failure sites for each vessel. The energy map associated with the graphite/epoxy vessels was found to decrease in the region of the impact damage in the 1.0 MHz frequency range. The Kevlar vessels showed the opposite trend, with the 1.0 MHz energy values increasing around the damage/failure sites.

1.0 INTRODUCTION

The technological improvements in many of today's aerospace structures are primarily due to advancements in materials and processes. As the performance requirements increase for these "advanced" materials, so does the need to accurately monitor the integrity of structural components fabricated from these material systems. Both nondestructive evaluation (NDE) and materials characterization are areas which continually need to be considered in the implementation of new materials into critical aerospace hardware. For these reasons, research efforts in NDE must keep pace with the development of new materials and processes.

Classically, NDE has been concerned with locating and identifying defects that could potentially hinder a structures ability to fulfill its mission. There are a number of NDE techniques which provide information about flaw size and location; including ultrasonics, eddy current, liquid penetrant, thermography and radiography to name a few, however, these techniques usually require a significant flaw size to exist in order for a minimum threshold of detection to be reached. Also, these techniques do not provide information as to the activation level of the flaw. In other words, will the flaw size increase with load, and if so, what effect will that have on the residual strength of the structure. Only one technique currently available actually does not depend upon flaw size, only that it is growing or active. This technique is acoustic emission (AE) testing.

Since AE does not depend upon size to characterize a flaw, only that it is growing , AE can be made extremely sensitive. Acoustic sensors and instrumentation available today can "hear" crack propagation events at such a minuscule level that the structure is not "appreciably" damaged. Thus acoustic emission testing has the potential to "proof-test" critical aerospace structures without impairing the ability of the structure to perform under normal operating conditions.

The sensitivity of AE NDE is primarily dependent upon the frequency range of the sensors used and the characteristics or physical properties of the test material. The strength "intensity" of the acoustic waves generated by a source are directly related to the energy released from flaw growth activity while ultrasonic wave propagation affects relate to the variations in time domain and waveform features of the received signal. Therefor, signal analysis requires an understanding of the complex interactions of the acoustic event with the material, the source mechanisms and the inherent nature of the instrumentation system. In general, AE signals have been characterized the same qualitative way for the last 15 years. Even with improvements in computing power, commercial instrumentation has not provided a noticeable improvement in acoustic emission signal analysis. Thus, this research is focused on providing some useful quantitative improvements in how acoustic emission signals are processed and interpreted.

The use of AE for monitoring composite structures during pressure testing has been accepted as a useful sensor technology. Characterization of the AE signals and interpretation of the structural properties contained in these signals as received during the test, still provides a challenge to the NDE research community. Much work has gone into identifying the individual failure mechanisms which create AE, with only a limited success. Most research has centered around special samples which fail in a prescribed mode [4]. In reality though, the propagation and modes of failure in a composite material are extremely complex and dependent on one another. Identification of a particular failure source from a given signal is extremely difficult, if not impossible. On the other hand, by studying a large number of signals, trends can be established which do relate to general failure modes. Since these distinguishing trends are often obscured by background clutter, an automated classifier is required to sort out what is important and what is not. Recent developments in artificial neural networks, have shown promise in sorting multidimensional data for distinguishing features that may in turn be used to predict an outcome. This research will demonstrate the use of neural network concepts for modeling the relationships between the AE signals recorded during the initial stages of loading and the ultimate failure of the structure.

In addition to AE, this study also provides an acousto-ultrasonics (AU) analysis of the regions in which the initiation of fracture is anticipated. Developed by Alex Vary at the Lewis Research Center, this technique has shown an ability to determine "weakest link" regions within a structure. AU is performed by injecting a known ultrasonic pulse (or stress wave) into a structure and measuring the relative attenuation or frequency shifts generated as a result of the interactions of that stress wave with the material volume. The similarity of AU to AE is carried over into the data analyses phase since AE hardware and software can be used for signal analysis of AU experiments. The major difference is that AE listens for stress waves emitted by crack or flaw propagation and AU provides its own stress wave energy, measuring the relative ability of the structure to dissipate that energy. Regions in which the energy is highly dissipated/concentrated or where drastic frequency shifting occurs are normally regions in which fracture will ultimately begin.

AU testing will be based on the ASTM standard currently under consensus ballot by ASTM, with the exact sequence of procedures best fitting the vessels under examination being developed during the course of this research effort. The incorporation of AU to map the quality of pressure vessels before pressure loading should provide benefits for interpretation of other NDE test data, as well as demonstrate the capabilities of AU to a broader audience. By performing AU scans on the composite vessels prior to the hydroburst testing and then monitoring the occurrence and location of AE "failure" during the pressure tests, information about how well the stress wave theory of AU predicts where failure will occur can be made. The AE events will provide real time information that fracture is occurring in those regions which were determined to be weaker structurally by AU.

In summary, the purpose of this task is to develop methods to evaluate the structural integrity of composite pressure vessels using both AE and AU techniques. Acousto-ultrasonic evaluation of the extent and effects of impact damage to pressure vessels will be investigated before hydroburst testing. During hydroburst, AE data will be acquired permitting the measurement of active flaw growth and burst pressure prediction models to be developed.

2.0 ACOUSTIC EMISSION

Impact damage, experienced in-service, is a problem that plagues the composites industry. Damage that may appear only superficial can often times have a detrimental effect on the performance of a composite structure [1]. Conventional NDE techniques typically map only the locations and shapes of impact damage and are not able to quantify its effects on the structure. Acoustic emission testing on the other hand, which records active flaw growth as the structure is loaded, provides the means to measure the reduction in structural performance that has been produced by an impact load or other abnormality. This research effort demonstrates a method for quantitatively proof testing impact damaged composite pressure vessels at sub-critical loads through a neural network analysis of their cumulative AE amplitude distribution data.

Acoustic emission signal analysis has been used to measure the effects of impact damage on the burst pressure of 14.61 cm diameter filament wound pressure vessels. The AE data were collected from a total of 101 vessels (31 inert propellant filled) constructed from graphite and Kevlar fiber with an epoxy matrix. The physical properties of the pressure vessels are described in Section 2.1.2. A summary of the AE test matrix is provided in Table 1.

	Inert Propellant Backing	Fiber type	Resin type	Quantity
Graphite/Epoxy	Yes	IM7	3501-6	6
			977-2	6
			X8553-45	5
			Total	17
Graphite/Epoxy	No	IM7	3501-6	12
			977-2	12
			X8553-45	12
			Total	36
Kevlar/Epoxy	Yes	Kevlar 49	DPL862/W	14
Kevlar/Epoxy	No	Kevlar 49	DPL862/W	19
Graphite/Epoxy (Tall)	No	IM7	977-2	15
			Grand Total	**101**

Table 1. Acoustic emission test matrix.

Impact damage was produced by means of a dead weight drop fixture utilizing both 12.7 mm blunt (BT) and 1.0 mm sharp (ST) hemispherical impactor tips with impact energies ranging from zero up to twenty-seven N • m. Burst pressure prediction models were developed by correlating the cumulative AE amplitude distribution collected during low level hydroproof tests (approximately 25% of the average expected burst pressure for an undamaged vessels) to known burst pressures using back propagation neural networks. The neural network models were trained from a subset of the vessels from each fiber/resin system and tested using the remaining vessels from that class.

A Physical Acoustics Corporation (PAC) SPARTAN-AT® performs the data acquisition during the hydroburst tests. The PAC program SA-LOC.EXE is configured to collect the AE and parametric pressure data during each test. The AE data file "PR###.DTA" is converted to ASCII text format "PR###.BAS" by the PAC program ATASC.EXE. The AE data file is trimmed to contain only the data from the first 25% of loading by running the QuickBasic program AEHITS.BAS (Appendix 6.1). Here the amplitude distribution "histogram" is computed and arranged for latter analysis, along with the burst pressure if known, in a network file "PR###.NNA". Finally, a neural network input file is organized by grouping the individual amplitude distribution files using a text editor, such as MS-DOS Editor, the network is trained and finally tested generating the results file "PR.NNR". For this research effort, NeuralWorks Professional II/PLUS® software, by NeuralWare, Inc, "NW2.EXE" was used to construct the neural network models. The network settings will be described for each model developed in a latter section of this report. Consult the reference and tutorial manuals for specific operation of the NeuralWare program.

SA-LOC.EXE => PR###.DTA

⇓

ATASC.EXE => PR###.BAS

(DOSSHELL.EXE => View file PR###.BAS for time cut-off @ 25% of ultimate)

⇓

AEHITS.BAS => PR###.NNA

⇓

NW2.EXE => PR.NNR

Note: PR = Test filename prefix
= File number

2.1 EXPERIMENTAL

2.1.1 Hydroburst Facility

The MSFC "portable" hydroburst chamber was used to test the pressure vessels. The hydroburst facility consists of a test chamber, air driven water pump and instrumentation to provide the pressure level. A schematic of the chamber is shown in Figure 1 along with the AE system and supporting instrumentation. A detail of the pumping system is provided in Figure 2.

During the time that the first thirty-six empty graphite/epoxy vessels were tested (Fall 1993) many problems were encountered with the repeatability and accuracy of the recorded pressures. A lack of a consistent pressure standard and pressurization schedule coupled with the limited number of samples for each test point (consisting of a variable impact energy, impactor and resin) made subsequent AE burst pressure prediction modeling virtually impossible by introducing to many uncontrolled and unknown variables into the already full test matrix.

Measures were taken to overcome these problems by establishing a reference from which to check the output of the pressure transducer against and a computer generated pressurization schedule was established. The pressure standard was facilitated through the use of a high precision Bourdon tube pressure gage. Here, by periodically checking the output of the pressure transducer against the gauge, the correct burst pressures could be confidently measured.

To ensure repeatability in the pressure cycles the output from the pressure transducer was collected by an DAS-8 OMEGA® A/D board controlled by a LABTECH NOTEBOOK® program. The LABTECH program displayed the desired pressurization ramp and the actual signal from the pressure transducer so that the test operator could regulate the air pressure driving the water pump, matching the desired pressurization ramp. A 69 kPa/sec pressurization rate was set for each ramp. The LABTECH program stores the pressure histories with a 10 Hz sampling rate for future reference and to determine the burst pressure of each vessel.

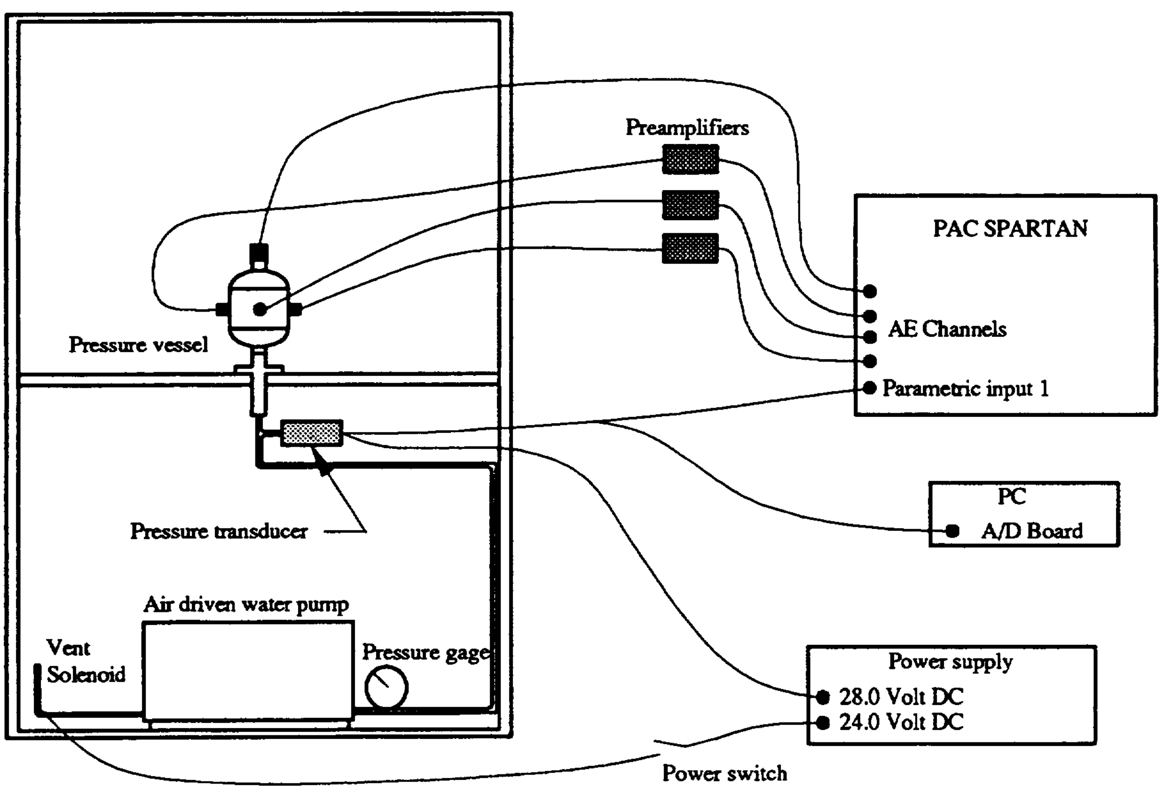

Figure 1. Hardware configuration.

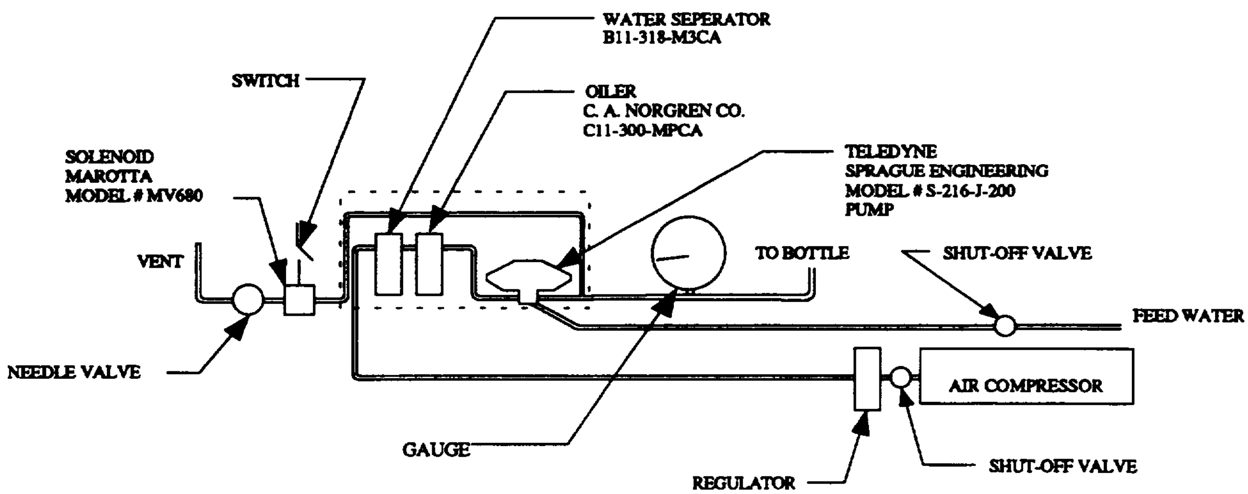

Figure 2. Pressure pump.

2.1.2 Pressure Vessels

The graphite/epoxy vessels included in this work were all tumble wound and rotisserie cured using a Hercules IM-7 graphite fiber prepreg with either a Hercules 3501-6 ATL, Hercules X8553-45 or Fiberite 977-2 epoxy resin. The cure cycle consisted of a one hour 65.6 °C precure followed by a three hour 177 °C cure, with 2.5 °C/minute temperature ramps. Inert propellant was packed into seventeen of the vessels, after washing out the sand mandrel, leaving only a one inch diameter cylindrical hollow core through its mid-section (Figure 3).

The Kevlar/epoxy vessels were tumble wound "wet" and rotisserie cured using Kevlar 49 fiber and Dow DPL862/W resin. Here, the cure cycle consisted of a one hour precure at 121 °C, followed by a three hour cure at 177 °C. The temperature ramps were maintained in the 0.5 to 2.5 °C range. Fourteen of the Kevlar vessels were packed with inert propellant in a similar manner to the graphite vessels.

One of the problems that had been encountered early on in this program was manufacturing consistency (See Section 2.3). An investigation into optimizing the manufacturing techniques was performed by fabricating tall (30.5 cm hoop length) graphite/epoxy bottles (Figure 4) made from IM7 fiber and 977-2 resin. The five manufacturing techniques are presented in Table 7 of Section 2.5.1. As an additional benefit to these tests, the ability to scale the neural network burst pressure prediction models could be investigated. None of the tall vessels were impact damaged.

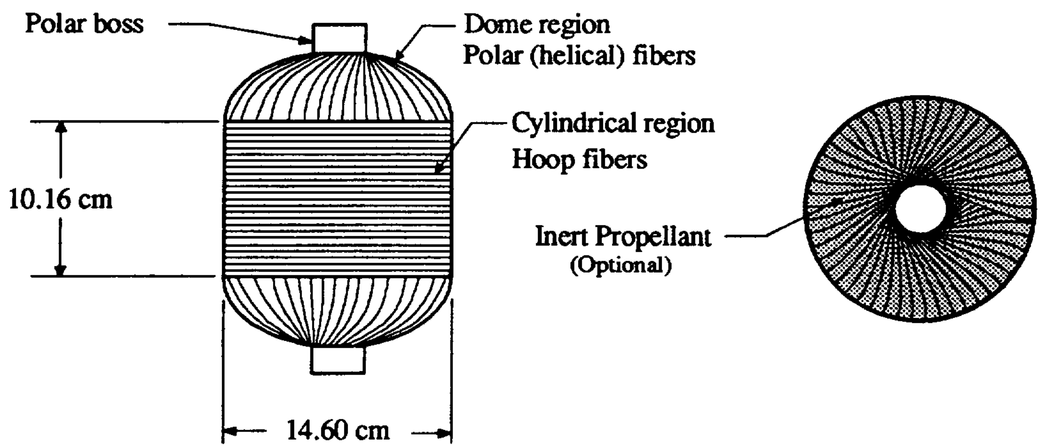

Figure 3. Standard 14.61 cm diameter pressure vessel geometry.

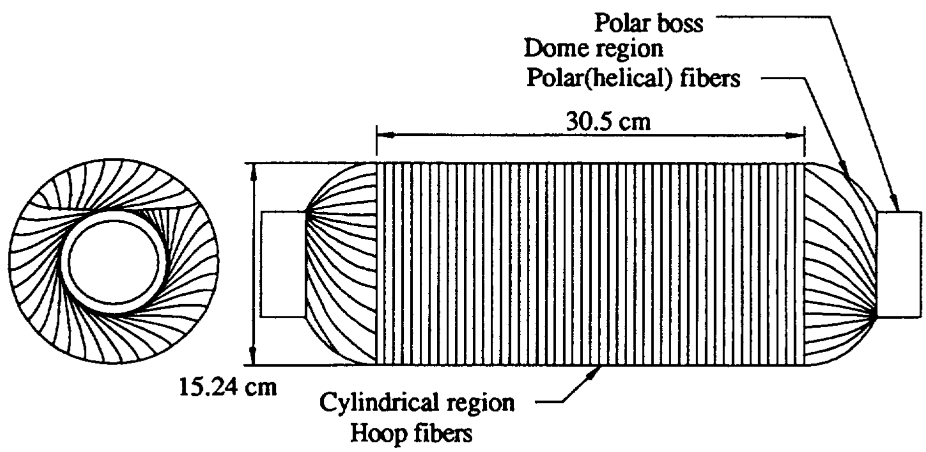

Figure 4. Tall 15.24 cm diameter pressure vessel geometry.

2.2 BACK PROPAGATION NEURAL NETWORKS

A back propagation neural network was developed to model the effects of the impact damage on burst pressure using NeuralWorks Professional II/PLUS software, by NeuralWare, Inc. The back propagation neural network paradigm is well suited to the problem of prediction using AE data since it can automatically map the descriptive features from a multidimensional input vector into a desired output response, such as the values of an amplitude histogram to burst pressure. Processing elements (PE) of the back propagation neural network (Figure 5) are used in a manner analogous to biological *neurons* creating the architecture necessary to provide the basis for learning [3]. The PE performs a simple summation of the weighted input values producing a single output response based upon a continuous transfer function. The transfer function serves to apply progressively smaller step sizes to the update delta weights as the normalized training error decreases and keep the PE output values at a reasonable level, typically between ±1.0. For this work, a hyperbolic transfer function (Figure 6) was used in each of the network models.

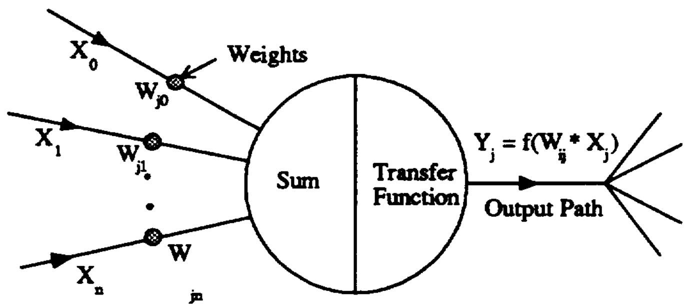

Figure 5. The processing element.

$$f(z) = \frac{e^{z} - e^{-z}}{e^{z} + e^{-z}}$$

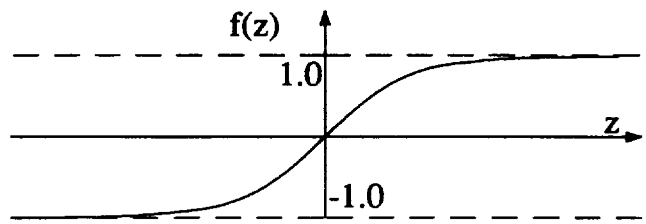

Figure 6. Hyperbolic tangent transfer function.

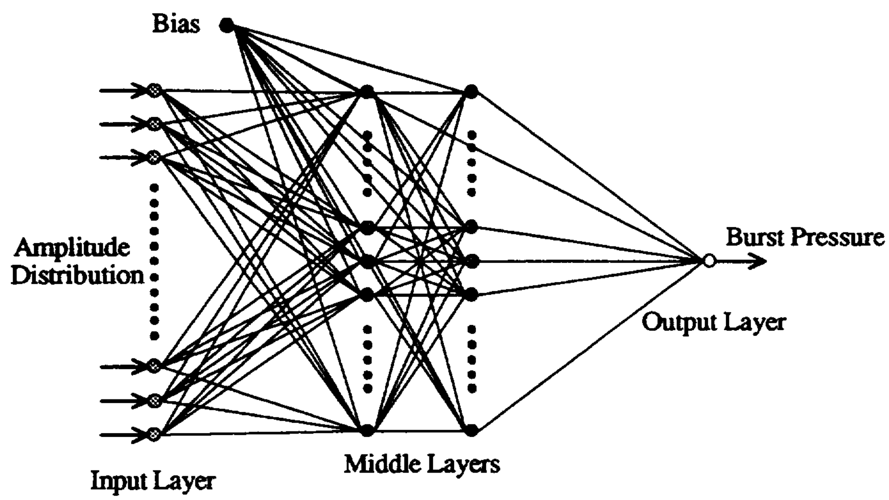

Figure 7. Back propagation neural network.

The PE in a back-propagation neural network are arranged into an input layer, an output layer and at least one middle, or hidden layer (Figure 7). The input layer provides a way to introduce data into the network. Here, for example the discrete values of the amplitude distribution histogram would be entered as an input vector. Each input processing element is fully connected by a series of weighting factors to the middle layer and these in turn are fully connected by another series of weighting factors to the output layer. If more than one middle layer is used, their PE are also fully connected. The middle layers serves to map nonlinear variations in the data set. A bias processing element may also be weight connected to the PE of the middle and output layers to serve as an offset value in the network. Ultimately, the weighting factors serve as the memory of the trained network by providing a multiplier between a preceding processing element's output value and an ensuing processing element's input value.

The learning process begins by assigning initially randomized weights to the interconnections of the network and calculating an output value in response to an input vector. The input and desired output vectors are typically scaled to values less than unity so as to help keep the PE summations from saturating the transfer function. A global error results from the sum of the differences between the desired output and the actual output over a specified epoch size. An epoch is defined as a single input-output data set. A measure of the local error "e" at the j^{th} processing element in layer "s" is given by the rate of change of the global error with respect to the summed input to the processing element. Only a portion of the actual local error is passed to each weighted connection by multiplying by a constant known as the "learning coefficient". The learning coefficient is kept as small as realistically possible to allow the network to converge on the absolute error minimum. Care must be taken when training a network not to get caught in local minima since these often lead to poor repeatability in the projected output. To overcome this problem a momentum term is added to the delta weight conversion to keep the network moving towards the absolute minimum by adding a portion of the previous delta weight "$(\Delta W)_p$" adjustment back to the new delta weight. There is no analytical way of determining for a given application before a test begins what values should be used for the learning coefficient and the momentum. Typically though, a learning coefficient of less than 0.1 and momentum in the range of 0.5 to 0.9 provides workable convergence times and training resolution.

$$\Delta W_{ji}^{[s]} = (\text{learning coefficient}) * e_j^{[s-1]} * x_j^{[s-1]} + (\text{momentum}) * \left(\Delta W_{ji}^{[s]}\right)_p$$

2.3 UN-FILLED 14.61 CM DIAMETER GRAPHITE/EPOXY VESSELS

The unfilled graphite/epoxy vessels(Table 2), impacted with a blunt 12.7 mm hemispherical tip, were hydroburst between July and October, 1993. The test code defines the AE data file name prefix for each test. For completeness, the burst pressure results of those tests have been included in this report. Several instrumentation and manufacturing variations/problems were encountered during this first round of testing that adversely effected the usefulness of the AE data for burst pressure prediction modeling. First, and foremost, the actual burst pressures are in question as a result of faulty pressure transducers and a lack of a stable pressure reference. Two pressure sensors failed, and had to be replaced, as a result of the back-shock created when the vessels ruptured. The calibration factor was periodically reset based upon shunt resistance values and also rezeroed, but with fluctuations in "house" water pressure and electronic noise creating variations as high as 689.5 kPa to 1034.2 kPa in the initial "reference" pressure level a consistent burst pressure reading is doubtful. The pressurization schedule was followed very loosely making AE hit rate and damage propagation measurements impossible to analyze. Also, the AE system timing parameter defining the hit lockout (HLT) interval was changes from 100 μs to 300 μs which invalidated any comparison between those individual data sets. Finally, several of the vessels failed at points away from the impact site. In some instances the failure was on the opposite side of the vessel as the impact. This was thought to be due to manufacturing defects that were more critical than the impact damage or a side effect of the way the vessels were held during the impact.

Neural network modeling of data for the purpose of prediction relies heavily on the repeatability and consistency of the data set. The network can only take into account variations that it has been trained on. Just as with statistical analysis, the ability of a network to *learn* is limited to a function of the number of samples presented to it during the training phase. For practical purposes only the data from 3 to 5 vessels from each sample class "resin type for this work" are hydroburst to train the network. This keeps the *real* expense of *destructive* testing at a minimum. Since the network is given only a limited number of samples, if any one is contaminated with an incorrect expected output "burst pressure" then a false model will be developed. The model will thus bias all future predictions with the error incurred by the incorrect training pressure reading.

Fabrication Number	Bottle I.D.	Burst (MPa)	Resin type	Test code	HLT (μs)	(MPa/volt)	Energy (N • m)
91PV-003	A001-002	12.53	3501-6	AA	100	4.626	9.49
92PV-005	C065-066	19.26	3501-6	AN	300	22.93	9.49
91PV-003	A015-016	11.92	3501-6	AO	300	22.93	9.49
92PV-005	C081-082	17.30	3501-6	AB	100	4.626	6.78
92PV-005	C085-086	19.14	3501-6	AP	300	22.93	6.78
92PV-005	C083-084	18.46	3501-6	AQ	300	22.93	6.78
91PV-003	A021-022	18.04	3501-6	AC	100	4.626	4.07
91PV-003	A019-020	15.93	3501-6	AR	300	22.93	4.07
91PV-003	A011-012	15.35	3501-6	BH	300	22.93	4.07
91PV-003	A009-010	14.85	3501-6	AD	100	4.626	0.00
92PV-003	C075-076	19.59	3501-6	AZ	300	22.93	0.00
92PV-005	C073-074	18.45	3501-6	BA	300	22.93	0.00
92PV-007	C133-134	18.82	977-2	AE	300	4.626	9.49
92PV-007	C153-154	17.76	977-2	AH	300	4.626	9.49
92PV-007	C123-124	8.880	977-2	AI	300	4.626	9.49
92PV-007	C147-148	18.83	977-2	AG	300	4.626	6.78
92PV-007	C121-122	23.13	977-2	AJ	300	4.626	6.78
92PV-007	C145-146	20.42	977-2	AK	300	23.20	6.78
92PV-007	C149-150	22.17	977-2	AF	300	4.626	4.07
92PV-007	C111-112	22.70	977-2	AL	300	22.93	4.07
92PV-007	C157-158	20.17	977-2	AM	300	22.93	4.07
92PV-007	C125-126	20.51	977-2	BB	300	22.93	0.00
92PV-007	C127-128	22.01	977-2	BC	300	22.93	0.00
92PV-007	C143-144	19.26	977-2	BD	300	22.93	0.00
92PV-001	A041-042	13.76	8553-45	AS	300	22.93	9.49
92PV-006	C097-098	21.89	8553-45	AT	300	22.93	9.49
92PV-001	A031-032	18.22	8553-45	AU	300	22.93	9.49
92PV-006	C103-104	13.53	8553-45	AV	300	22.93	6.78
92PV-001	A039-040	19.14	8553-45	AW	300	22.93	6.78
92PV-001	A037-038	13.64	8553-45	BI	300	22.93	6.78
92PV-006	C101-102	19.83	8553-45	AY	300	22.93	4.07
92PV-006	C107-108	N.A.	8553-45	BJ	300	22.93	4.07
92PV-006	C105-106	13.64	8553-45	AX	300	22.93	4.07
92PV-006	C095-096	22.81	8553-45	BE	300	22.93	0.00
92PV-006	C089-090	22.58	8553-45	BF	300	22.93	0.00
92PV-006	A045-046	20.75	8553-45	BG	300	22.93	0.00

Table 2. Summary of unfilled graphite/epoxy pressure vessels.

The vessels were acoustically monitored with four PAC R15I sensors mounted with vacuum bag sealant tape. One sensor was attached to the wave guide pipe plug screwed into the top polar boss, while the remaining three sensors were bonded symmetrically around the mid-hoop line of each vessel. The same AE system setting described in Section 2.4 were used during this series of tests. A pressurization schedule consisting of three phases was used to load the vessels. First, the vessels were ramped (68.95 kPa/sec) to 6.895 MPa and held for two minutes. During that time AE data was collected for potential burst pressure prediction modeling. After unloading, the vessels were again ramped to 6.895 MPa and held for a variable time while the shearographic and video image correlation images were acquired. The vessels were then loaded to 13.790 MPa and held at pressure for another two minutes. Pressure was again released, so that the AE sensors could safely be removed, and the vessel reloaded to failure.

A plot of the final burst pressures versus impact energy is provided in Figure 8.

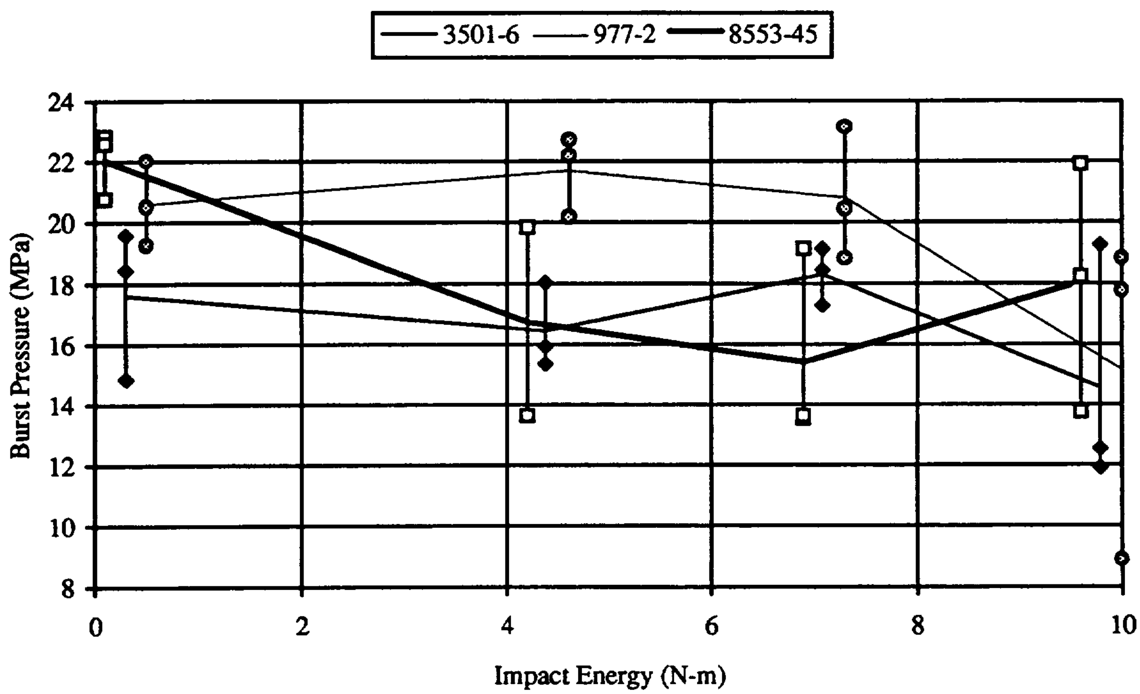

Figure 8. Burst pressure results of unfilled graphite/epoxy pressure vessels.

2.4 INERT FILLED GRAPHITE/EPOXY 14.61 CM DIAMETER VESSELS

The acoustic activity produced during hydroproof testing of seventeen inert propellant filled 14.61 cm diameter graphite/epoxy pressure vessels is presented. Four AE sensors were used to monitor the acoustic activity, three located symmetrically around the mid-line of the hoop region and one on the top polar boss (Figure 9). The sensors were all bonded to the vessel with hot melt glue. All of the pressure vessels were constructed from a Hercules IM-7 graphite fiber, while the resins types were split evenly into three groups using either a Hercules 3501-6 ATL, Hercules X8553-45 or a Fiberite 977-2 resin.

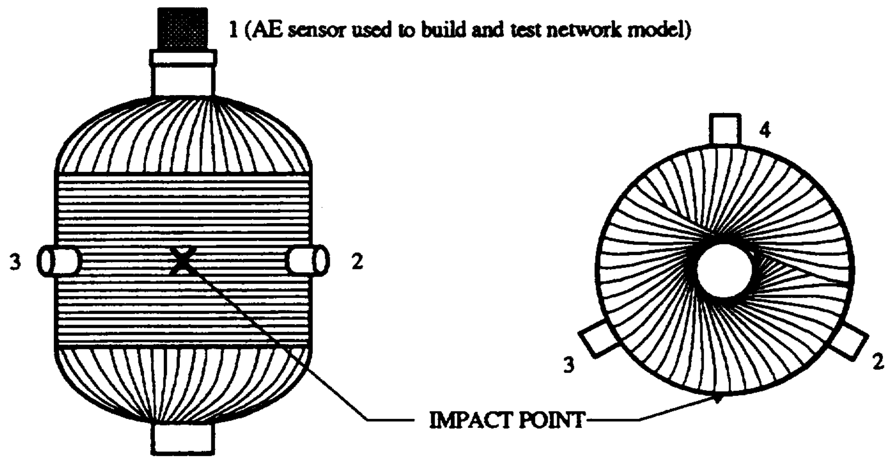

Figure 9. Transducer placement.

A pressurization cycle was selected that would be convenient for the AE testing, as well as for the optical NDE techniques (shearography and sub-pixel video image correlation) also used to monitor the vessels (Figure 10). The first proof cycle to 5.516 MPa (approximately 25% of the expected burst pressure) provided a consistent AE data set for later use in developing burst pressure prediction models and to ensure that the containment chamber door could be safely opened for the optical NDE techniques. By monitoring the continuation of AE activity during a two minute hold at 5.516 MPa the level of creep damage could be measured. Here, a large amount of AE activity during a hold would signify that the vessel was near failure making it unsafe to continue pressurization with the chamber door open. The vessels were then unloaded by opening the pump vent switch, the containment door opened, and the vessels stepped back up to 5.172 MPa in 1.724 MPa increments. Five minute holds were allowed between each pressure ramp to allow time to collect the optical data for each step. After the 5.172 MPa hold the chamber door was closed and the vessels were proofed to 6.895 MPa. Following a two minute hold at 6.895 MPa to allow time for any creep activity to stabilize (noted by the absence of AE) the door was reopened and the final optical measurements made. The vessels were then unloaded, the hoop AE sensors removed, the door re-shut and a final pressure ramp straight to failure applied.

The pressure vessels' acoustic activities were collected during the hydroburst with the PAC SPARTAN AE system. A PAC R15I (150 kHz, 40 dB integral preamplifier, 100 kHz to 300 kHz bandpass filter) transducer was bonded with hot melt glue on the pipe plug used to seal the upper polar boss (Figure 9). Three PAC R15 (150 kHz) transducers were bonded symmetrically around the mid-hoop line and connected to external PAC 1220A preamplifiers (40 dB gain, 100 kHz to 300 kHz bandpass filter). A 20 dB internal gain and 60 dB signal threshold were used to establish the system's sensitivity. The AE system's timing parameters defined the acoustic hits with a 30 μs peak detection time, 80 μs hit detection time and a 300 μs hit lock-out time. With these settings, lead breaks performed approximately two inches from each sensor produced signal amplitudes in the 80 dB range, verifying good sensor coupling.

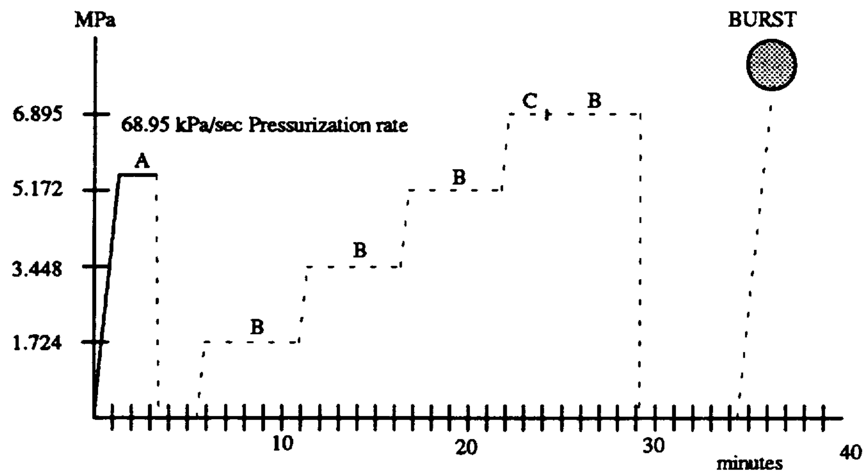

A => 2 minute hold at 5.516 MPa
B => 5 minute hold at 1.724, 3.448, 5.172 and 6.895 MPa
C => 2 minute hold at 6.895 MPa

Figure 10. Pressurization schedule.

AE Parameters	Peak definition time (PDT)	30 μs
	Hit definition time (HDT)	80 μs
	Hit lockout time (HLT)	300 μs
	Total system gain	60 dB
	Threshold	60 dB
External Parameters	Parametric multiplier	2020 psi/volt (13.93 MPa/volt)
Location Parameters	Wave speed	200000 inch/sec (508000 cm/sec)
	Lockout	18 inch (45.72 cm)
	Over calibration	1 inch (2.54 cm)

Table 3. System test parameters.

A calibrated dead weight drop fixture produced impact damage in the mid-hoop region of each vessel ranging from that which was barely visible to obvious fiber breakage. One vessel from each resin class was used as a control sample and left undamaged. The remaining vessels were split into equal groups and impacted with either the sharp or blunt hemispherical tip described in beginning of Section 2.0. Two impact levels were used with each tip (1.63 N•m. and 3.53 N•m for the sharp tip, 6.78 N•m and 10.98 N•m for the blunt tip) to produce a broad range of damage conditions. Electronic shearography (ES) and sub-pixel digital video image correlation (SDVIC) techniques showed that the blunt tipped impactors generally produced a wide damaged zone with some localized delaminations while the sharp tip tended to break fibers at the impact point [2]. Typical, full field strain measurements generated using the SDVIC system are provided in Figure 11, demonstrating the extent and effect of impact induced fiber damage. Delamination zones are shown in Figure 12, for both blunt and sharp tipped impactors, as detected by the ES system.

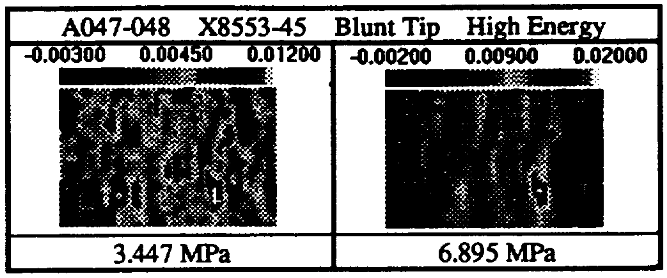

Figure 11. Full field strain measurements indicating regions of fiber damage using SDVIC.

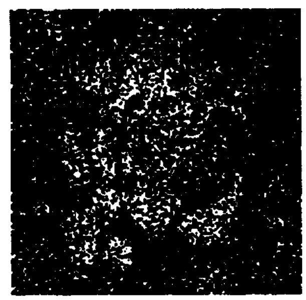

Figure 12. Delamination zone as imaged from the ES system.

2.4.1 Test Summary

The three resin systems were acoustically very different. The amount of AE activity recorded on channel 1, for example, through the end of the first hold at 5.516 MPa varied from an average of 517 hits for the 3501-6 resin, to 118 hits for the 977-2 resin, to only 11 hits for the 8553-45 resin (Figure 13). These results were expected, since the 977-2 and X8553-45 resin systems were formulated to be tougher than the brittle 3501-6 resin system, thereby providing a structure that could better redistribute stresses around stress concentrations rather than failing.

Based upon the limited test data collected, the 977-2 resin system appears to provide the highest burst pressures and the least sensitivity to impact damage. In the undamaged state the 977-2 resin produces a vessel that is 5% stronger than one fabricated from the 8553-45 resin system and 20% stronger than one fabricated from the 3501-6 resin system. The impacted vessels made from the 977-2 resin are on average 32% stronger than those made from the 3501-6 resin and 21% stronger than those made from the 8553-45 resin. Even with the small sample size (one vessel for each damage level and material type) these percentages are significant and warrant future study.

The burst pressures are plotted versus impact energy in Figure 14 for the seventeen vessels. Overall, the 977 resin system produced the greatest burst pressures and showed the least sensitivity to impact damage. As expected the burst pressures decreased with increasing sharp tip impact energy. The blunt tip impacted vessels though, showed an increase in burst pressure with larger impact energies. The delaminations generated during these impacts appear to be stress relieving the individual hoop plies, creating a more uniform overall stress state, and thus producing a higher net burst pressure.

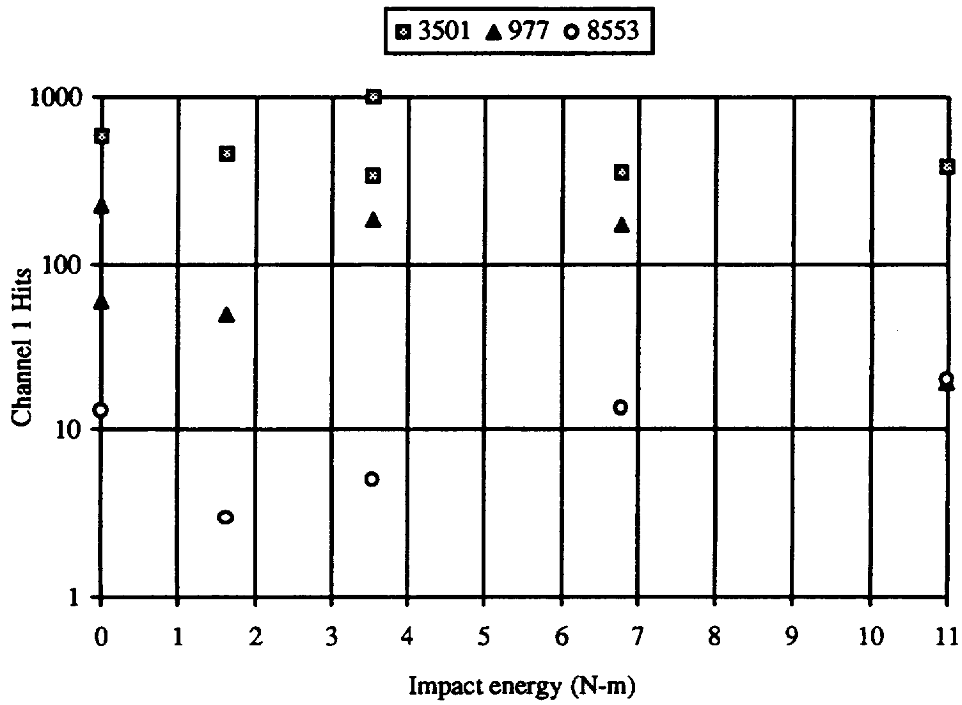

Figure 13. Acoustic activity versus impact energy.

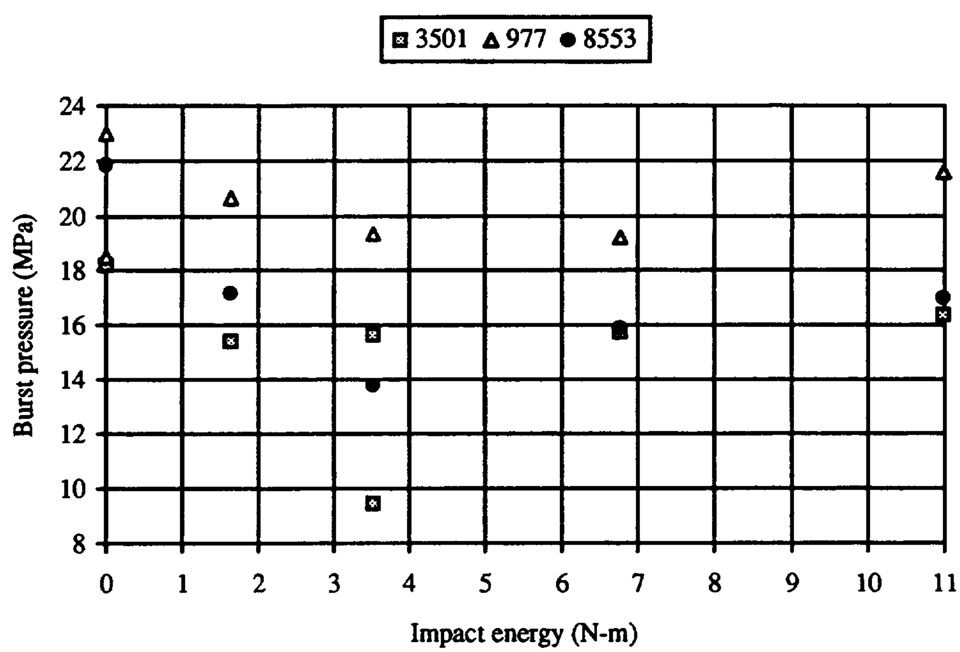

Figure 14. Burst pressure results.

Resin type	Bottle I.D.	Impact status	AE Code	Burst pressure (MPa)
Hercules 3501-6	A003-004	None	GBIA003	18.20
	C077-078	BT-10.98 N•m	GBIC077	16.36
	C069-070	BT-6.78 N•m	GBIC069	15.71
	A013-014	ST-1.63 N•m	GBIA013	15.39
	A023-024	ST-3.53 N•m	GBIA023	15.62
	A017-018	ST-3.53 N•m	GBIA017	9.453*
Fiberite 977-2	C115-116	None	GBIC115	22.99
	C139-140	None	GBIC139	18.49
	C117-118	BT-10.98 N•m	GBIC155	21.60
	C155-156	ST-3.53 N•m	GBIC155	19.33
	C141-142	BT-6.78 N•m	GBIC141	19.21
	C131-132	ST-1.63 N•m	GBIC131	20.66
Hercules X8553-45	A025-026	None	GBIA025	21.86
	A029-030	BT-6.78 N•m	GBIA029	15.87
	C087-088	ST-1.63 N•m	GBIC087	17.16
	A047-048	BT-10.98 N•m	GBIA047	16.98
	C093-094	ST-3.53 N•m	GBIC093	13.76

* Dome Failure

Table 4. Summary of burst pressures for inert filled graphite/epoxy vessels.

2.4.2 Neural Network Analysis

A back propagation neural network was developed to model the effects of the impact damage on burst pressure for each of the three fiber/resin systems. The amplitude distribution data from channel one (Appendix 6.2), between 60 dB and 100 dB were introduced to the network through a 41 neuron input layer. The first of the two 13 neuron middle layers was fully connected by a series of weighting factors to the input layer, and then to each other. Burst pressure values were generated by a single output neuron that was fully weight connected to the second middle layer. Finally, a bias neuron (output of 1.0) was weight connected to the middle and output layer neurons to serve as a constant reference or offset value in the network. During training the network adjusts the bias weights just as it does the other interconnection weights to reduce the overall output error. The input vector was normalized to a range of 0.0 to 1.0 by the NeuralWare program and the output values, burst pressures, scaled to fit into a range of -0.8 o 0.8. A small learning coefficient, 0.001, was necessary to provide adequate delta weight resolution during training and momentum of only, 0.1, was required to give an reasonable convergence rate. The epoch size was set at 3, to match the number of training set vectors, permitting an average of the entire training error to be used for each delta weight calculation. A hyperbolic tangent transfer function was utilized to keep the output of the PE in check, i.e. between -1.0 and 1.0.

Three independent, yet similar, networks were trained using three vessels from each resin class after building a training file consisting of the amplitude distribution corresponding to a high, medium and low burst pressure for each class. Each network was trained on the cumulative amplitude distributions from the dome sensor (AE system channel 1) and known burst pressures until a 5% convergence criteria was met on the modeled burst pressures. In all cases, less than

5000 training cycles were required to reach the convergence criteria. The results of this training exercise is presented in Table 5.

Once trained, the networks were tested on the remaining vessels from each resin class. A summary of the predicted burst pressure values are provided in Table 6. Burst predictions were made with an average prediction error of only 5.0% including an outlier with an error of over 19%. Excluding this outlier the average prediction error drops to a low 2.9%. The final network weights are given in Appendix 6.3a, b and c. The weights describe the 700+ coefficient equation relating the amplitude distribution to burst pressure for each material system. Although it is theoretically possible to infer the physical nature of a problem from a network model using the relative weight magnitudes, in this particular situation the extremely large number of weights makes that impractical.

Resin Type	Bottle I.D.	Actual Burst (MPa)	Predicted Burst (MPa)	% Error
Hercules	A003-004	18.19	17.93	-1.5
	C077-078	16.36	16.42	0.4
3501-6	A017-018	9.453	9.832	4.0
Fiberite	C115-116	22.99	22.81	-0.8
	C141-142	19.21	19.20	-0.00
977-2	C131-132	20.66	20.74	0.4
Hercules	A025-026	21.86	21.53	-1.5
	A047-048	16.98	17.01	-0.1
X8553-45	C093-094	13.76	14.04	2.1
			Abs(Average)	1.2

Table 5. Neural network training results.

Resin Type	Bottle I.D.	Actual Burst (MPa)	Predicted Burst (MPa)	% Error
Hercules	C069-070	15.71	15.35	-2.3
	A013-014	15.39	16.24	5.6
3501-6	A023-024	15.62	18.70	19.7
Fiberite	C139-140	18.49	19.25	4.1
	C117-118	21.60	21.46	-0.6
977-2	C155-156	19.33	20.24	4.7
Hercules	A029-030	15.87	15.74	-0.8
X8553-45	C087-088	17.16	17.59	2.5
			Abs(Average)	5.0 (2.9)*

* Average error excluding outlier

Table 6. Neural network prediction results.

2.5 TALL GRAPHITE/EPOXY 14.61 CM DIAMETER VESSELS

The burst pressures of fifteen "un-filled" 12 inch tall IM7/977-2 (graphite/epoxy) vessels were predicted using the neural network model developed for the short (Section 2.4) 977-2 class filled vessels. The primary purpose for these tests were to investigate the effects of different manufacturing techniques on burst pressure. As a side benefit, the ability to "scale" a neural network model from subscale to larger structures could be investigated.

The vessels were not impacted, and as such shearography and SDVIC were not performed. Since the optical NDE techniques were not used a slightly modified pressure cycle (Figure 15) could be used. Instead of the ramp to 5.516 MPa, hold, unload and reramp to 6.895 MPa; the vessels were directly ramped to 6.895 MPa, held, unloaded and finally ramped to failure. The same sensor pattern as used on the standard size 14.61 cm diameter graphite/epoxy bottles was incorporated with the tall vessel tests (Figure 16). The network was trained and tested using the cumulative AE amplitude distribution data collected during the initial pressure ramp to 5.516 MPa from the dome sensor (AE channel 1).

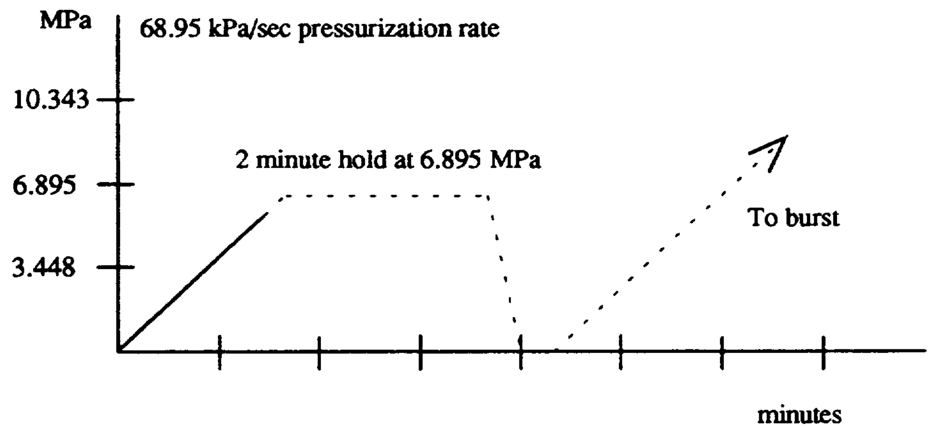

Figure 15. Pressurization cycle for tall graphite/epoxy vessels.

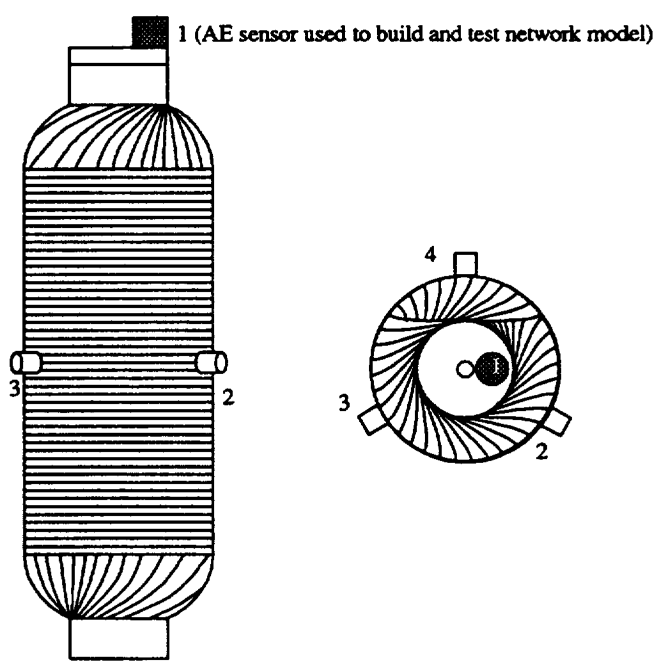

Figure 16. Sensor locations for tall graphite/epoxy vessels.

2.5.1 Test Summary

The burst pressures are summarized in Table 7 along with a description of the manufacturing process and failure location. The failure location is determined by the circumferential distance, measured clockwise from the vessel label. Post burst examination of the vessels indicated that failure initiated in the mid-hoop region for eight of the vessels and near one dome for the remaining seven vessels. The dome failures resulted in the ejection of the polar boss, splitting of the vessels along a longitudinal axis and buckling of the polar plies (created by the rapid unloading of the fibers at failure) radially from the initiation point. Vessels that failed in the mid-hoop region first, behaved in a similar fashion except that the domes remained intact after failure.

Overall, the series 5 vacuum bagged and oven cured vessels had the best "highest" burst pressures, averaging 22.43 MPa. The rotisserie cured series 6 vessels though, yielded only slightly lower burst pressures, averaging 21.69 MPa for a 3.3 % reduction in overall strength. The series 6 vessels were also the only ones to not have at least one dome failure. Figure 17 illustrates the burst pressure results for the five manufacturing processes.

Bottle I.D.	Burst (MPa)	AE Test code	Bottle series	Failure Loc.	Pramp/Pfail
A	20.61	GBT4A	94PV0004	0.5 D	T1.PRN
B	21.06	GBT4B	Autoclaved	11.5	T2.PRN
C	15.79	GBT4C		16.0 D	T3.PRN
Average	19.15				
A	22.93	GBT5A	94PV0005	6.5 D	T4.PRN
B	22.53	GBT5B	Vacuum Bag	5.0 D	T5.PRN
C	21.80	GBT5C	Oven cure	8.0 D	T6.PRN
Average	22.42				
A	20.91	GBT6A	94PV0006	17.5	T7.PRN
B	22.34	GBT6B	Rotisserie	0.5	T8.PRN
C	21.83	GBT6C		0.5	T9.PRN
Average	21.69				
A	17.86	GBT7A	94PV0007	12.0	T10.PRN
B	17.74	GBT7B	Low temp cure-PVA washed out-	16.0	T11.PRN
C	16.05	GBT7C	final cure	14.5D	T12.PRN
Average	17.22				
A	20.92	GBT8A	94PV0008	3.0	T13.PRN
B	21.40	GBT8B	Rotisserie	14.0 D	T14.PRN
C	20.33	GBT8C	350° and cured	5.0	T15.PRN
Average	20.88				

D = Dome Failure

Table 7. Test summary for tall graphite/epoxy vessels.

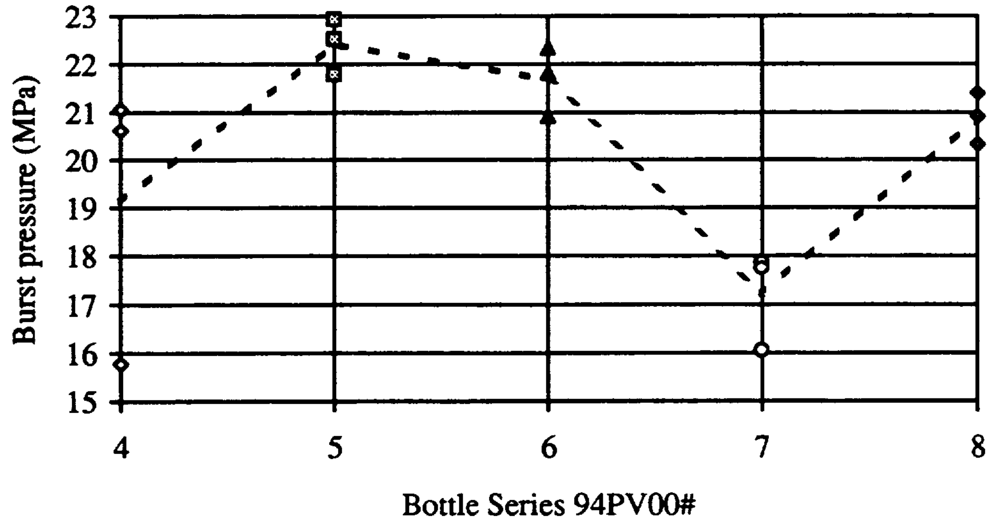

Figure 17. Burst pressure summary for the tall graphite/epoxy vessels.

2.5.2 Neural Network Analysis

The neural network results for the tall graphite/epoxy vessels show that provided the manufacturing processes are similar, good overall burst pressure predictions can be made from the trained network of the standard size vessels. Table 8 provides the prediction errors for all of the tall vessels along with the average error computed by the absolute value of prediction error for each vessel series. The lowest average error, 4.9 %, was found for the series 6 vessels were the same material and manufacturing processes were used as with the standard size vessels. A fair prediction error was also produced with the series 5 and 8 vessels. The network model had the most problem predicting the burst pressures of the series 7 vessels. Apparently, the different cure changed the mechanical properties of the vessels enough that their acoustic signature was unrecognizable by the model. Besides that series, only one outlier was found. The third vessel in the series 4 class of vessels has a burst pressure 4.826 MPa lower than the other two of that class. The network model was not able to pick up this variation netting an error of over 37 %.

More testing will need to be performed in this area to better define the limits of the network to be trained on subscale vessels for prediction on larger vessels. The main question to be answered is how will the network handle a potential change in the primary failure mechanism, which may happen as the geometry of the vessel changes? For the tall vessels presented herein, the failure was primarily localized in the hoop fibers just as was found on the standard vessels. But when the diameter of the vessels is increased though and the local curvature becomes smaller, what effect will that have on the propagation and formation of the principle failure modes? It is possible that for scaling to work the network will have to be trained on specially designed subscale vessels with similar failure modes present as in their full scale counterparts vessels.

Bottle series	AE test code	Failure location	Actual burst pressure (MPa)	Predicted burst pressure (MPa)	Prediction error
94PV0004 Autoclaved	GBT4A	0.5 D	20.61	19.84	-3.7
	GBT4B	11.5	21.06	21.45	1.8
	GBT4C	16.0 D	15.79	21.75	37.8
				Abs(Average)	**14.4**
94PV0005 Vacuum bag Oven cure	GBT5A	6.5 D	22.93	21.94	-4.3
	GBT5B	5.0 D	22.53	20.16	-10.5
	GBT5C	8.0 D	21.80	21.03	-3.5
				Abs(Average)	**6.1**
94PV0006* Rotisserie cure	**GBT6A**	**17.5**	**20.91**	**20.38**	**-2.6**
	GBT6B	**0.5**	**22.34**	**20.32**	**-9.0**
	GBT6C	**0.5**	**21.83**	**21.17**	**-3.0**
				Abs(Average)	**4.9**
94PV0007 Low temp cure-PVA removed-final cure	GBT7A	12.0	17.86	20.69	15.8
	GBT7B	16.0	17.74	19.55	10.2
	GBT7C	14.5D	16.05	18.90	17.8
				Abs(Average)	**14.6**
94PV0008 Rotisserie cured at 350°	GBT8A	3.0	20.92	19.22	-8.1
	GBT8B	14.0 D	21.40	22.80	6.5
	GBT8C	5.0	20.33	19.27	-5.2
				Abs(Average)	**6.6**

D = Dome Failure * = Similar manufacturing process to short inert filled vessels.

Table 8. Neural network results.

2.6 UN-FILLED KEVLAR/EPOXY 14.61 CM DIAMETER VESSELS

Nineteen "un-filled" 14.61 cm diameter Kevlar/epoxy pressure vessels were acoustically monitored during hydroburst with four AE sensors. Just as with the graphite/epoxy vessels, three AE sensors were mounted symmetrically around the mid-line of the hoop region with one sensor on the top polar boss (Figure 9) with hot melt glue. All of the pressure vessels were wet wound and rotisserie cured from a Dupont Kevlar fiber and Dow DPL862/W epoxy resin.

The pressure cycle was shortened slightly from the one used with the graphite/epoxy vessels by decreasing the hold at each 1.724 MPa step (labeled B in Figure 10 of Section 2.4) to only 2 minutes, as compared to the previous 5 minute holds. The reduction in the hold time was permitted as a result of not conducting shearography during the proof tests.

The system parameters of the PAC SPARTAN were kept the same as for the graphite/epoxy vessels except that the threshold was reduced to 50 dB. The reduction in threshold was deemed necessary due to the larger attenuation of the Kevlar vessels over the graphite vessels and the lower overall acoustic nature of the Kevlar/epoxy material system. Six (3 each filled and unfilled) Kevlar/epoxy vessels were tested before the threshold was changed to the lower value. Due to nonlinear roll-off in the threshold filter, it would be impossible to synthetically reconstruct the lost

AE events below 60 dB and since the data from 50 to 60 dB was significant, clipping the first 10 dB of the remaining vessels would be impractical. With these settings, lead breaks performed approximately two inches from each sensors produced signal amplitudes in the 70 dB range, verifying good sensor coupling.

A calibrated dead weight drop fixture produced impact damage in the mid-hoop region of each vessel ranging from that which was barely visible to obvious fiber breakage. Two vessels were used as a control sample and left undamaged. The remaining vessels were somewhat randomly impacted with either the sharp and blunt hemispherical tip. Overall, impacts ranged up to 16.15 N•m with the sharp tip and 21.02 N•m with the blunt tip. Just as with the graphite/epoxy vessels ES and SDVIC techniques showed that the blunt tipped impactors generally produced a wide damaged zone with some localized delaminations while the sharp tip tended to break fibers at the impact point. The major difference between the two fiber/resin systems was that less fiber fractures were apparent and the delaminations were more pronounced in the Kevlar vessels.

2.6.1 Test Summary

A summary of the burst pressures, threshold, impact status and number of channel one hits are presented in Table 9. The burst pressures are plotted versus impact energy in Figure 18 for the nineteen Kevlar vessels. It should be noted that vessel D254-255 was impacted twice, and is represented in the figure at a position denoted by the sum of the two impact energies. The summed energy value for D254 is shown strictly for reference should not be taken literally, as the energy from multiple impacts are not additive. The Pramp/Pfail column defines the pressure profile filenames for each test.

Bottle I.D.	Burst (MPa)	Threshold (dB)	AE code	Impact Status (N•m.)	Channel 1 Hits	Pramp/Pfail
D179-180	17.66	60	KBD179	ST-13.56	21	K4
D227-228	15.69	60	KBD227	BT-16.27	38	K5
D165-166	16.22	60	KBD165	ST-9.491	52	K6
D239-240	12.38	50	KBD239	BT-21.02	143	K7
D213-214	16.24	50	KBD213	ST-14.91	87	K9
D235-236	11.73	50	KBD235	BT-19.54	35	K16
D254-255	10.62	50	KBD254	BT-17.75/19.54	102	K13
D169-170	17.98	50	KBD169	ST-11.97	42	K12
D187-188	16.60	50	KBD187	BT-16.00	43	K11
D241-242	16.23	50	KBD241	BT-12.20	271	K14
D177-178	15.42	50	KBD177	ST-16.15	52	K10
D225-226	14.82	50	KBD225	ST-16.00	39	K15
D201-202	17.91	50	KBD201	ST-9.362	92	K23
D233-234	21.08	50	KBD233	NONE	201	K25
D237-238	15.95	50	KBD237	ST-13.29	7	K26
D161-162	15.51	50	KBD161	?	26	K27
D221-222	19.77	50	KBD221	NONE	31	K31
D215-216	17.26	50	KBD215	ST-9.633	122	K32
D163-164	15.13	50	KBD163	BT-14.78	24	K33

Table 9. Data summary for un-filled Kevlar/epoxy vessels.

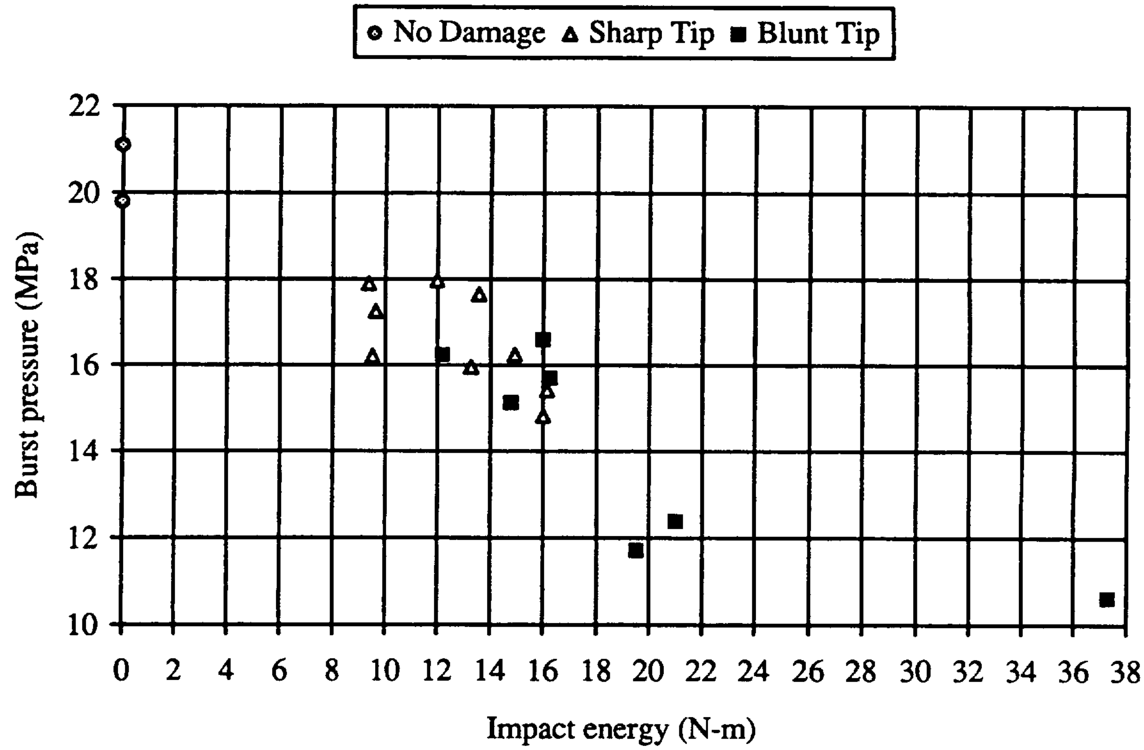

Figure 18. Burst pressure results for un-filled Kevlar/epoxy vessels.

2.6.2 Neural Network Analysis

A back propagation neural network was trained on the cumulative amplitude distributions, from the dome sensor (channel 1), of five vessels. The vessels were selected based upon their impact "damage" level and subsequent burst pressure. An implied requirement for developing robust neural network models is that the training set cover as many of the possible variations in the input and output vector as feasible. Ideally, hundreds or even thousands of input-output vector sets would be needed to train a neural network, but for practical considerations, i.e. time and cost, a limited number of samples must be used. Since, the sample size is restricted care must be taken when developing the training set to ensure that it be as broad based as possible.

The amplitude distribution data between 50 dB and 100 dB from channel one were introduced to the network through a 51 neuron input layer. The number of middle layer neurons was varied from as low as 3 to as high as 50 while keeping the learning coefficient fixed at 0.006 on the input to middle layer and 0.003 on the middle to output layer; and momentum equal to 0.8. The epoch size was set at 5 to again match the number of training data sets and a linear transfer function was incorporated into the network. The input vector "amplitude distribution" was scaled to fit between 0.2 and 0.8 while the output "burst pressure values were scaled to fit between -0.9 and 0.9. A 3% convergence criterion was set for defining the end of training. After each network was trained, two trial vessels were tested to see how well the network would respond to outside, other than training, data. Since the network is essentially solving an optimization problem where more unknowns "weights" exist than equations "input-output vector sets" a trained solution may not be a "globally" correct solution. In other words, it is possible during training for the network to model a trivial part of the input vector set to generate the correct output, instead of finding a "true" or physical correlation between the input and output vector. By testing these, trial, vessels the probability for success on future vessels will increase.

The best training/trial results were generated when 19 middle layer neurons were used in the network. The results Table 10 show the training, trial and *blind* test results. The blind test results being those which were introduced to the network, independently of any training process. Overall, the errors indicate that the network was able to model the effects of impact damage on burst pressure with the exception of the double hit blunt impact vessel. It is possible that due to the nature of the damage an entirely different failure mode was induced as the vessel was pressurized which the network was unable to identify.

The final network weights are given in Appendix 6.5 for reference.

Bottle I.D.	Impact Status (N•m)	Actual burst (MPa)	Predicted burst (MPa)	% error
Training results				
D187-188	BT-16.00	16.60	16.56	-0.19
D235-236	BT-19.54	11.73	11.98	2.15
D233-234	NONE	21.08	21.13	0.23
D177-178	ST-16.15	15.42	15.34	-0.54
D221-222	NONE	19.77	19.57	-1.01
Trial results				
D201-202	ST-9.362	17.91	16.91	-5.55
D163-164	BT-14.78	15.13	15.06	-0.47
Blind Test results				
D241-242	BT-12.20	16.23	16.99	4.71
D239-240	BT-21.02	12.38	12.79	3.32
D225-226	ST-16.00	14.82	14.94	0.81
D169-170	ST-11.97	17.98	18.89	5.08
D213-214	ST-14.91	16.24	15.86	-2.38
D237-238	ST-13.29	15.95	16.78	5.15
D161-162	UNKNOWN	15.51	16.10	3.85
D254-255	BT-17.75/19.54	10.62	15.92	49.84
D215-216	ST-9.633	17.26	17.03	-1.34

19 middle layer neurons

Table 10. Burst pressure prediction results.

2.7 INERT FILLED KEVLAR/EPOXY 14.61 CM DIAMETER VESSELS

A similar test procedure was conducted on the inert propellant filled vessels as was done for the empty vessels. Fourteen vessels in all were hydroburst, yet only eleven are used in the network models due to different AE test threshold settings.

2.7.1 Test Summary

Bottle I.D.	Burst (MPa)	Threshold (dB)	AE code	Impact Status (N•m)	Channel 1 Hits	Pramp/Pfail
D197-198	15.99	60	KBID197	ST-6.006	66	K1
D229-230	15.14	60	KBID229	BT-23.05	33	K2
D247-248	17.52	60	KBID247	BT-14.78	31	K3
D243-244	17.84	50	KBID243	ST-2.942	305	K4
D249-250	17.65	50	KBID249	ST-5.17	55	K17
D231-232	14.29	50	KBID231	ST-6.576	109	K18
D181-182	16.48	50	KBID181	ST-3.918	73	K19
D223-224	20.53	50	KBID223	NONE	135	K24
D191-192	14.47	50	KBID191	BT-27.50	58	K20
D205-206	21.17	50	KBID205	BT-6.711	102	K22
D245-246	15.51	50	KBID245	BT-18.02	33	K21
D185-186	20.86	50	KBID185	NONE	52	K28
D175-176	13.77	50	KBID175	BT-22.37	69	K29
D255-256	18.49	50	KBID255	ST-5.559	108	K30

Table 11. Data summary for inert propellant filled Kevlar/epoxy vessels.

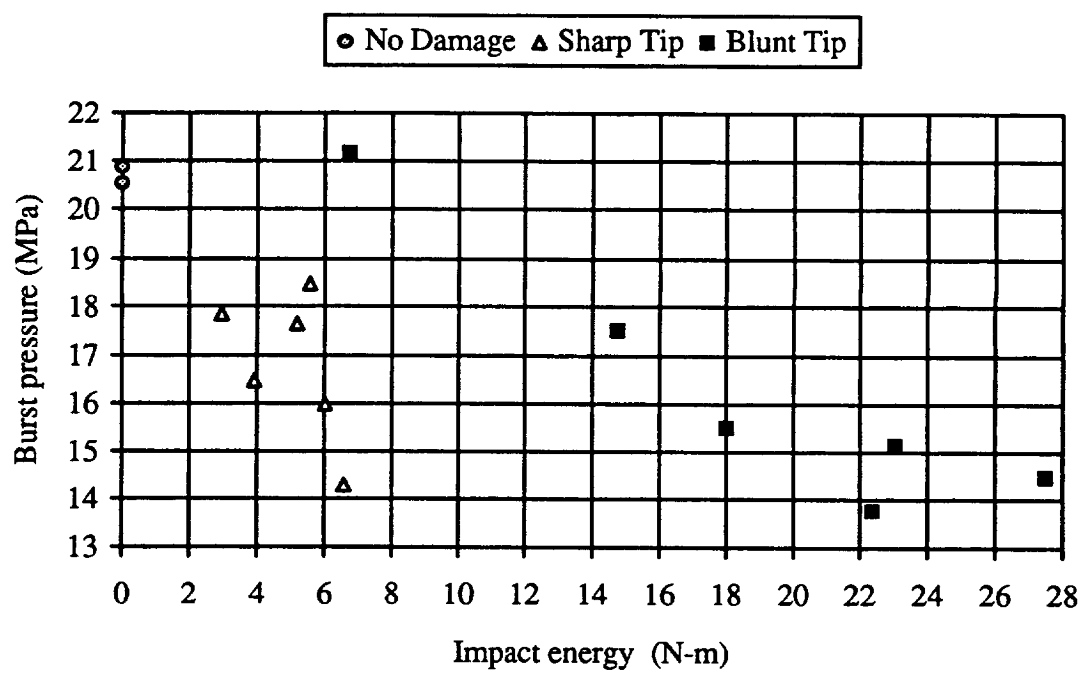

Figure 19. Burst pressure results for un-filled Kevlar/epoxy vessels.

2.7.2 Neural Network Analysis

The results of the filled vessels were similar to those of the un-filled vessels. This time though only 16 middle layer neurons were used to build the network. The best training and trial results were generated using a hyperbolic transfer function, 8% convergence criterion and by scaling the input vector to the range of 0.0 to 1.0 and the output values to between 0.0 and 0.8. Again the highest energy blunt impact produced the worst network prediction.

Bottle I.D.	Impact Status (N•m)	Actual burst (MPa)	Predicted burst (MPa)	% error
Training results				
D243-244	ST-2.942	17.84	17.80	-0.27
D231-232	ST-6.576	14.29	14.80	3.58
D185-186	NONE	20.86	19.73	-5.38
D175-176	BT-22.37	13.77	14.29	3.81
D205-206	BT-6.711	21.17	20.23	-4.45
Trial results				
D249-250	ST-5.17	17.65	17.67	0.10
D245-246	BT-18.02	15.51	16.28	5.00
Blind Test results				
D223-224	NONE	20.53	21.50	4.69
D181-182	ST-3.918	16.48	16.78	1.84
D191-192	BT-27.50	14.47	18.94	30.84
D255-256	ST-5.559	18.49	18.71	1.18

16 middle layer neurons

Table 12. Burst pressure prediction results.

2.8 CONCLUSIONS (AE)

- This research effort provides a means for quantitatively proof testing composite pressure vessels that have experienced some form of impact damage in service.

- The result of this work demonstrate that the effects of impact damage on the burst pressures of graphite/epoxy vessels can be made using a four layered back propagation neural network. Here, two 13 neuron middle layers were required to model the effects of the impact damage.

- Three layer neural network models were adequate for the Kevlar/epoxy vessels, both inert propellant filled and empty. The network architecture for the unfilled vessels included 19 middle layer neurons while the filled vessels utilized a 16 neuron middle layer. Both networks used a 51 PE input layer and a single output PE.

- The potential to scale the neural network model for a particular manufacturing process shows promise as was demonstrated on the tall graphite/epoxy vessels.

2.9 RECOMMENDATIONS (AE)

- The effects of scale on the network models needs to be addressed in greater detail by conducting scaled tensile tests and hydroburst tests of larger diameter vessels.

- The network models could be made more efficient by removing, or pruning, portions of the input vector, amplitude distribution, that had significantly smaller weights than the rest of that layer. By pruning the network the number of unknowns could be reduced when training, which often can lead to a more robust network.

- It may be possible to generate burst pressure prediction models from other parameters of the AE data. For example, the loading schedule used for this research would allow a study into correlating the Felicity ratio of the recorded AE to burst pressure.

3.0 ACOUSTO-ULTRASONICS

3.1 THEORY

Acousto-ultrasonics serves as a NDE tool by combining the technologies of AE and ultrasonics. The AU system records the response of a structure to an ultrasonic pulse, similar to that of through-transmission ultrasonics. A pulser driving an ultrasonic transducer is configured to inject a single strain wave (acoustic signal) into the structure. The signal passes through the structure and is transformed by the complex interactions of itself with the material volume and then is received by a broadband AE transducer. The parameters of the recorded acoustic signal, or event, then carries with it a fingerprint of the integrity and quality of the material between the pulser and receiver. By analyzing the frequency (power) spectrum of the received signal a correlation with the material properties and overall residual strength of the structure can often be deduced.

A stress wave factor (SWF) is defined as a measure of the received signals strength. The stress wave factor can take on many forms ranging from a simple amplitude measurement to an integration of the power spectrum. Researchers have devised many different ways to calculate the SWF for specific structural cases. For this work the energy associated with specific frequency bands of the power spectrum was chosen to represent the SWF. The SWF (waveform energy) for the inert filled graphite/epoxy vessels were computed on two intervals selected in the range from 25 to 375 kHz and 375 to 700 kHz, based on an apparent grouping in the power spectrum curves. The Kevlar/epoxy vessels were tested utilizing a system with a larger bandpass, allowing the frequency spectra be investigated up to 2.0 MHz. The 750 kHz to 1250 kHz portion of the frequency spectra provided the best resolution for measuring the extent of damage in the Kevlar/epoxy vessels and locating the ultimate failure location.

The basic requirement for a valid SWF is that it provide an indication as to the structural quality of a pressure vessel before an impact as well as be directly related to the amount of damage attained from an impact. The SWF will also be related to manufacturing variations such as voids in the resin or misaligned fibers and experimental variables including contact pressure and degree of sensor coupling.

3.2 AURES

A basic requirement for AU testing is that sensor contact pressure be uniform and that a sufficient number of measurements be made to completely map the region of interest. As described in Section 3.3, the process of taking AU measurements by hand is not only time consuming but also lacks resolution and repeatability. These problems were partially solved by developing a acousto-ultrasonic robotic evaluation system (AURES). The AURES incorporates the robotic controls from a Rhino® robot with a PC based ultrasonic measurement system to create an automated AU measurement system. With the AURES many more measurements can be made over the surface of the vessels, in less time and with more repeatability, than were done by hand. The AURES has proven to be very versatile, allowing AU mapping of drone wing panels, compressed gas container welds, powder formed impact cages as well as the pressure vessels described in this report. A schematic of the AURES configured for the 14.61 cm diameter pressure is shown in Figure 20.

The program RBTBOT.M (Appendix 6.7) controlling the AURES was written in the MATLAB working environment. MATLAB essentially works as a batch driver, allowing execution of the robot control, data acquisition and FFT programs. Robot control is facilitated through three QuickBasic executable files. The programs UPRBT.EXE (Appendix 6.8) and SPINBT.EXE (Appendix 6.9) are both position oriented programs not requiring feedback from the load cell. UPRBT simply lifts the sensor pair two inches after each measurement, while the program SPINBT steps the bottle through 40 equally spaced angular (9° each) positions. The third program, DOWNRBT.EXE (Appendix 6.10), works in conjunction with a load cell to ensure that contact pressure remains constant for each measurement. The ultrasonic receiver of the AURES is instrumented with a Omega Engineering, Inc. subminiature LCK series 1 kg capacity compression type load cell. A balance beam type arm is adjusted so that the same contact pressure is also applied to the pulse transducer. The load cell output is feed to an instrumentation amplifier (1000x gain) which intern is input to one side of a comparator. The other side of the comparator is regulated by a simple voltage divider so that the load (voltage) from the load cell can be used to turn the comparator on and off. The electronic circuit and calibration procedures are given in Appendix 6.11 and 6.12. The DOWNRBT program moves the robot arm down until it either reaches its travel limit or compresses the load cell enough to trip the comparator and shut itself "the robot" down. The procedures for running the AURES are presented in Appendix 6.13.

The AU signal is recorded by a Digital Wave broadband receiver. The signal is amplified by a Digital wave PA2040G 40 dB preamplifier powered by a 28 volt DC supply. The input signal is generated by a Harrisonic 1.0 MHz (1.27 cm diameter) ultrasonic sensor driven by a Panametrics pulser/receiver unit. The signals are recorded by a Physical Acoustics Corp. (PAC) A/D board running in a 90 MHz Pentium PC. The A/D is configured to digitize the waveforms with a 32 MHz sampling rate over 4096 points or 128 μs window.

A summary of the AURES instrumentation system is provided in Figure 21. The vessel cradle and sensor holders are described in more detail in Appendix 6.15 through 6.17.

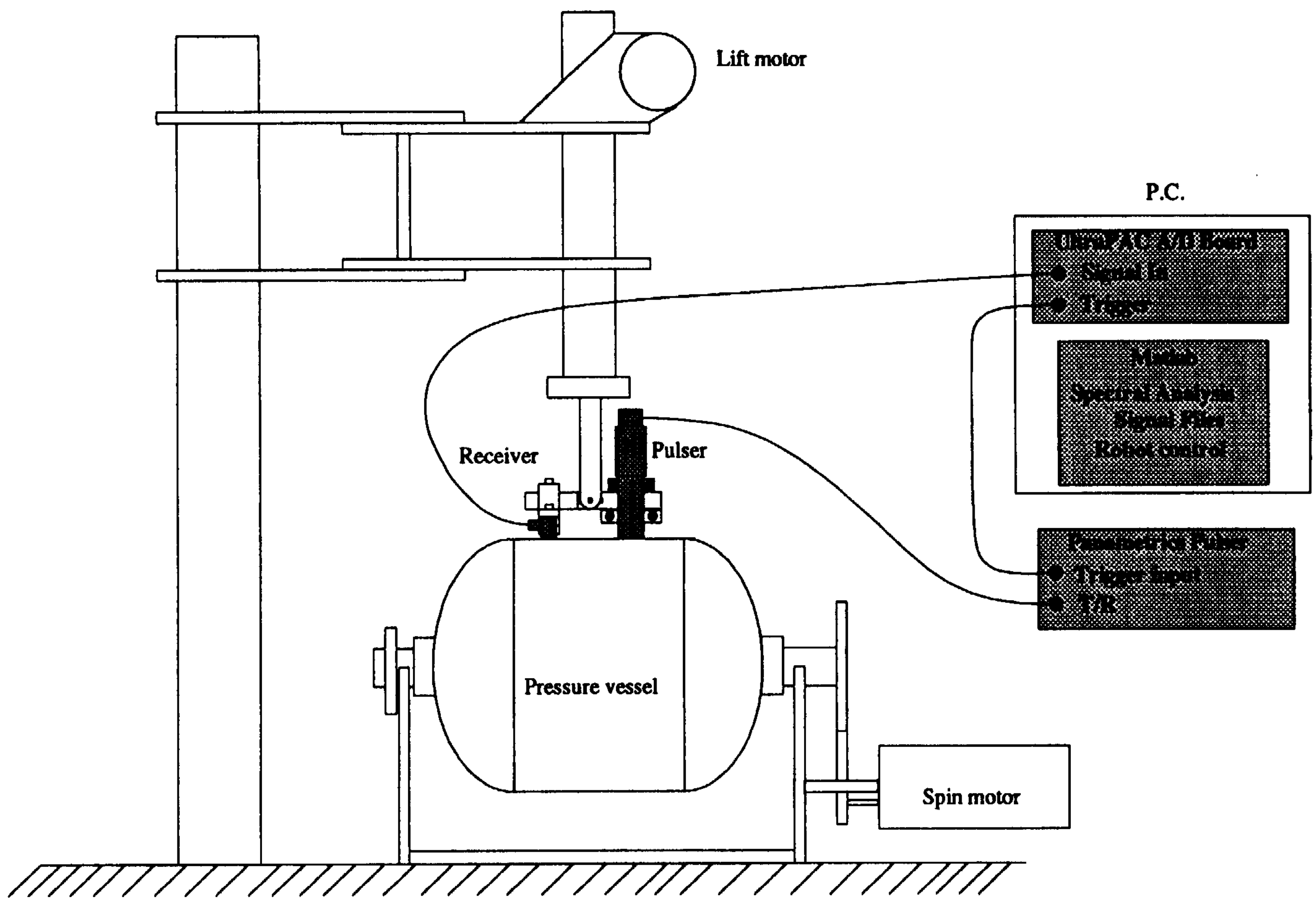

Figure 20. The AURES.

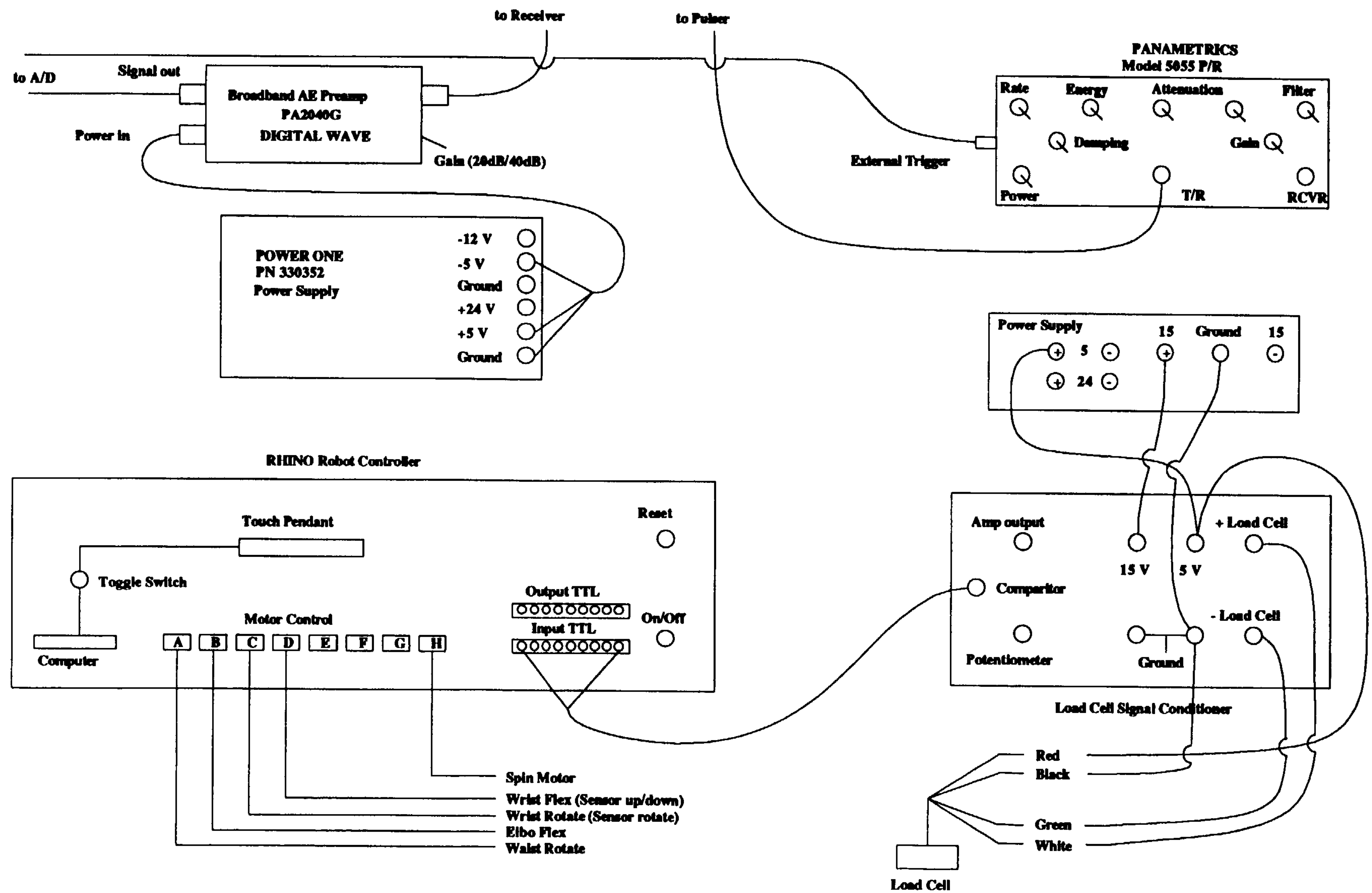

Figure 21. AURES instrumentation.

3.3 INERT FILLED GRAPHITE/EPOXY 14.61 CM DIAMETER VESSELS

The AURES was not completed at the time the first of the filled graphite/epoxy vessels were scheduled for hydroburst. Instead, an AU system was assembled to map the inert filled graphite/epoxy vessels by combining a standard ultrasonic pulser and AE recording system. The heart of the AU system was a PAC SPARTAN AE system which measured and stored the AE signal parameters as well as the signal waveform. A PAC model WDI (100 to 1000 kHz) broadband receiver was used to record the response of the material to an ultrasonic pulse generated by a Harrisonic 500 kHz ultrasonic transducer driven by a Panametrics model 5055PR pulser. The receiver and pulser were coupled to the surface using Sonotrace ultrasonic couplant. The pulser was triggered by a signal from a Wavetek Pulse/Function generator so as to generate a single waveform. The AU system is shown in Figure 22.

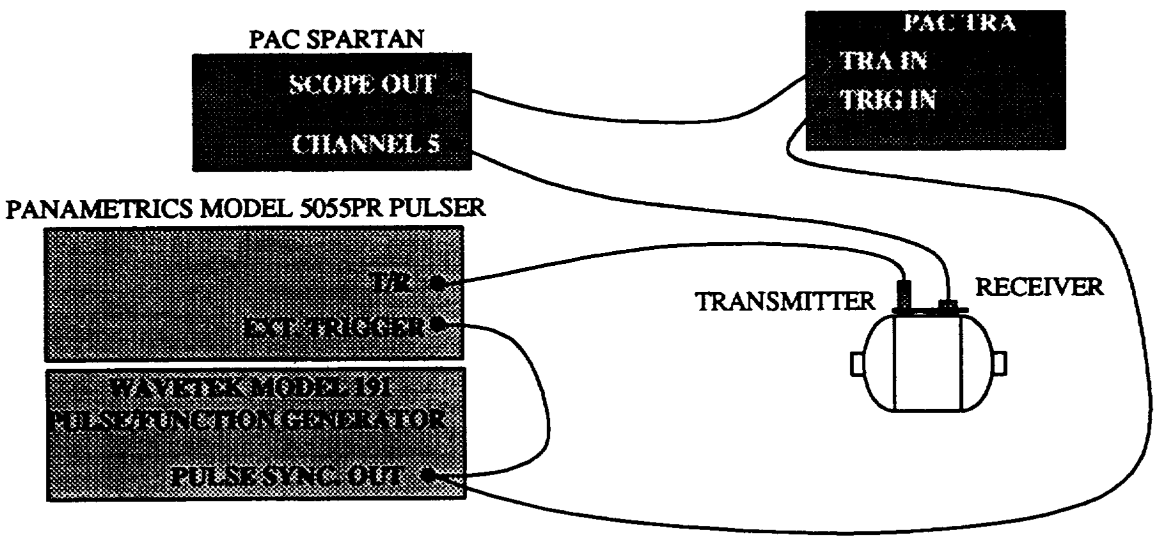

Figure 22. Acousto-Ultrasonic system schematic.

Twelve graphite/epoxy vessels (Table 13) were mapped with this system to determine the extent of damage in the impact zone. Measurements were taken by hand along and perpendicular to the hoop fiber direction for these twelve bottles. The power spectrum and resulting spectral energy were tabulated for each acoustic signal. The energy was then plotted versus bottle location as a test of the AU system to quantify the extent of impact damage.

Transducer spacing and contact pressure is often a problem associated with AU measurements. To help overcome these problems two simple holders were constructed from 0.635 cm thick Plexiglas providing a means to both position the transducers relative to each other and press them to the structure. A simple flat holder (Figure 23) was used for making measurements perpendicular to the hoop direction while a hinged version (Figure 24) was constructed for making measurements around the hoop direction of the vessel. A two pound (8.9 N) steel weight was bonded to each holder to provide the required constant contact pressure. The holders were designed to maintain a 3.81 cm sensor spacing.

Fabrication number	Bottle I.D.	Resin type	Impact status (N•m)
92PV005	C069-070	3501-6	BT-6.78
92PV005	C077-078	3501-6	BT-10.98
92PV003	A013-014	3501-6	ST-1.63
92PV003	A017-018	3501-6	ST-3.53
92PV007	C141-142	977-2	BT-6.78
92PV007	C117-118	977-2	BT-10.98
92PV007	C131-132	977-2	ST-1.63
92PV007	C155-156	977-2	ST-3.53
92PV001	A029-030	8553-45	BT-6.78
92PV001	A047-048	8553-45	BT-10.98
92PV006	C087-088	8553-45	ST-1.63
92PV006	C093-094	8553-45	ST-3.53

Table 13. Graphite/epoxy vessels mapped by acousto-ultrasonics.

The recorded AU signals were first converted to ASCII format through the PAC program TRA2DAD.EXE (Appendix 6.18). This program generates a data file consisting of a seven line header followed by a sequential string of values representing the digitized waveforms. For this work the sampling rate was set at 16 MHz for a total of 8192 points, a 512 μs window. The ASCII data file is then run through the BASIC program "TRA2MLAB.BAS" which eliminates the header and puts the file into MATLAB format. The program "ENGYDATA.M" (Appendix 6.19) is executed by MATLAB to compute the power spectra and resulting energy for the two frequency bands (25 to 375 kHz and 375 to 700 kHz). Finally, the energy table from MATLAB is processed by another BASIC program "OUTPUT.BAS" (Appendix 6.20) which computes the average of the readings for one position and orders the data into a convenient form.

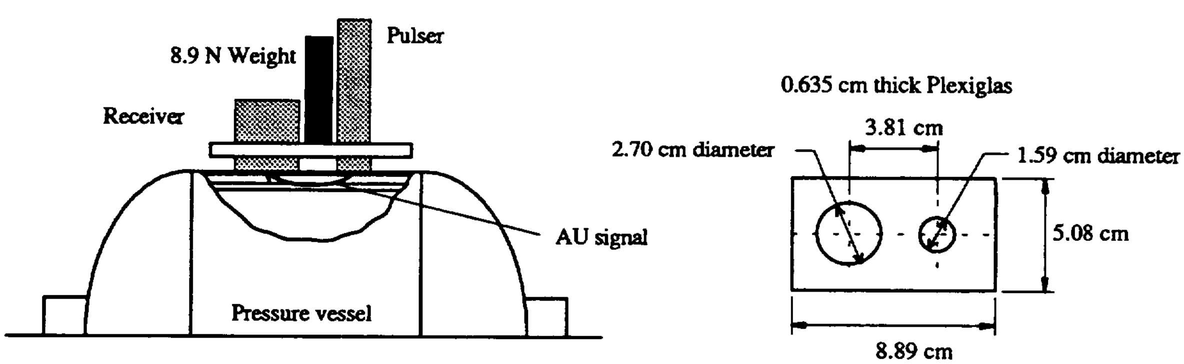

Figure 23. Flat transducer holder.

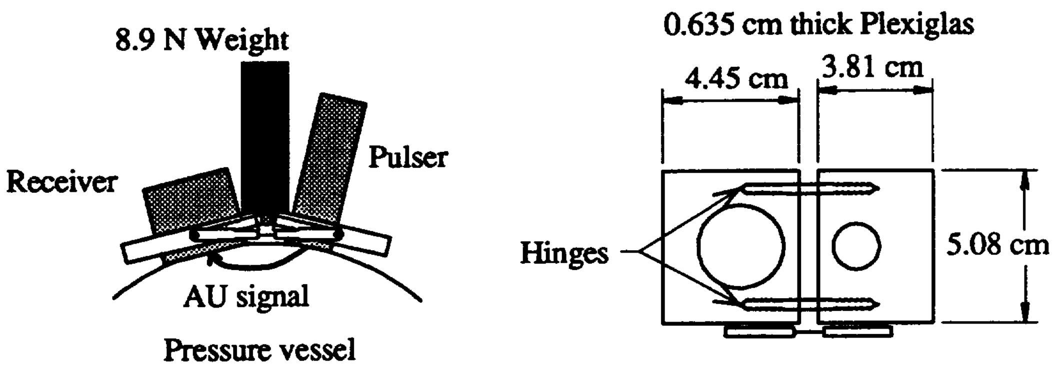

Figure 24. Hinged transducer holder.

3.3.1 Data Summary

Three measurements were made at each sensor position in an attempt to reduce the effects of contact pressure variations and local surface roughness on the data set. For the longitudinal direction, measurements were taken on 2.54 cm circumferential spacing in the vicinity of the impact point and 5.08 cm spacing elsewhere (Figure 25). Three sets of measurements were taken at each circumferential position (top, middle, bottom) to measure the extent of damage along the length of the vessels.

The AU signal was also taken from top to bottom along the hoop region in the damage zone. Here, AU measurements were taken at seven positions spaced 1.27 cm apart through the impact point (Figure 26). Again three measurements were taken at each location and averaged.

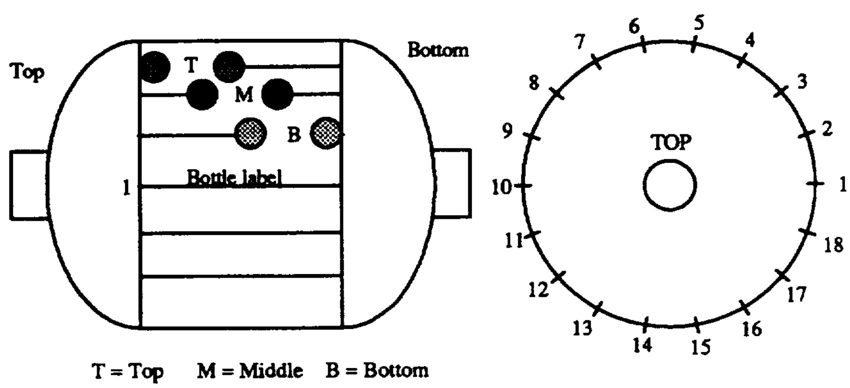

Figure 25. Bottle position and sensor locations for longitudinal measurements.

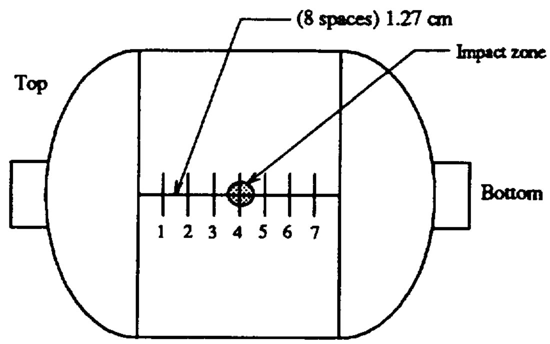

Figure 26. Hoop data transducer positions.

3.3.2 Energy/Location Plots and Discussion

The results presented in Figures 27 through 38 depict the average partitioned energies for each hoop and middle circumferential position. The top and bottom energy values have been omitted from the circumferential measurement graphs as they provided no additional information. A open circle indicates the impact point for the circumferential measurements. The impact point for the hoop direction is always at position number four.

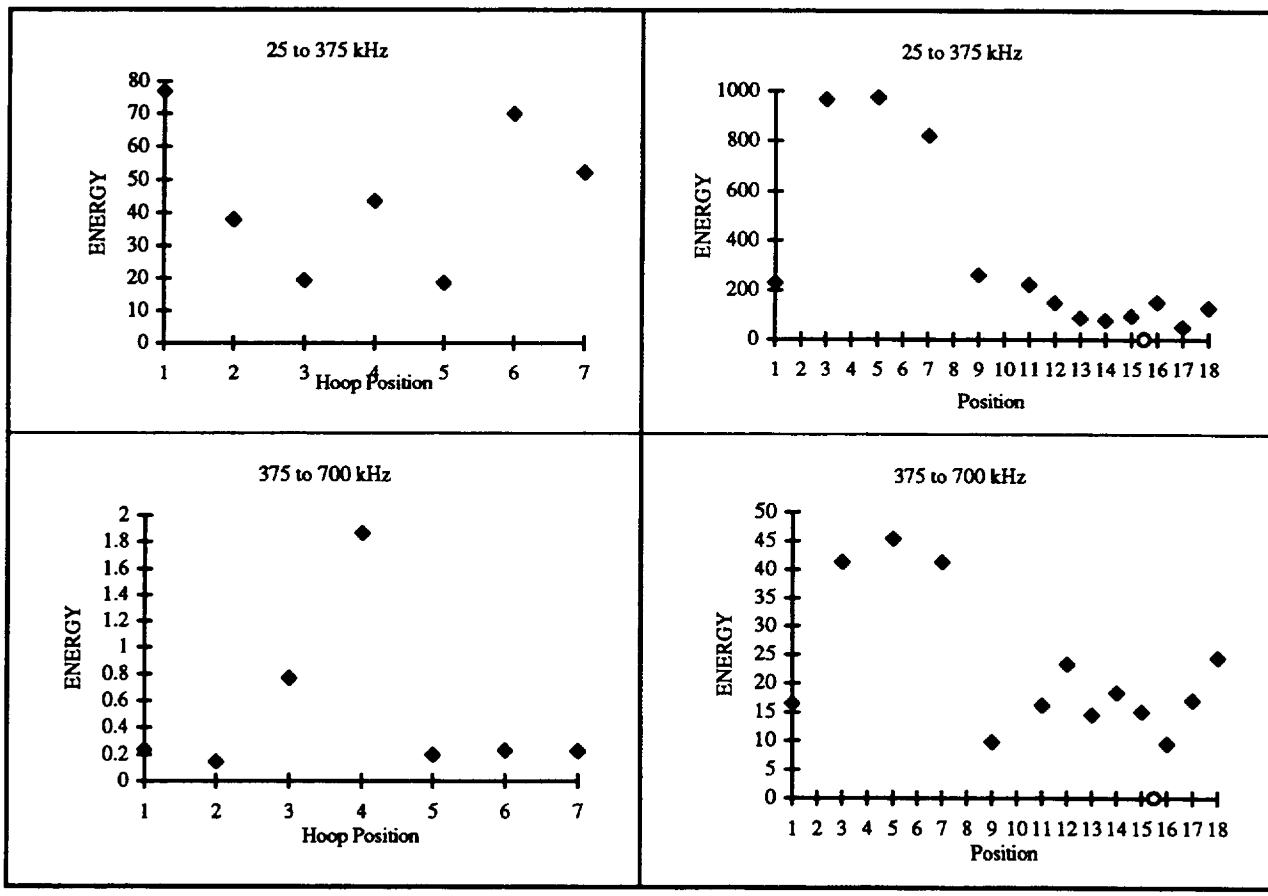

Figure 27. Energies for vessel A029-030 (8553-BT-6.78 N•m).

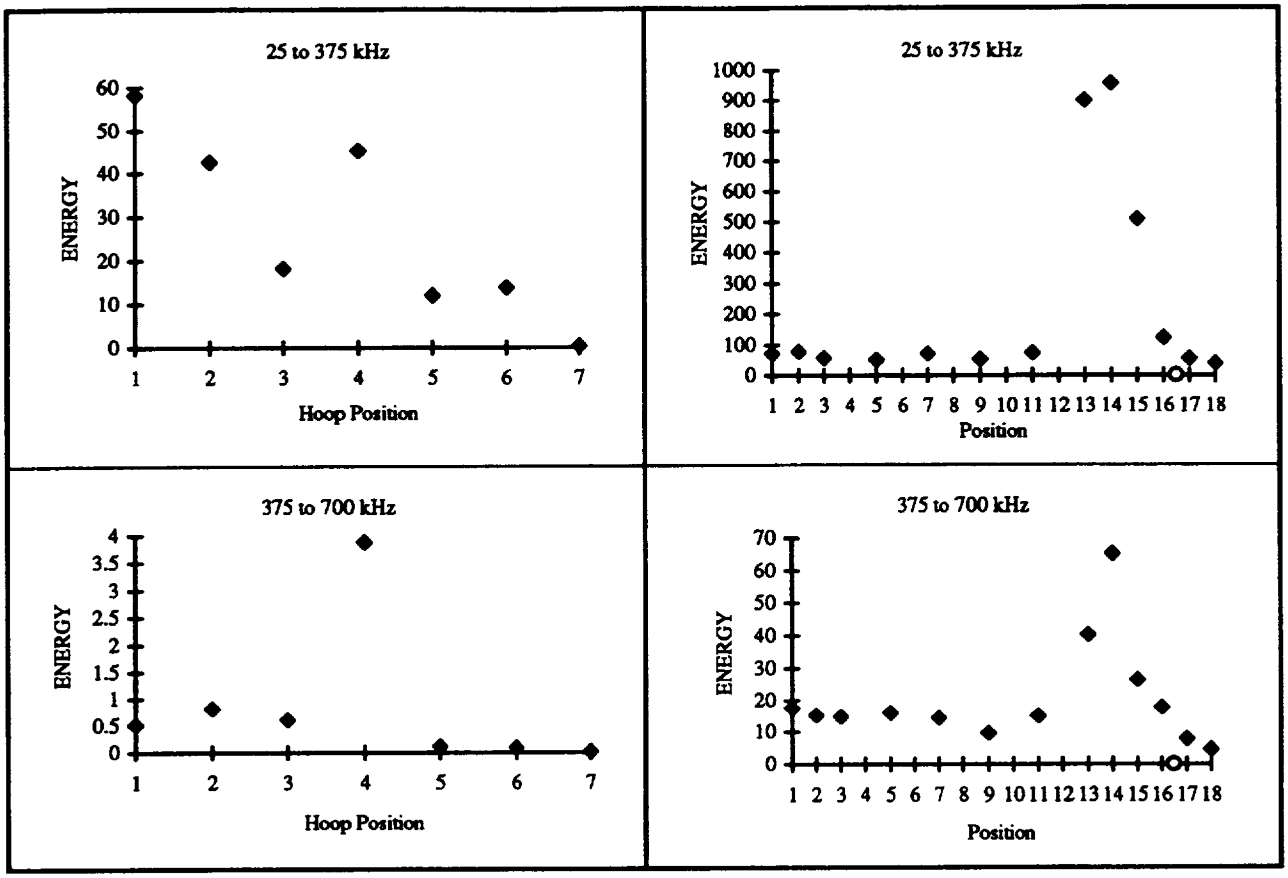

Figure 28. Energies for vessel A047-048 (8553-BT-10.98 N • m).

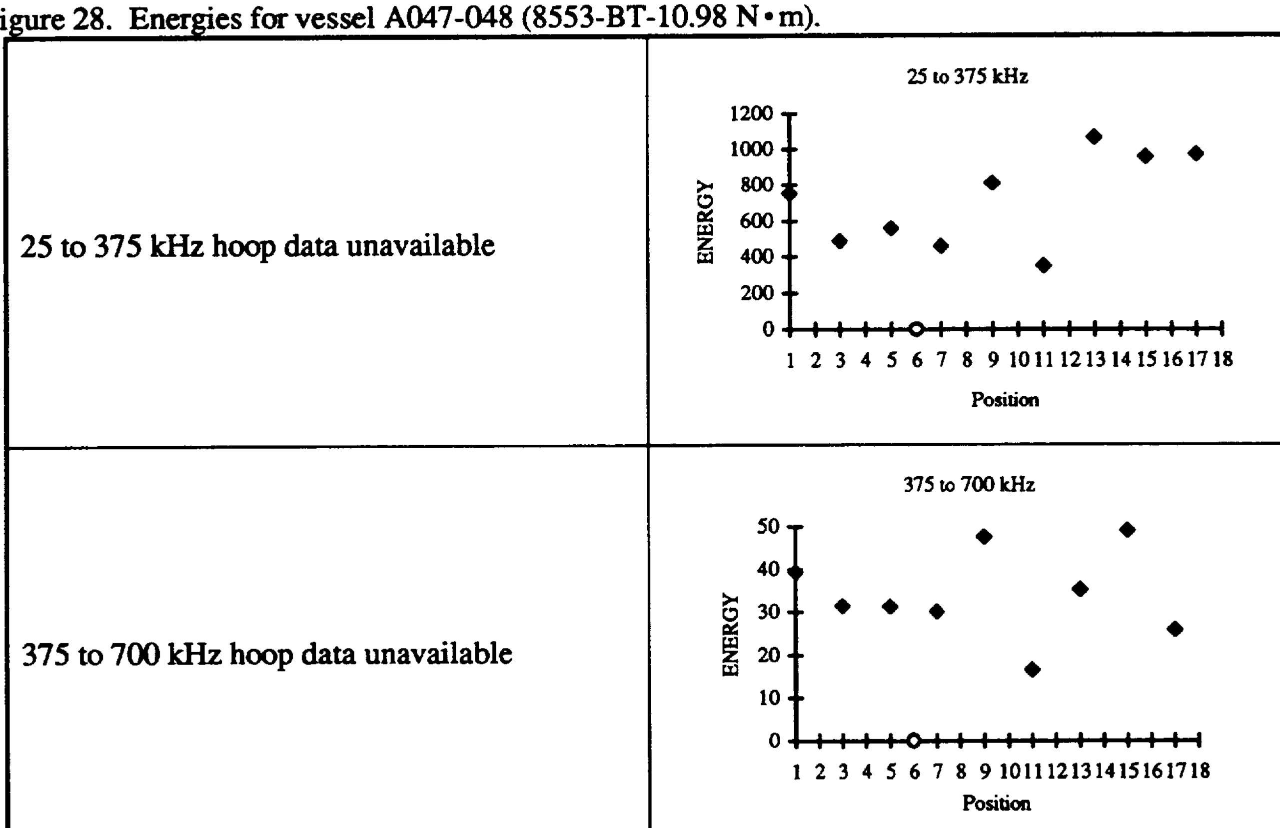

Figure 29. Energies for vessel C087-088 (8553-ST-1.63 N • m).

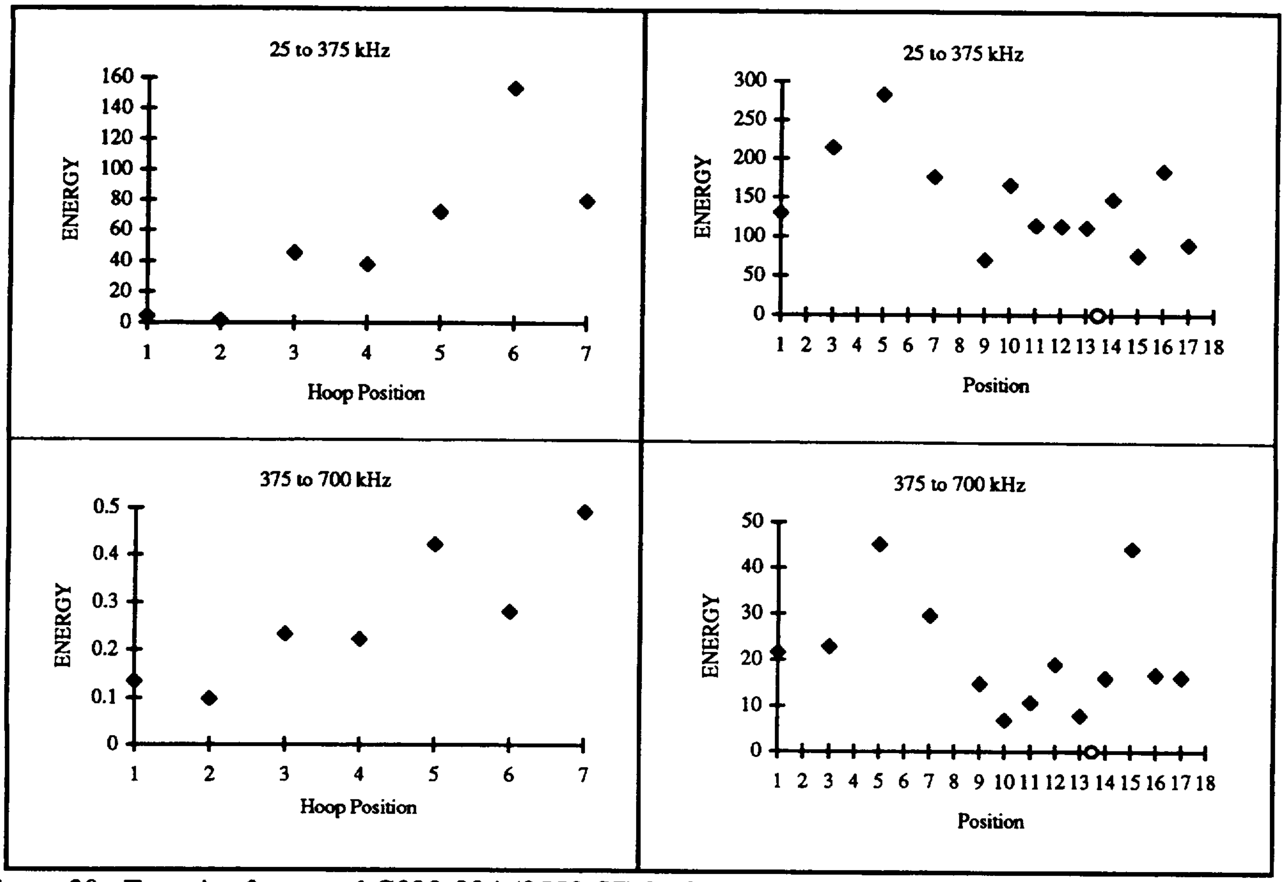

Figure 30. Energies for vessel C093-094 (8553-ST-3.53 N•m).

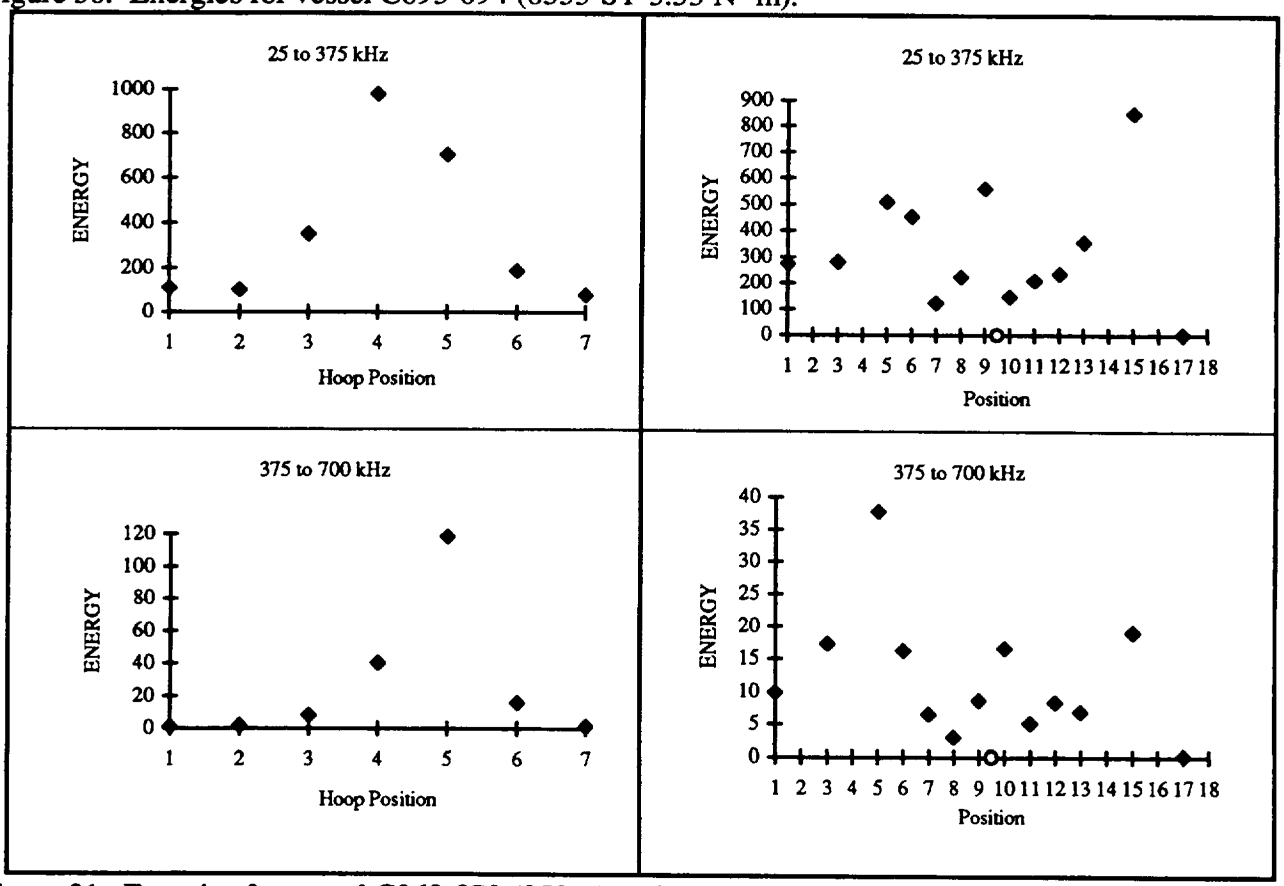

Figure 31. Energies for vessel C069-070 (3501-BT-6.78 N•m).

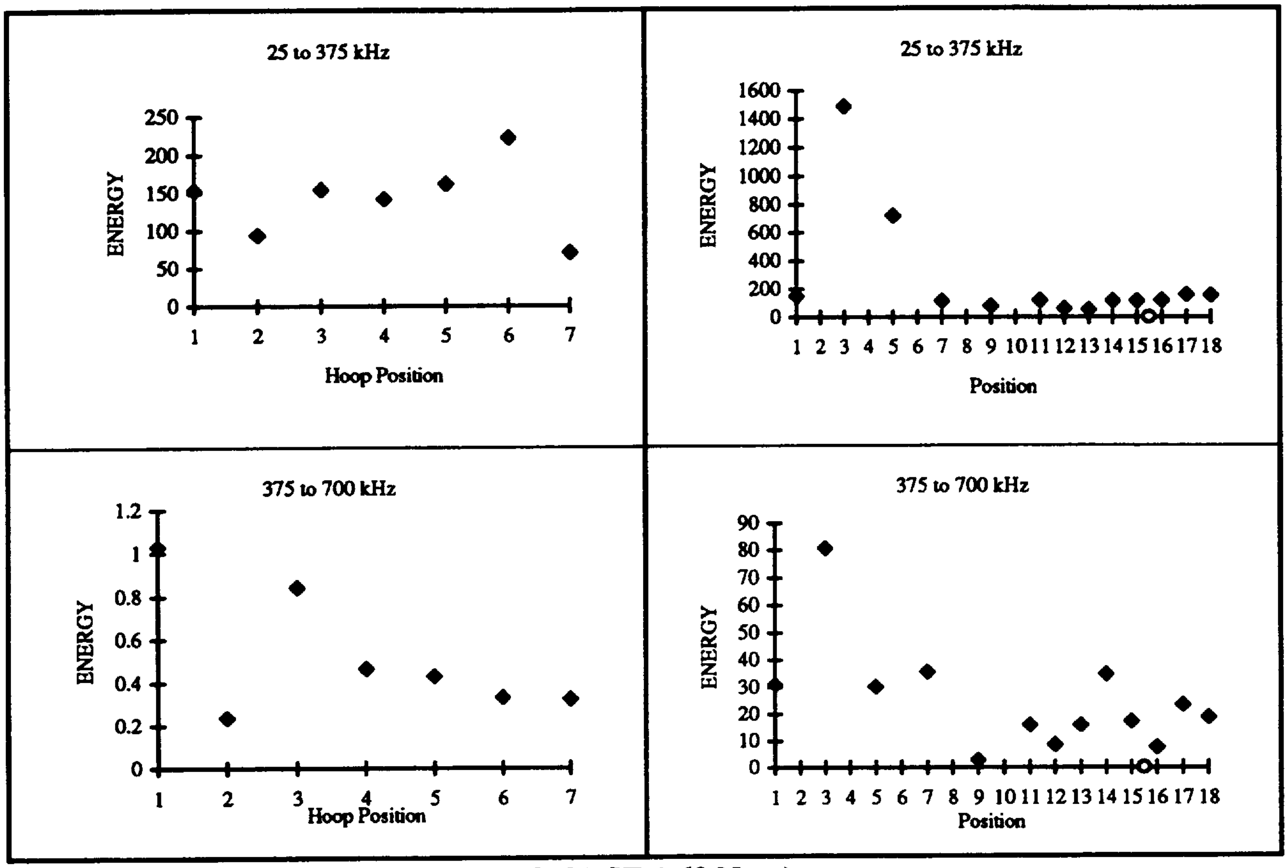

Figure 32. Energies for vessel A013-014 (3501-ST-1.63 N•m).

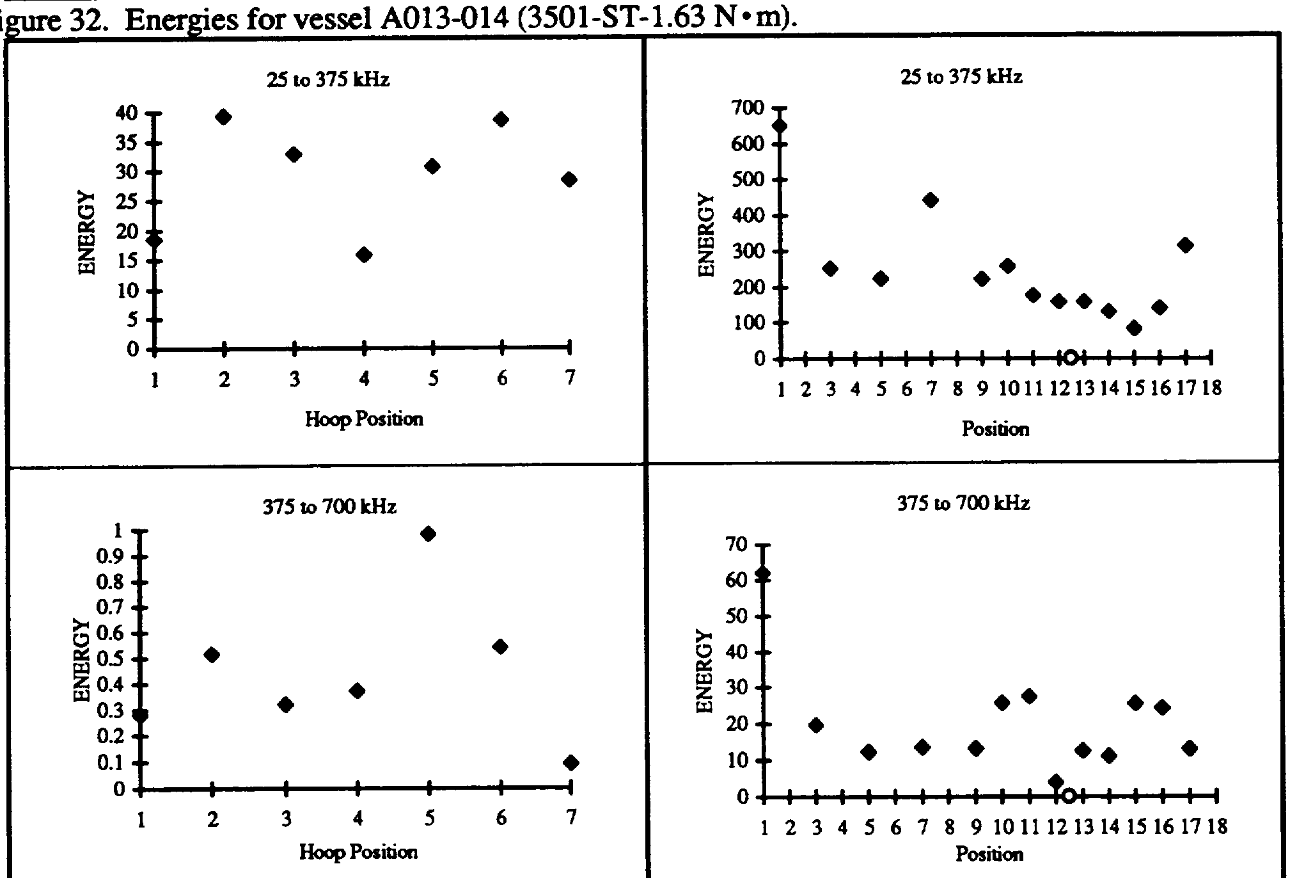

Figure 33. Energies for vessel A017-018 (3501-ST-3.53 N•m).

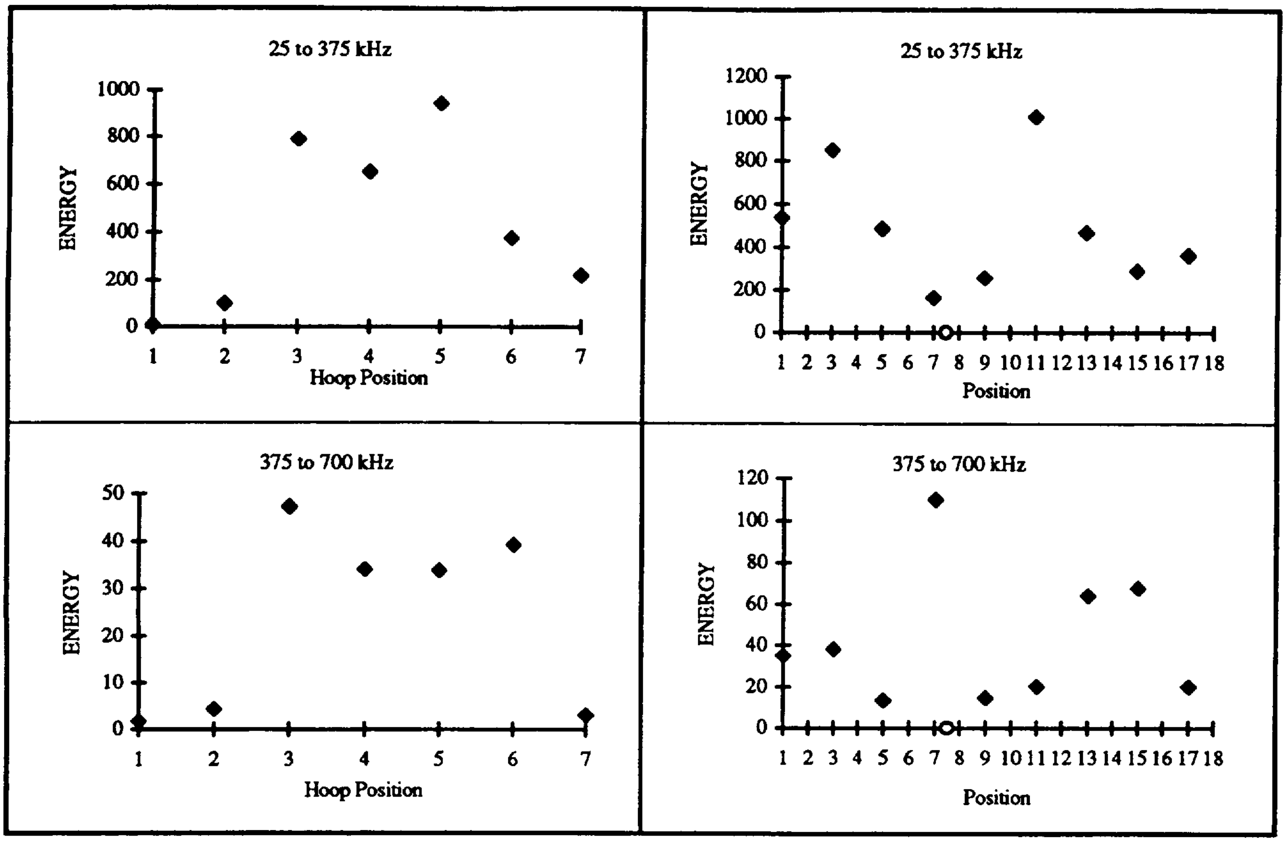

Figure 34. Energies for vessel C077-078 (3501-BT-10.98 N•m).

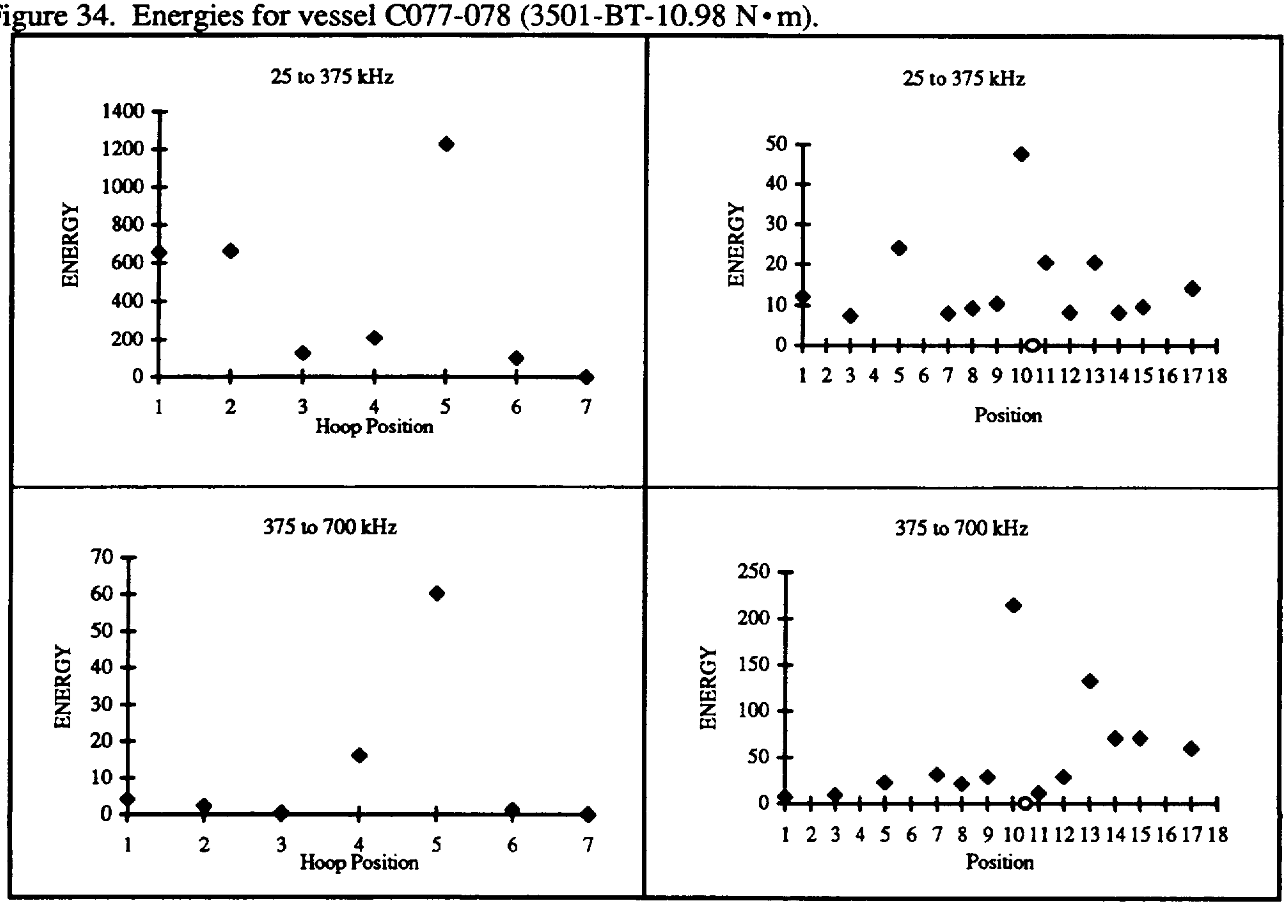

Figure 35. Energies for vessel C117-118 (977-BT-10.98 N•m).

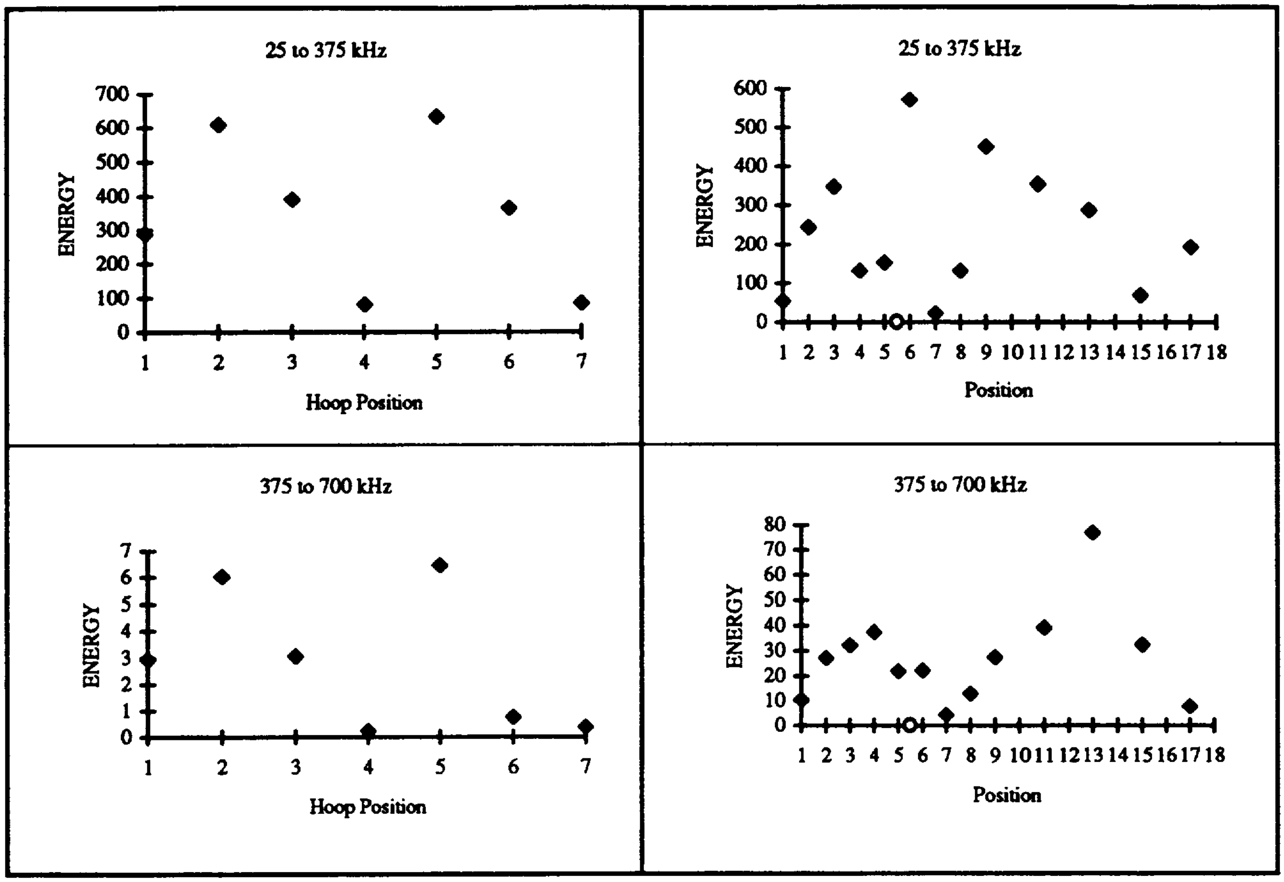

Figure 36. Energies for vessel C131-132 (977-ST-1.63 N•m).

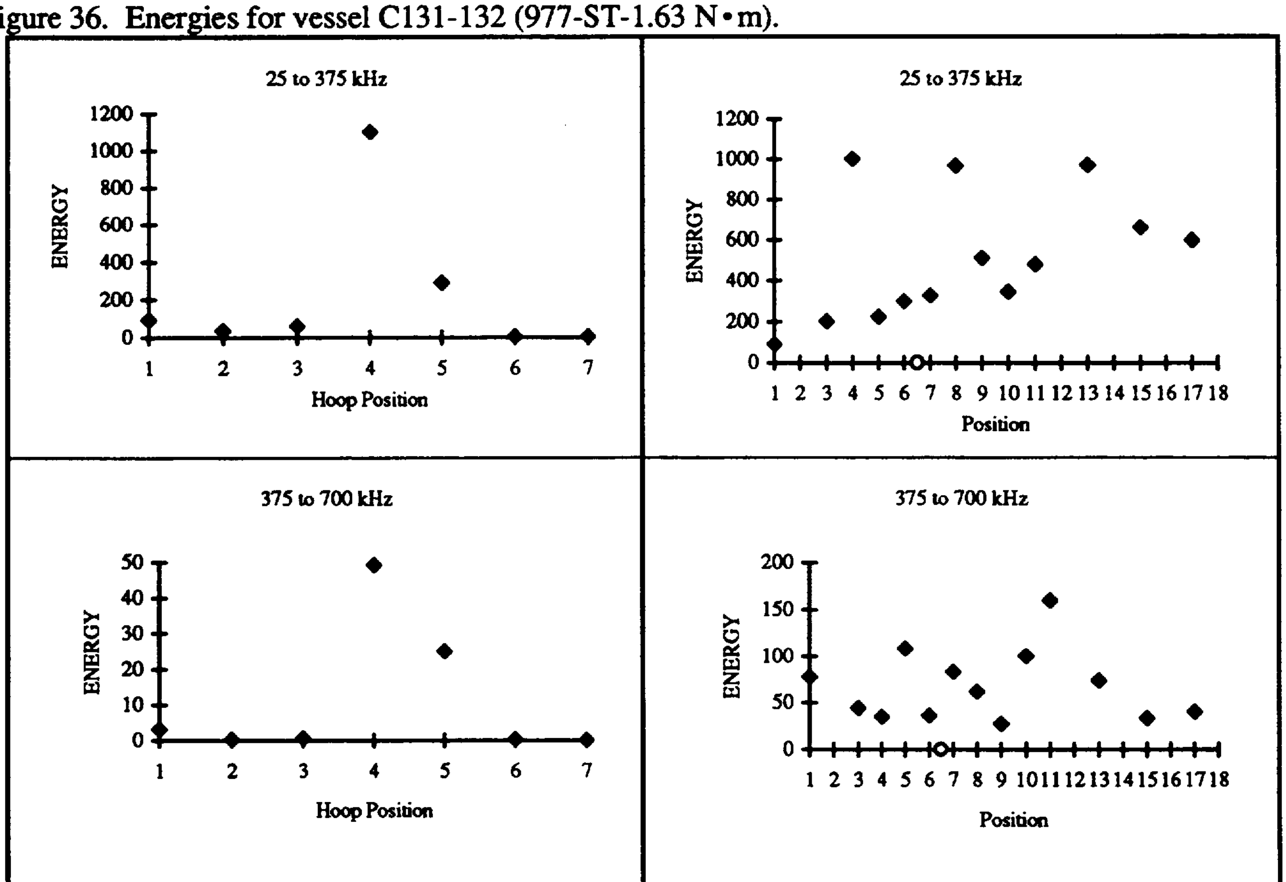

Figure 37. Energies for vessel C141-142 (977-BT-6.78 N•m).

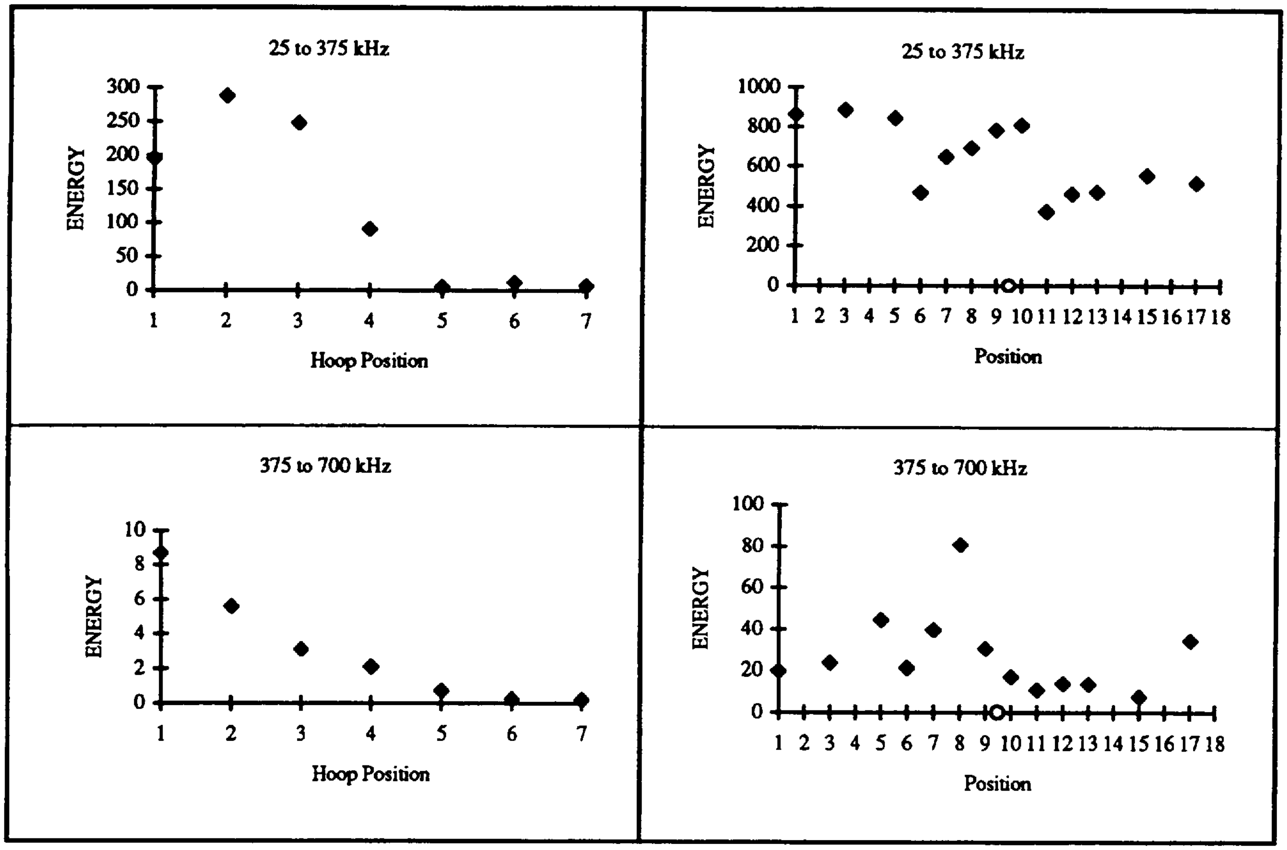

Figure 38. Energies for vessel C155-156 (977-ST-3.53 N•m).

The energy bands selected for this preliminary study did not provide an adequate SWF for identifying the impacted regions of the pressure vessels. In general, the energy values for the circumferential measurements tended to decrease in the damage zone while the hoop energy values tended to increase at the impact point. Overall, no conclusive trends could be found in the energy profiles to establish a measurement of the impact position or severity.

There were two major sources for the inability of this AU system to detect the flawed regions. First, a high degree of surface roughness and curvature combined with a large sensor contact area lead to poor couplant repeatability. The individual values used to compute the averages produced variations greater than 100% in some cases. Wave guides were constructed from brass and Plexiglas to reduce the footprint of the transducers in an attempt to help reduce the problem of local surface roughness. The combined attenuation of the wave guides and the bottles reduced the already weak AU signal to an impractical level though, such that the background noise dominated the power spectrum. Figure 39 illustrates the wave guides that were constructed for the study.

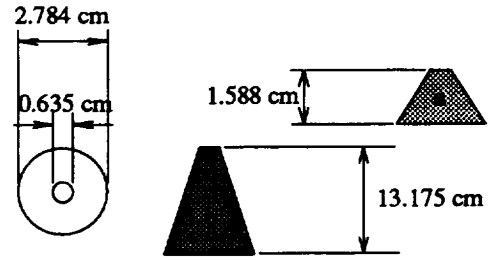

Figure 39. Wave guides.

The second reason that the system was not able to detect the damage zone was that the AU signal had to pass through a "filtered" channel board of the AE system before it could be stored by the TRA system. This meant that the 100 to 300 kHz bandpass filter located on the channel board would block some if not all of the high frequency information of the AU signal. Since the signal was already weak due to the attenuation of the pressure vessel, very little of the high frequency components were recorded. The damage detection threshold of an AU system is directly related to the frequency of the transmitted signal. A small crack or discontinuity acts as a low pass filter, blocking high frequency components of the signal. The lower frequency components will pass through a damaged region with little or no effect to its attenuation while higher frequencies will be blocked by the damage. Therefor, since what is being measured by an AU system is the variation in the signals characteristics from on location on the structure to another, if the higher frequencies are attenuated by the recording system no variations will be measured. The amount that a signal will be attenuated by the filter can be seen in the amplitude frequency response of the channel board shown in Figure 40.

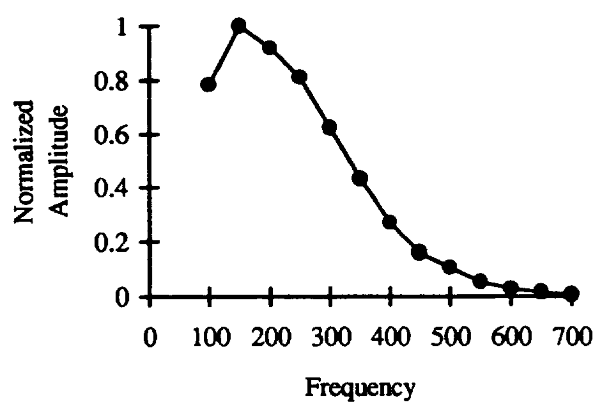

Figure 40. Amplitude frequency response of SPARTAN system.

The problems encountered with this preliminary work led to the development of the AURES. The AURES eliminates virtually all of the sensor contact repeatability and tedium problems found when taking measurements by hand. The ultrasonic receiver used with the AURES (0.635 cm diameter) is less effected by surface roughness than the 2.54 cm diameter WDI sensor. By using load cell feedback consistent pressure could be maintained for each measurement with the AURES. Also, the bandwidth of the AURES permits frequency analysis up to 2 MHz, which greatly enhances the potential of the AU signal analysis.

Two inert filled graphite/epoxy vessels were mapped using the AURES system (Table 14). Two hundred measurements were taken over forty equally spaced circuferential positions (5 measurements per position) to map the damage state of the vessels. The results are presented in Figures 41 and 42.

Fabrication number	Bottle I.D.	Resin type	Impact status
92PV003	A007-008	3501-6	ST-2.85 N•m.
92PV001	A033-034	8553-45	BT-6.78 N•m

Table 14. Graphite/epoxy vessels mapped by acousto-ultrasonics.

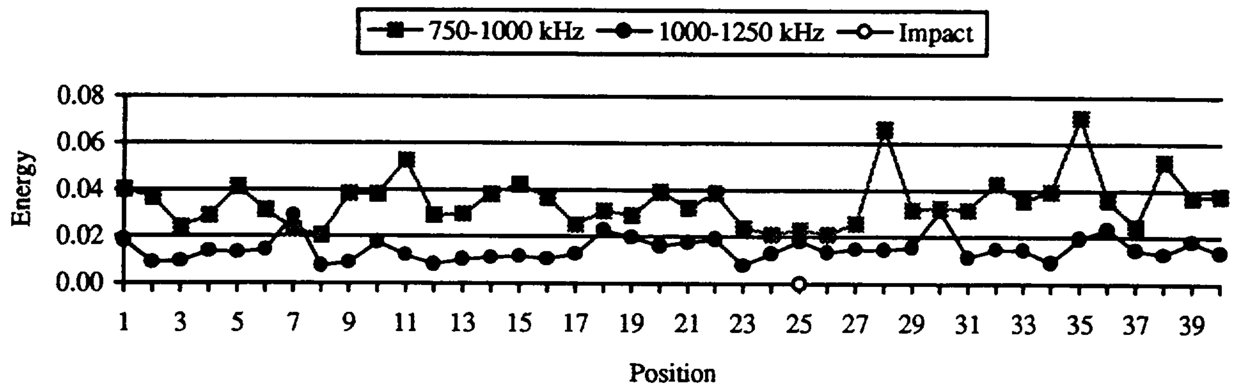

Figure 41. Energies for vessel A007 - Sharp Tip 2.85 N•m.

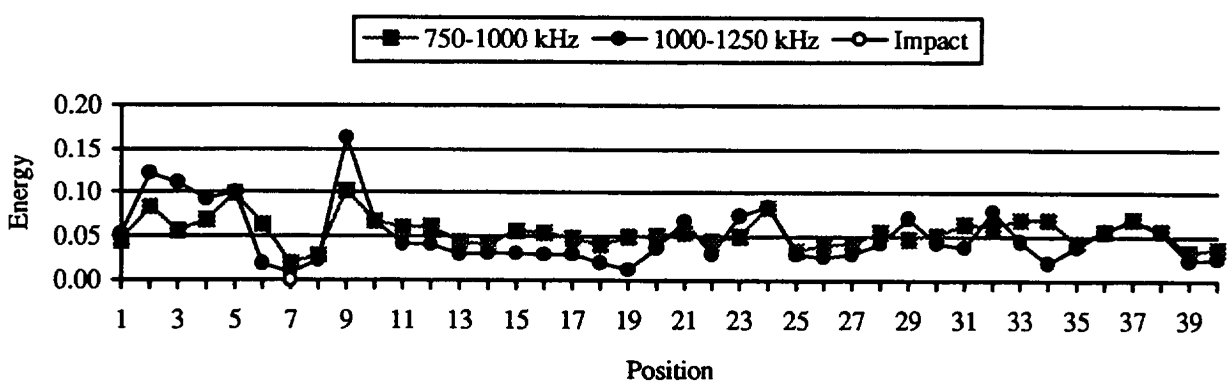

Figure 42. Energies for vessel A033 - Blunt Tip 6.78 N•m

The energy computed from the 750 to 1000 kHz frequency interval showed the same trend as was found using the hybrid AE/ultrasonic system. That is, the AU energy associated with the damage zone is less than that of the remaining vessel. To a lesser degree, the 1000 to 1250 kHz zone could also be used to locate damage. It is interesting to note that a second region of lower energy is found nearly 180° from the impact site. Although, the energy reduction is not as great, the results indicate that secondary damage may exist. This damage may be a side effect of the way the vessels were cradled during impact, with the cradle-vessel contact producing some damage at impact.

3.4 INERT FILLED KEVLAR/EPOXY 14.61 CM DIAMETER VESSELS

The AURES was used to AU map 13 inert propellant filled vessels featuring various levels of impact energies. A Harrisonic 1.0 MHz pulser injected the ultrasonic energy into the vessel while a Digital Wave broadband receiver recorded the AU signal. The sensors were spaced two inches apart along the longitudinal axis of the vessels and were centered on the bottles length. A thin bead of Soundsafe ultrasonic couplant was applied around the vessels in the path of the sensors and a 31.03 kPa (0.25 volt) contact pressure was set into the comparator. The pulse energy of the Panametric pulser unit was set to 4 (400 volt).

3.4.1 Data Summary

The vessels are identified in Table 15 along with the impact locations, AU code and impact status. The AU code references the filename given to each test so that the individual vessel data sets can be located on the storage diskettes. The impact locations provide the approximate center of the impact point. When three digits are given the impact point is nearly centered on the middle digit, while two digits implies that the impact point is centered between those values.

Bottle I.D.	Impact Location	Test date	AU test code	Impact Status (N•m)
D249-250	7-8-9	4-17-95	I	ST-5.18
D231-232	37-38	4-17-95	J	ST-6.58
D181-182	37-38	4-17-95	K	ST-3.92
D223-224	none	4-9-95	N	none
D191-192	5-6-7	4-9-95	O	BT-27.5
D205-206	8-9-10	4-9-95	P	BT-6.71
D245-246	35-36	4-9-95	Q	BT-18.02
D175-176	6-7	7-31-95	U	BT-22.37
D185-186	none	8-1-95	W	none
D255-256	3-4	7-31-95	X	ST-5.56
D257-258	4-5	8-1-95	Y	BT-14.78
D159-160	33-34	10-25-95	AB	ST-5.31
D219-220	27-29-31	10-25-95	AD	BT-20.39

BT = Blunt Tip (0.5 inch) ST = Sharp Tip (1 mm)

Table 15. Inert filled vessel AU data summary.

3.4.2 Energy/Location Plots and Discussion

The spectral energies were computed over eight, 250 kHz, intervals, from nearly DC up to 2.0 MHz. Of these bands, the 750 kHz to 1000 kHz and 1000 kHz to 1250 kHz bands provided the best resolution to measure the extent of the impact damage. Typical signals and their power spectra are given in Figure 43 for a damaged and undamaged zone. The results of the AU analysis are presented in Figures 44 through 56.

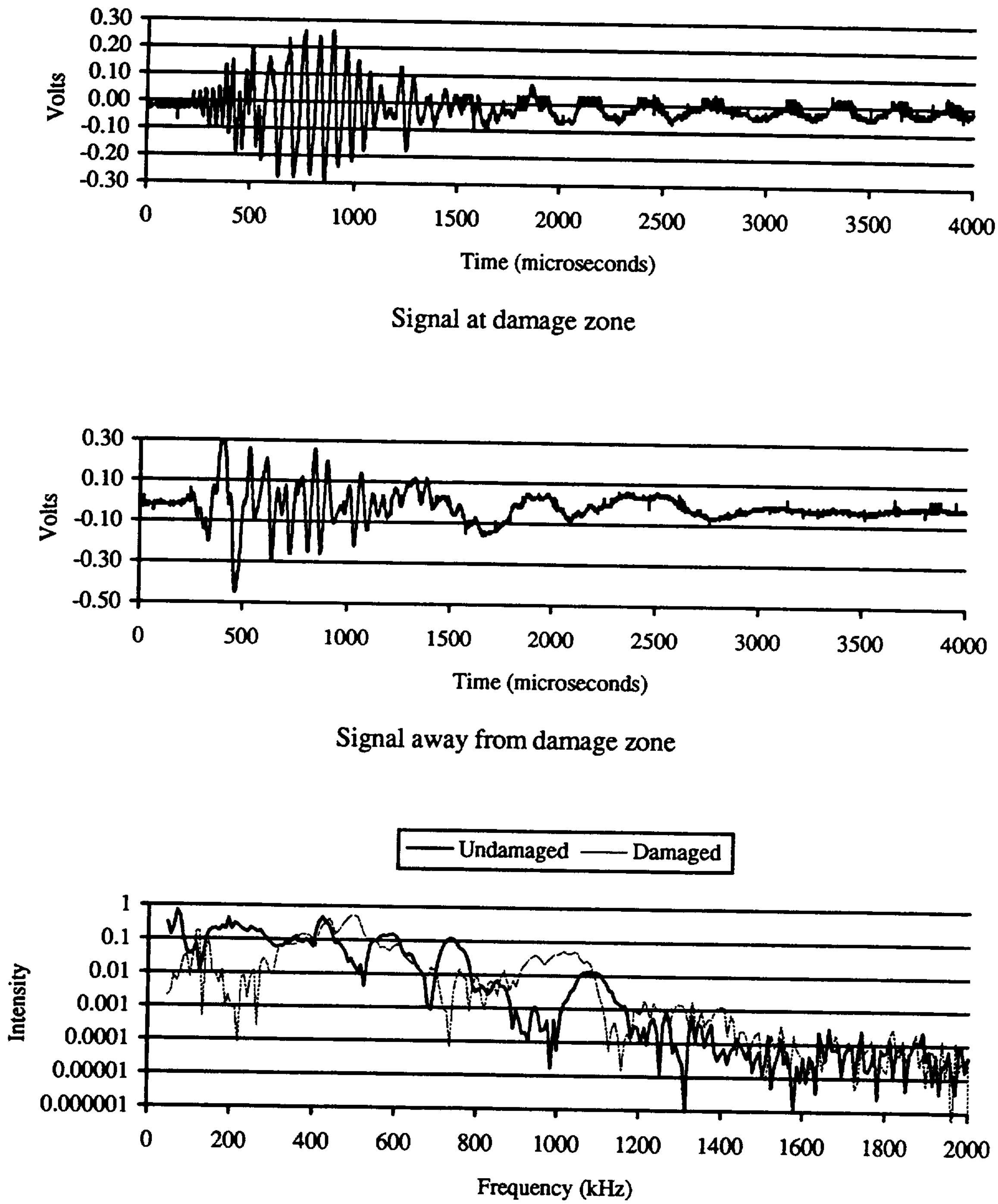

Figure 43. Signal variations between damaged and undamaged zones.

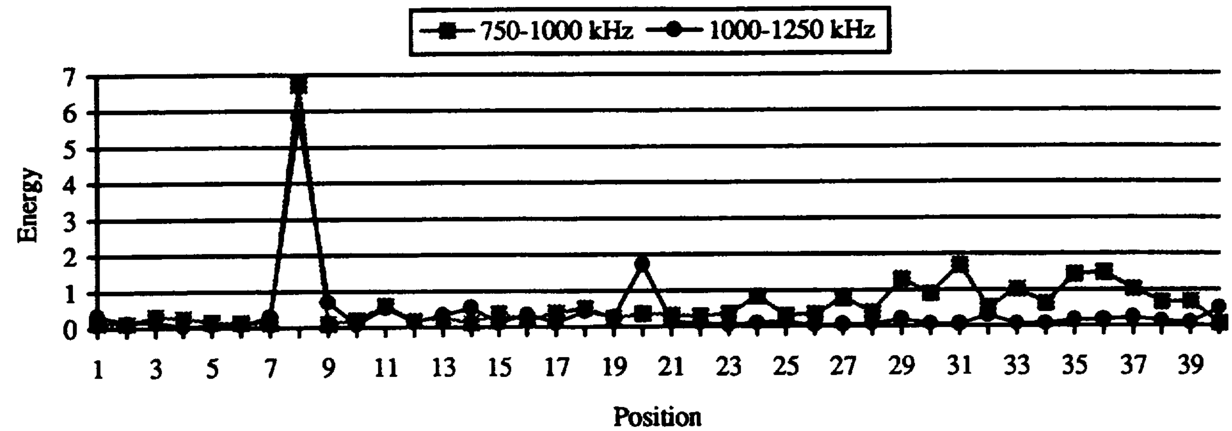

Figure 44. Energies for vessel D249 - Impact at position 8 - Sharp Tip 5.18 N • m.

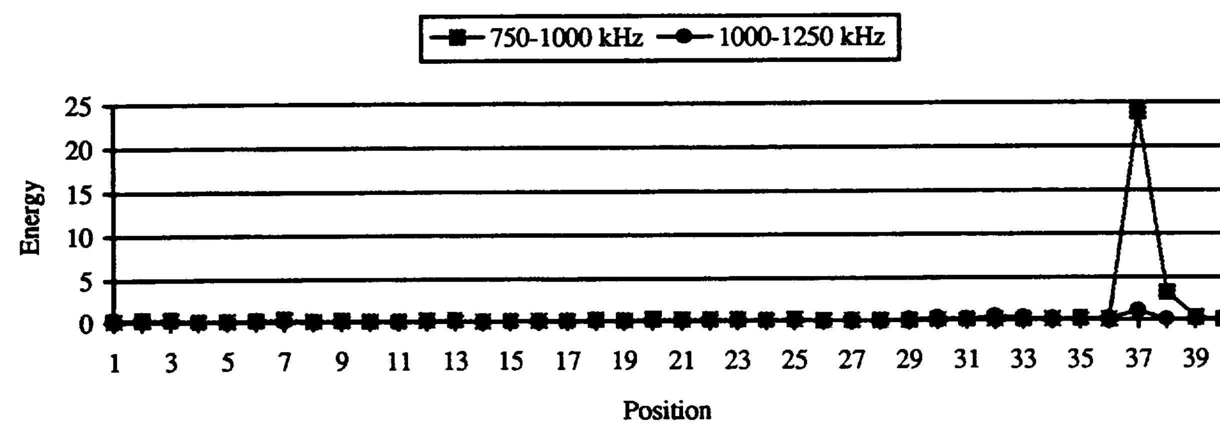

Figure 45. Energies for vessel D231 - Impact at position 37.5 - Sharp Tip 6.58 N • m.

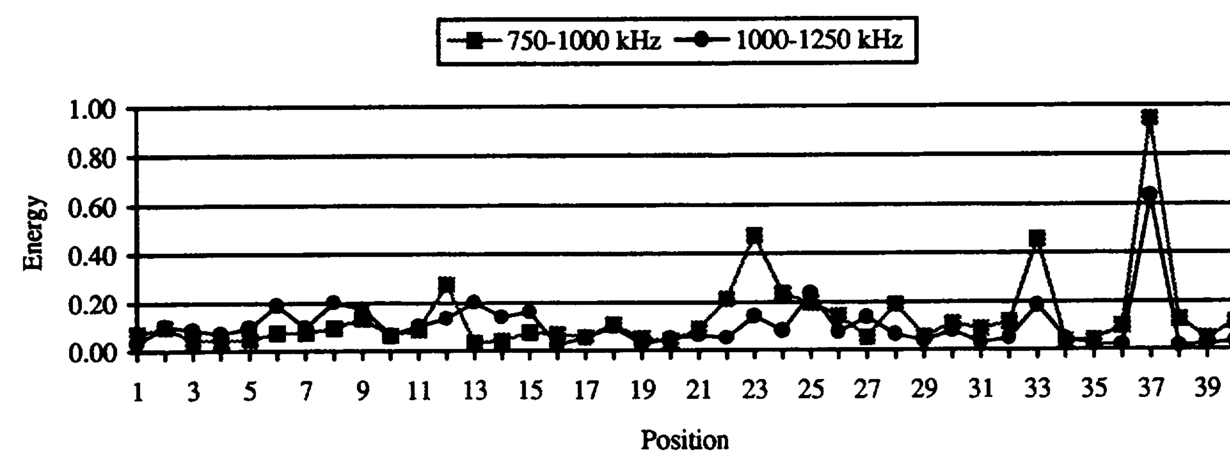

Figure 46. Energies for vessel D181 - Impact at position 37.5- Sharp Tip 3.92 N • m.

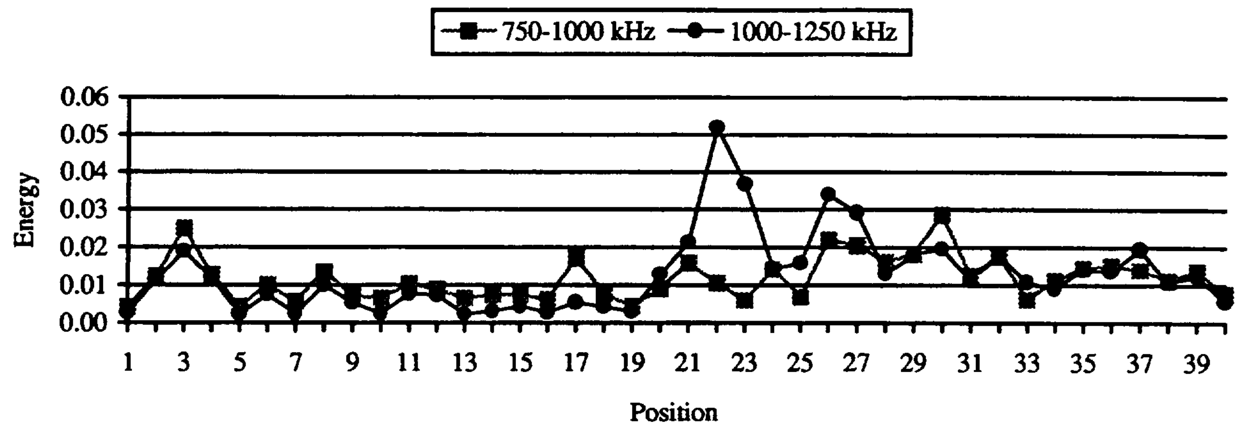

Figure 47. Energies for vessel D223 - No impact - Failure at position 30.

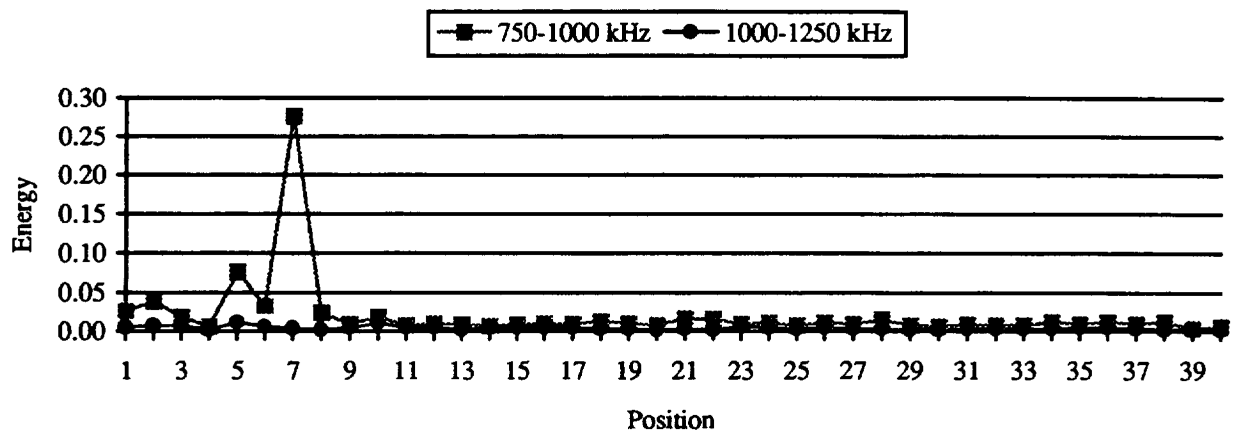

Figure 48. Energies for vessel D191 - Impact at position 6 - Blunt Tip 27.50 N • m.

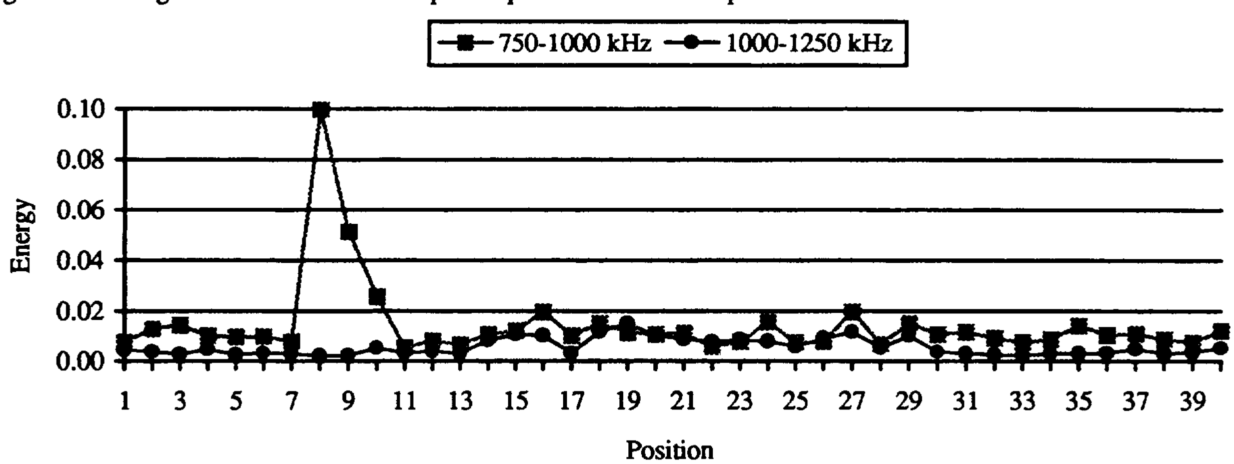

Figure 49. Energies for vessel D205 - Impact at position 9 - Blunt Tip 6.71 N • m.

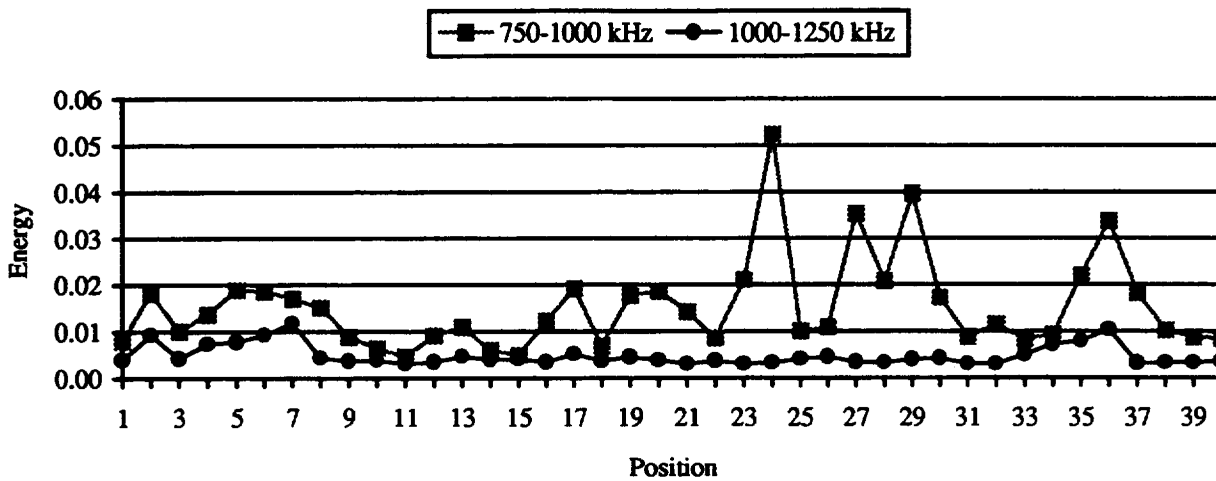

Figure 50. Energies for vessel D245 - Impact at position 35.5 - Blunt Tip 18.02 N•m.

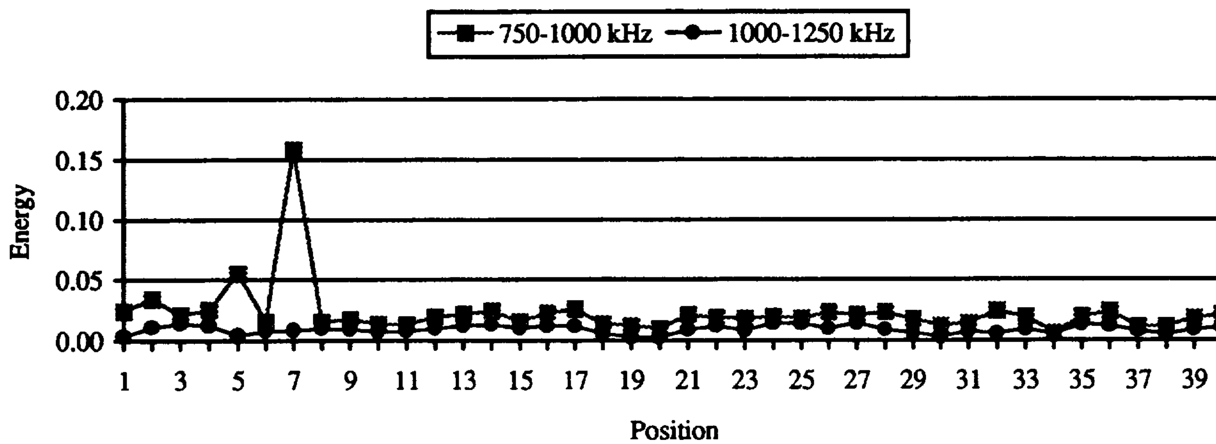

Figure 51. Energies for vessel D175 - Impact at position 6.5 - Blunt Tip 22.37 N•m.

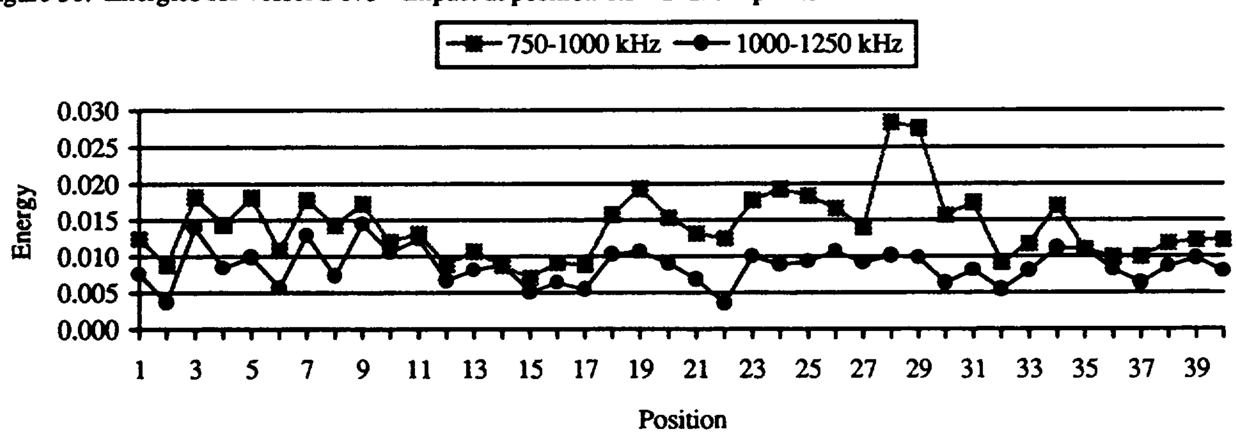

Figure 52. Energies for vessel D185 - No impact - Failure at position 28.

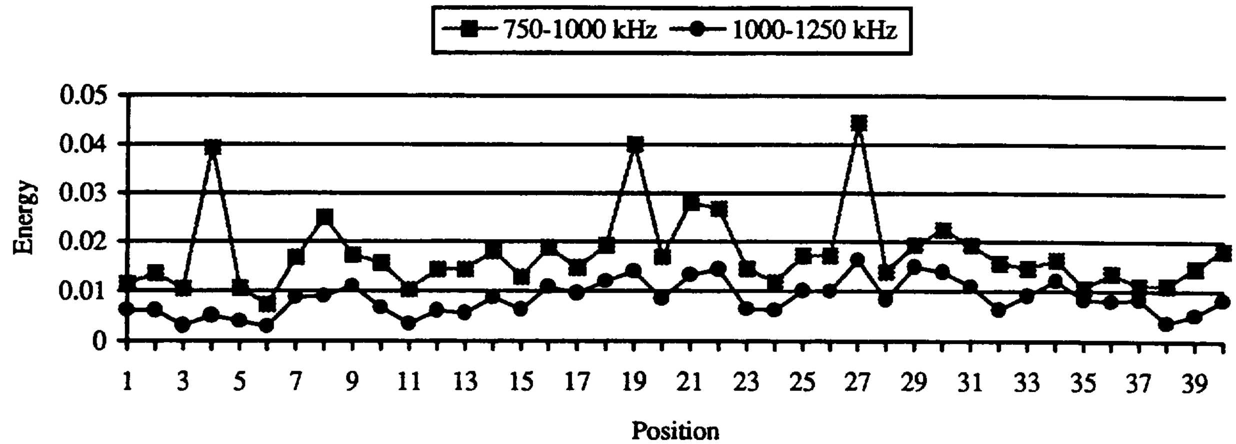

Figure 53. Energies for vessel D255 - Impact at position 3.5 - Sharp Tip 5.56 N•m.

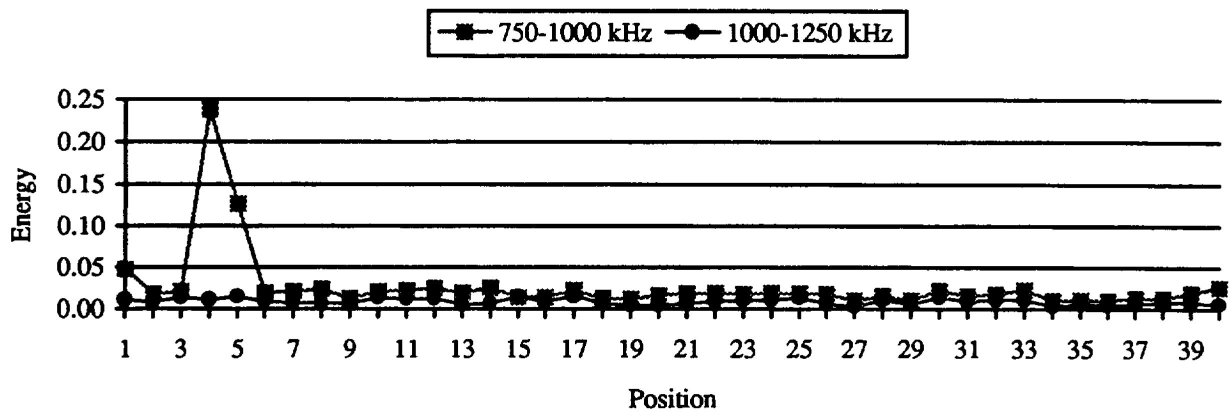

Figure 54. Energies for vessel D257 - Impact at position 4.5 - Blunt Tip 14.78 N•m.

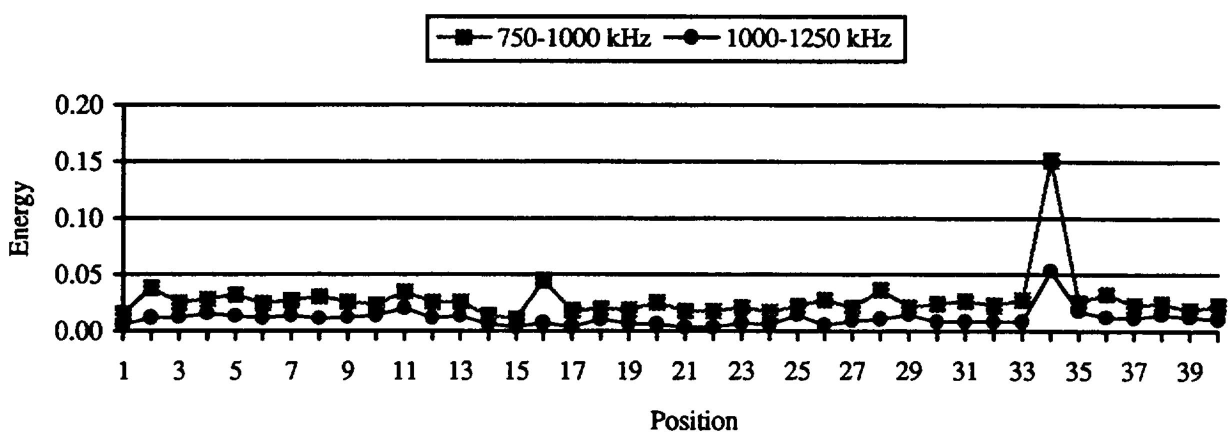

Figure 55. Energies for vessel D159 - Impact at position 33.5 - Sharp Tip 5.31 N•m.

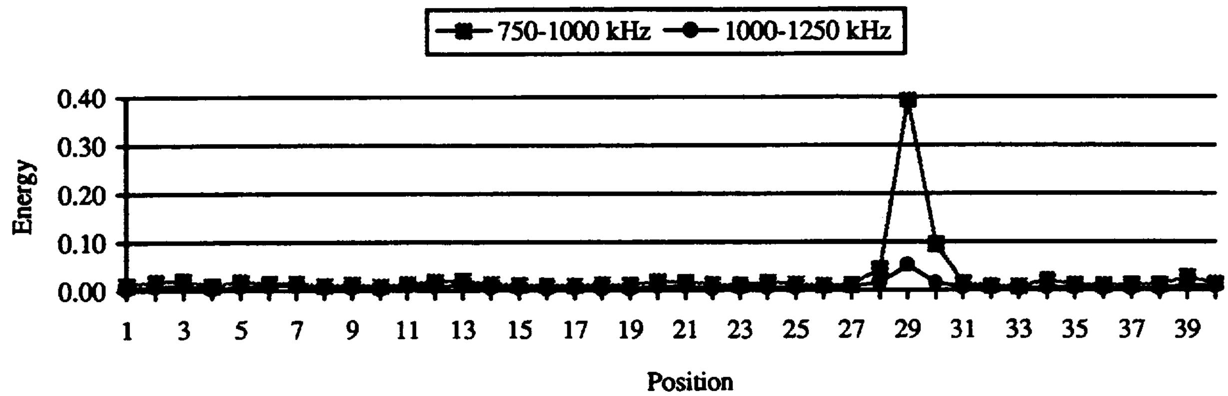

Figure 56. Energies for vessel D219 - Impact at position 29 - Blunt Tip 20.39 N•m.

The impact locations were very pronounced in the energy plots for the Kevlar vessels. In every case, the energy from the 750 to 1000 kHz band increased several orders of magnitude at and around the impact site. The 1000 to 1250 kHz frequency band was not as good a measure of the impact location but it did provide additional information when the lower frequency interval was not as clear.

Most important to note though, was the capability of the AU system to locate the failure initiation point of the unimpacted vessels. The overall energy magnitudes were the same for the damaged and undamaged vessels, with only slight increases in energy around suspect zones for the undamaged vessels. For example, the AU system mapped regions of high energy for vessel D185 at position 28, and vessel D223 at position 30; in both cases failure initiated at or near those regions.

3.5 EMPTY KEVLAR/EPOXY 14.61 CM DIAMETER VESSELS

The AURES was used to AU map 17 empty Kevlar/epoxy vessels featuring various levels of impact energies. A Harrisonic 1.0 MHz pulser injected the ultrasonic energy into the vessel while a Digital Wave broadband receiver recorded the AU signal. The sensors were spaced two inches apart along the longitudinal axis of the vessels and were centered on the bottles length. A thin bead of Soundsafe ultrasonic couplant was applied around the vessels in the path of the sensors and a 31.03 kPa (0.25 volt) contact pressure was set into the comparator. The pulse energy of the Panametric pulser unit was set to 4 (400 volt).

3.5.1 Data Summary

The vessels are identified in Table 16 along with the impact locations, AU code and impact status. The same impact location code as for the inert filled vessels was followed.

3.5.2 Energy/Location Plots and Discussion

The spectral energies were computed over eight, 250 kHz, intervals, from nearly DC up to 2.0 MHz. Of these bands, the 750 kHz to 1000 kHz and 1000 kHz to 1250 kHz bands provided the best resolution to measure the extent of the impact damage. The results (Figures 57 through 73) of these tests were the same as for the empty Kevlar vessels in that the energy values increased drastically around the impact site.

Bottle I.D.	Impact Location	Test date	AU test code	Impact Status (N•m)
D171-172	23-24	4-13-95	A	?
D235-236	38-39	4-13-95	B	BT-19.54
D254-255	4-8-12	4-13-95	C	BT-17.75/19.54
D169-170	33-34-35	4-14-95	D	ST-11.97
D187-188	7-8	4-14-95	E	BT-16.00
D241-242	9-10-11	4-14-95	F	BT-12.20
D177-178	36-37	4-14-95	G	ST-16.15
D225-226	36-37	4-14-95	H	ST-16.00
D201-202	3-4	6-8-95	L	ST-9.36
D233-234	none	6-9-95	M	none
D237-238	4-5	7-28-95	R	ST-13.29
D163-164	4-5-6	7-28-95	S	BT-14.78
D215-216	4-5	7-28-95	T	ST-9.63
D221-222	none	7-28-95	V	none
D161-162	35-36	8-21-95	Z	?
D207-208	29-30-31	10-25-95	AA	ST-12.74
D203-204	9-10	10-25-95	AC	BT-15.55

Table 16. AU data summary.

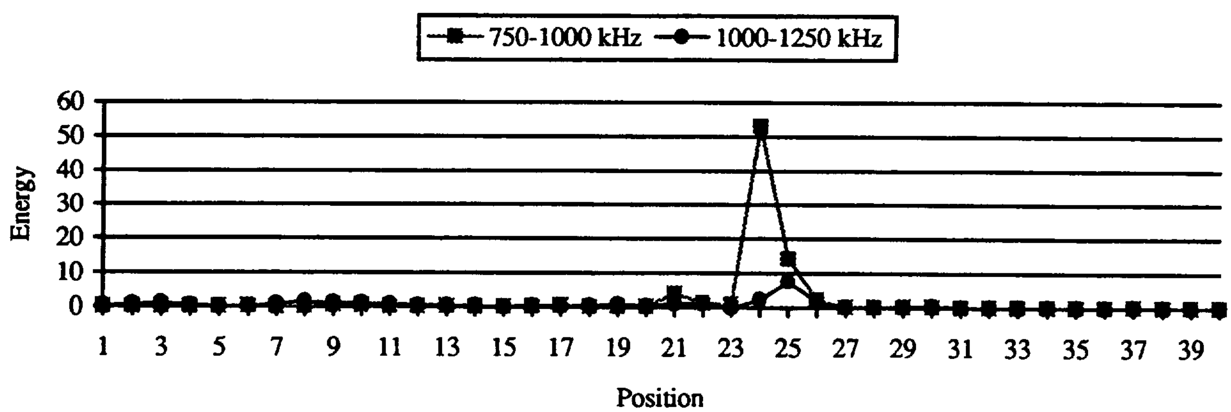

Figure 57. Energies for vessel D171 - Impact at position 23.5.

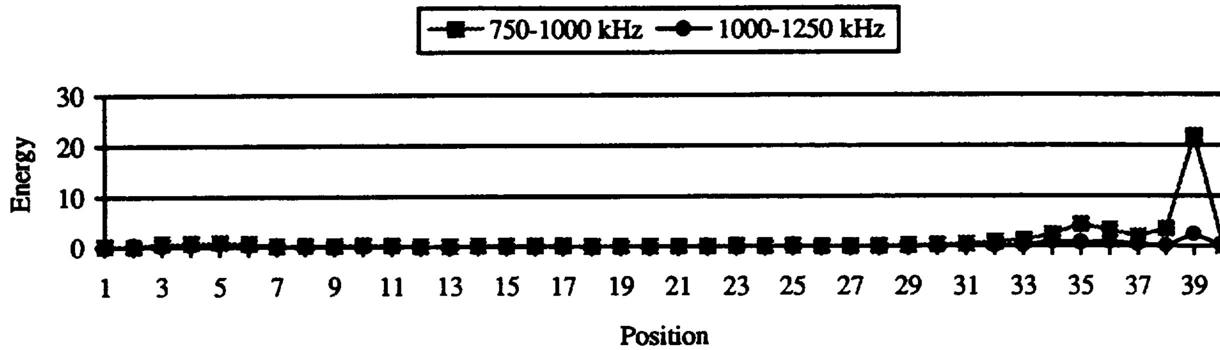

Figure 58. Energies for vessel D235 - Impact at position 38.5 - Blunt Tip 19.54 N•m.

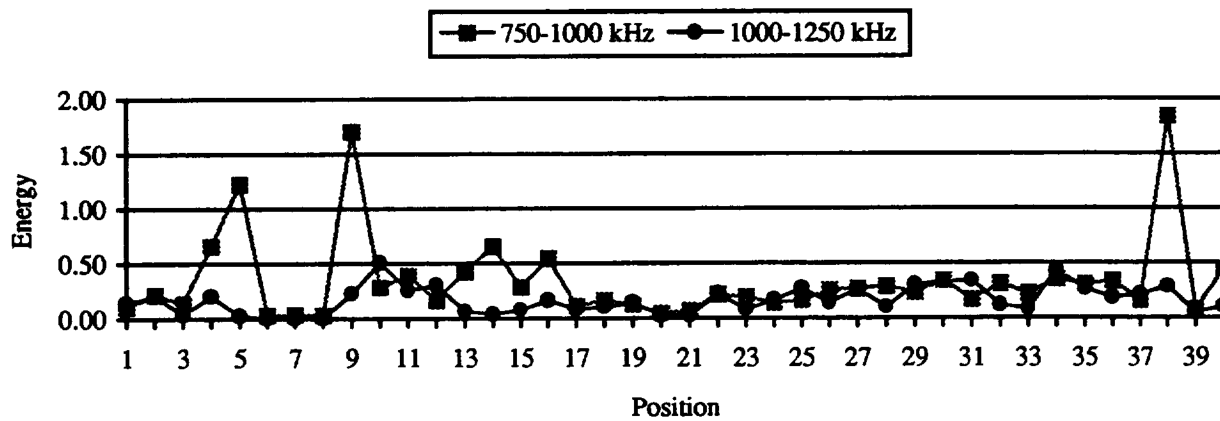

Figure 59. Energies for vessel D254 - Impact at position 8 - Blunt Tip 17.75/19.54 N•m.

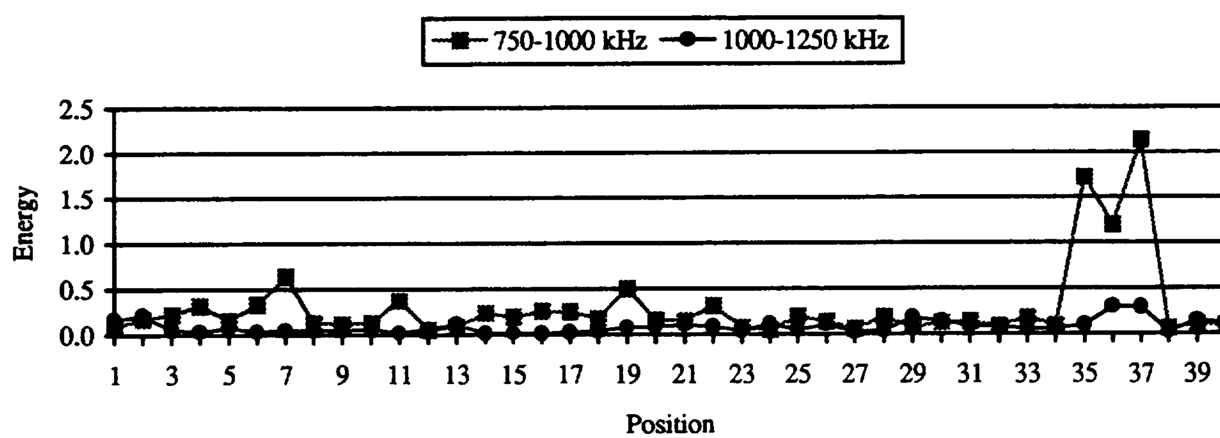

Figure 60. Energies for vessel D169 - Impact at position 34 - Sharp Tip 11.97 N•m.

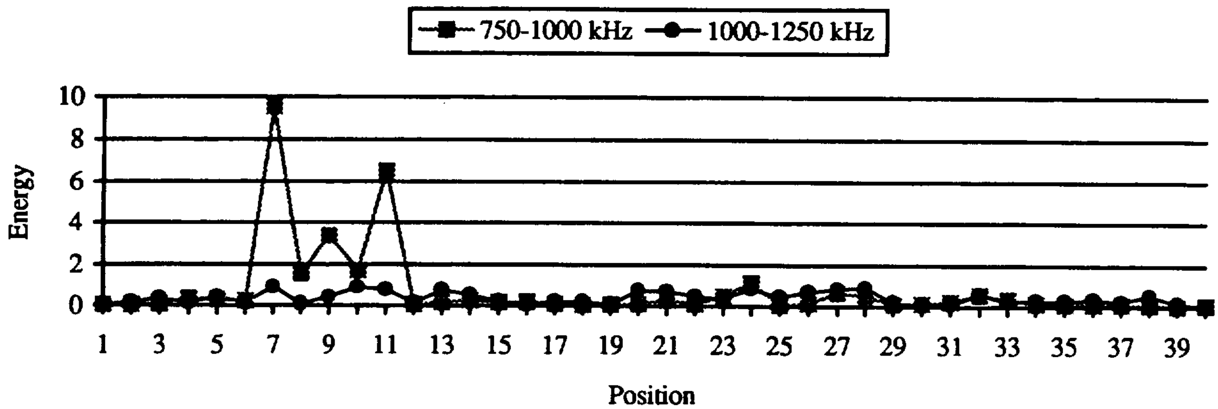

Figure 61. Energies for vessel D187 - Impact at position 7.5 - Blunt Tip 16.00 N • m.

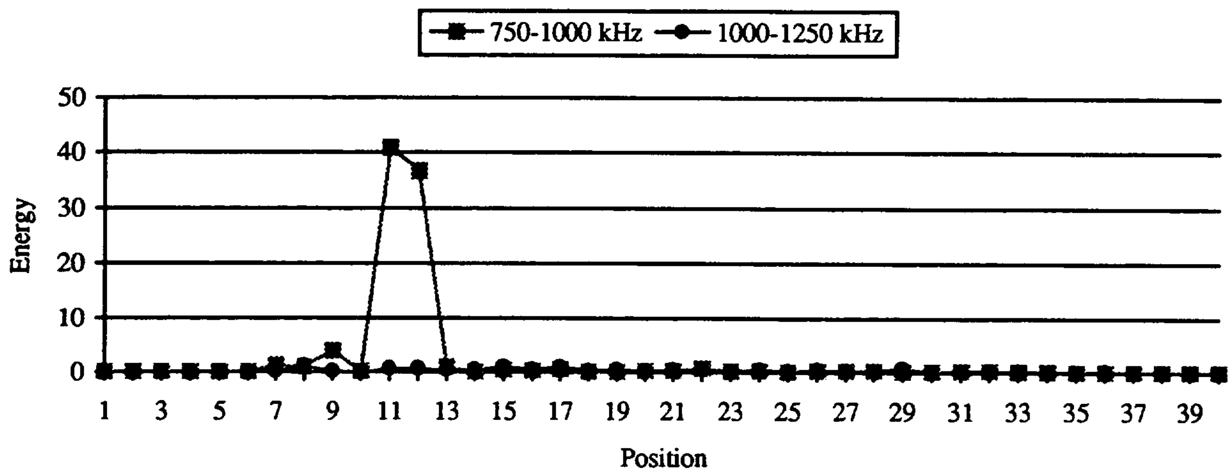

Figure 62. Energies for vessel D241 - Impact at position 10 - Blunt Tip 12.20 N • m.

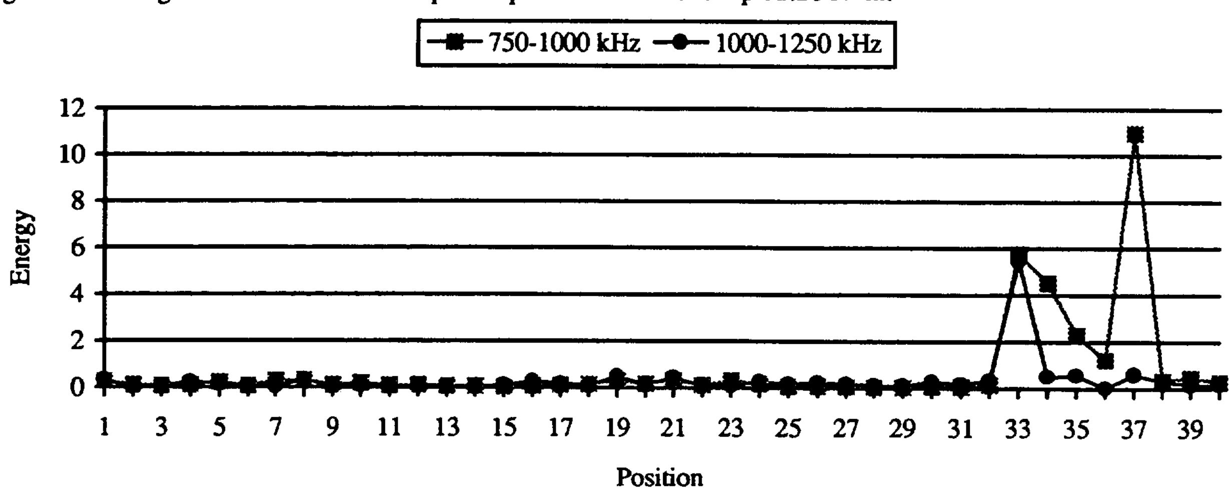

Figure 63. Energies for vessel D177 - Impact at position 36.5 - Sharp Tip 16.15 N • m.

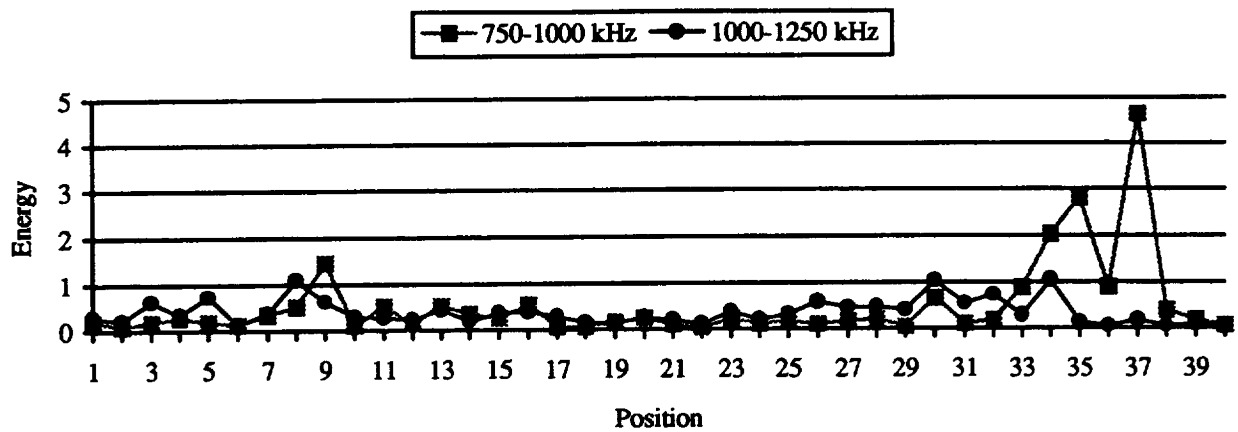

Figure 64. Energies for vessel D225 - Impact at position 36.5 - Sharp Tip 16.00 N • m.

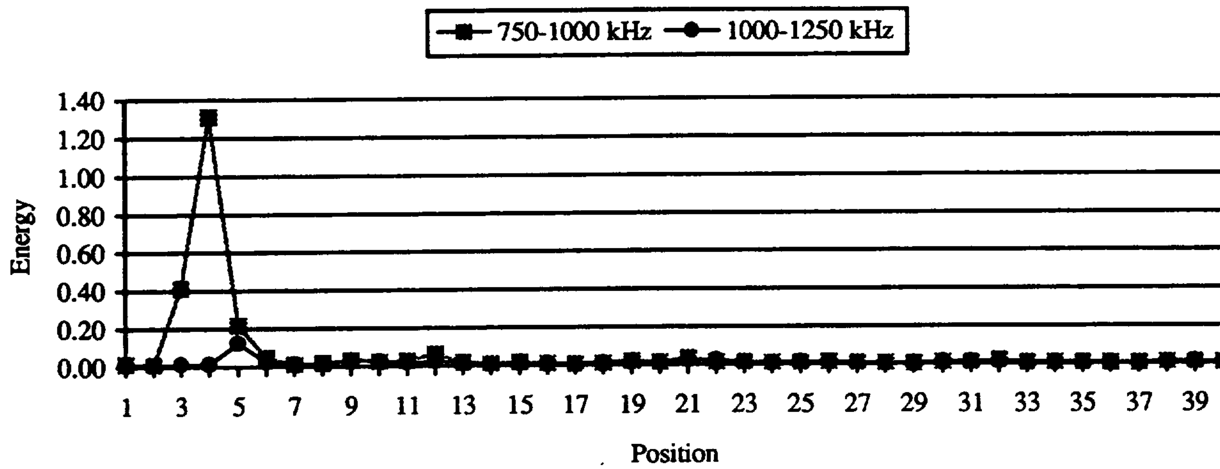

Figure 65. Energies for vessel D201 - Impact at position 3.5 - Sharp Tip 9.36 N • m.

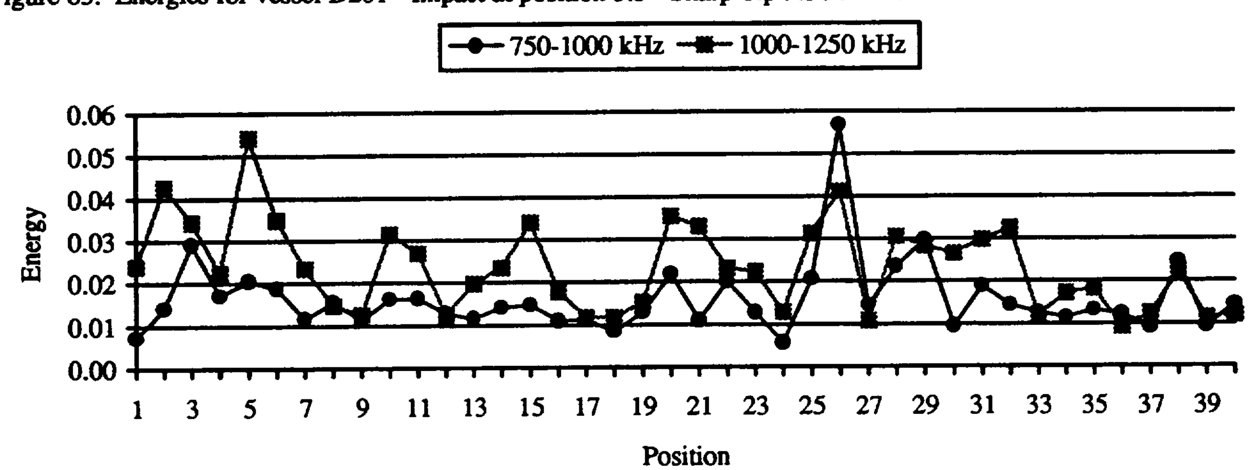

Figure 66. Energies for vessel D233 - No impact - No identifiable failure initiation point.

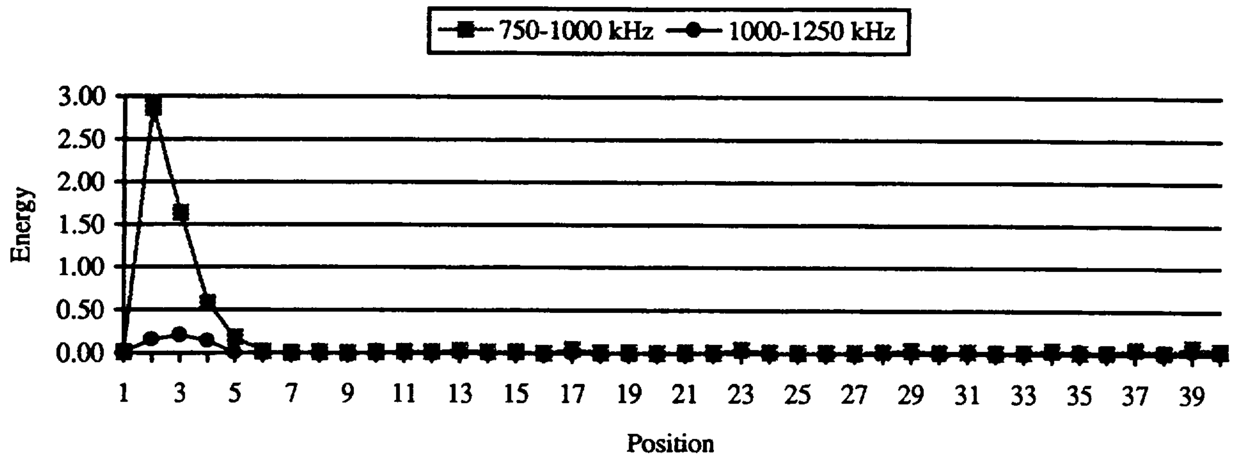

Figure 67. Energies for vessel D237 - Impact at position 4.5 - Sharp Tip 13.29 N • m.

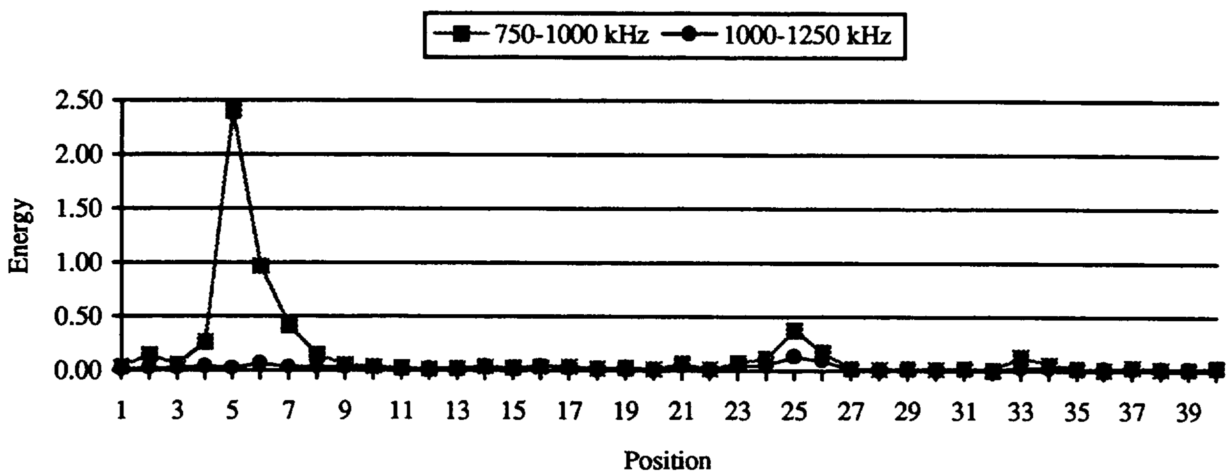

Figure 68. Energies for vessel D163 - Impact at position 5 - Blunt Tip 14.78 N • m.

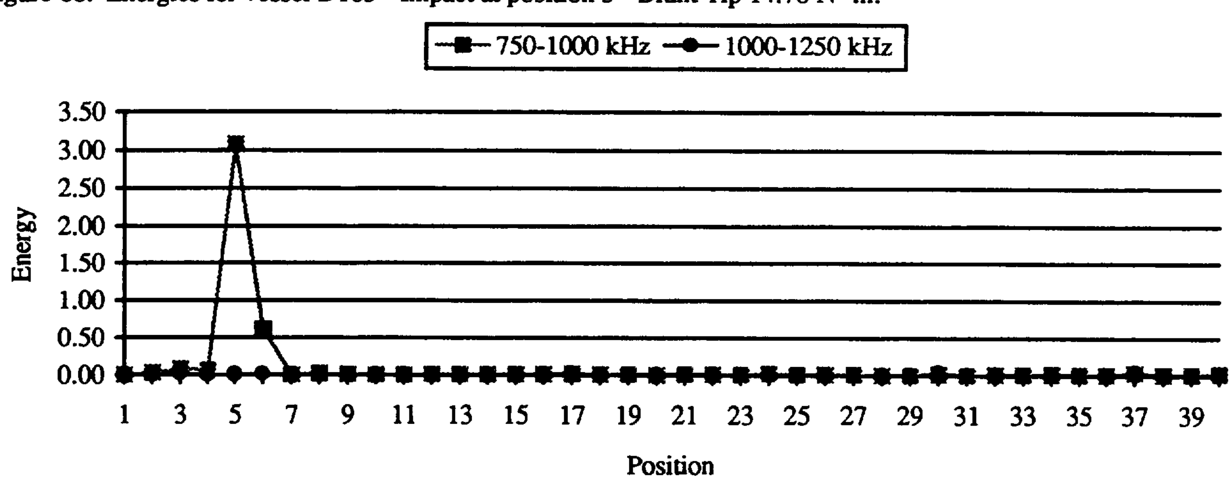

Figure 69. Energies for vessel D215 - Impact at position 4.5 - Sharp Tip 9.63 N • m.

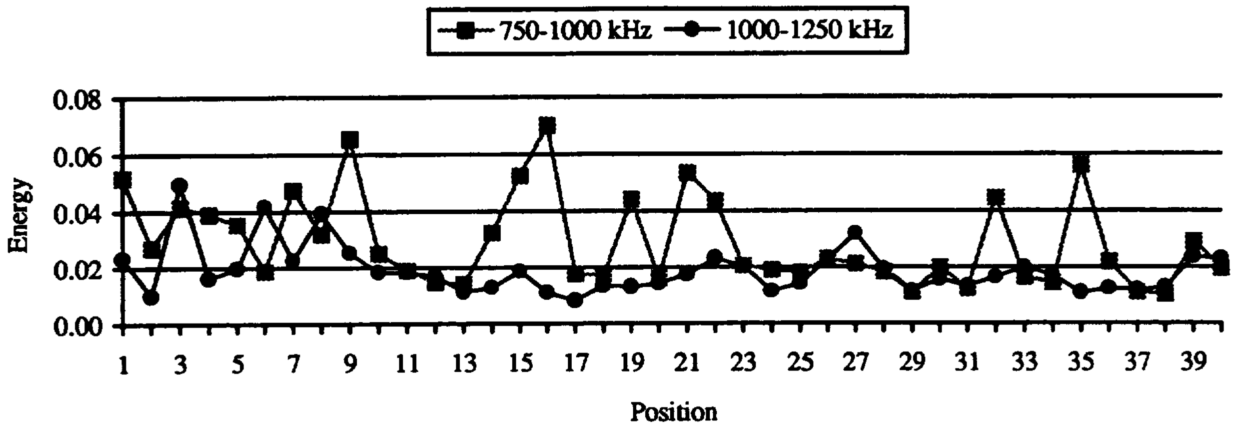

Figure 70. Energies for vessel D221 - No impact - Failure initiation at location 16.

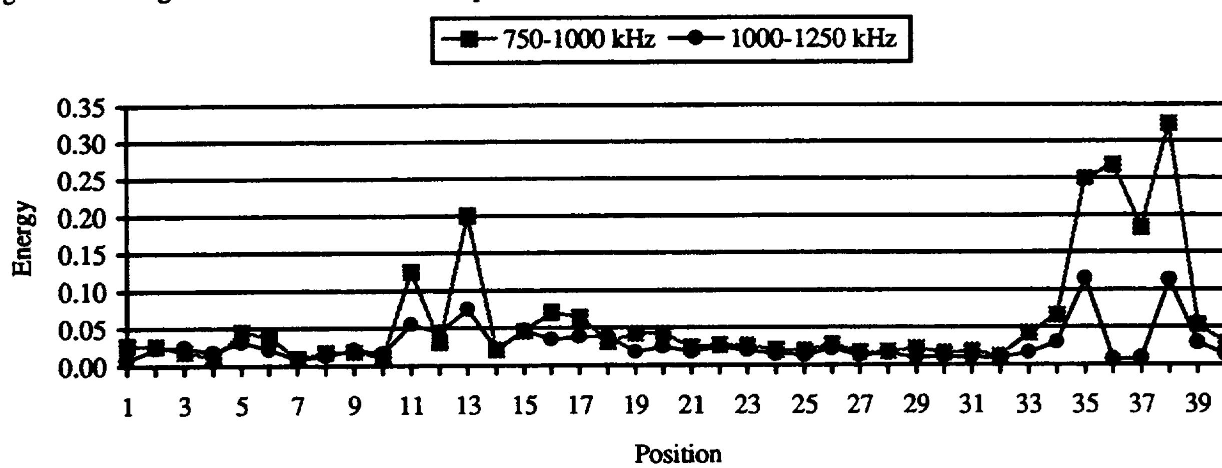

Figure 71. Energies for vessel D161 - Impact at position 35.5 - Unknown energy.

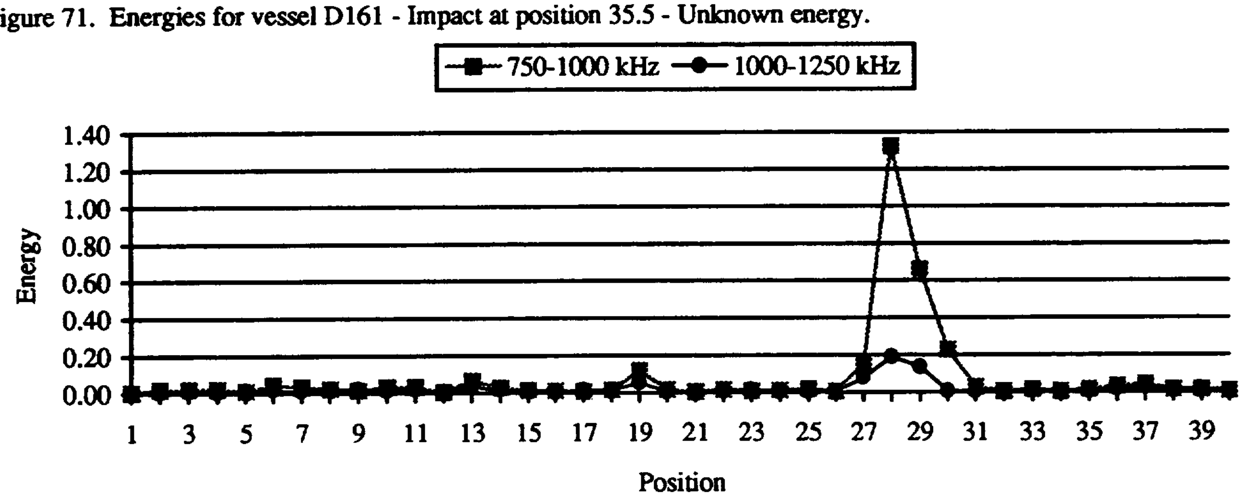

Figure 72. Energies for vessel D207 - Impact at position 30 - Sharp Tip 12.74 N • m.

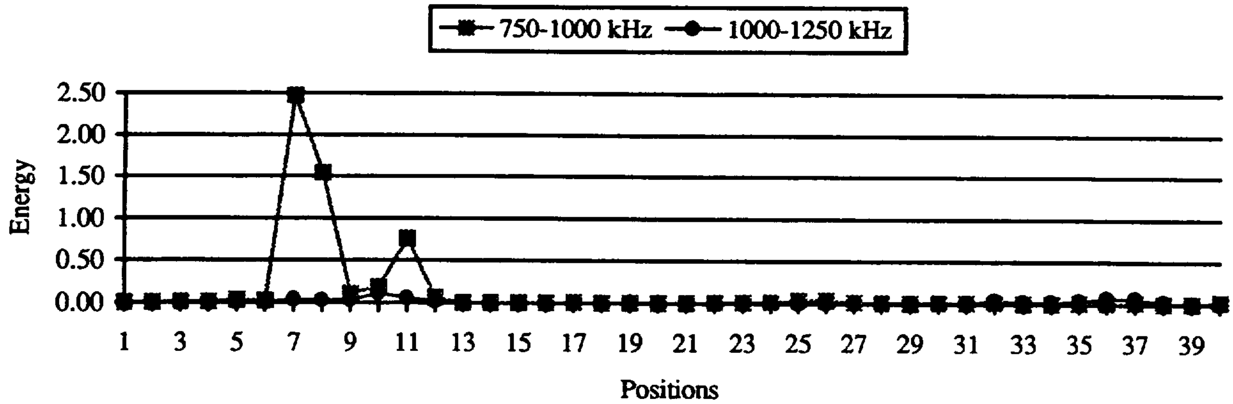

Figure 73. Energies for vessel D203 - Impact at position 9.5 - Blunt Tip 11.47 N•m.

Just as with the inert propellant filled Kevlar vessels, a large increase in the energy of the 750 to 1000 kHz frequency band was found in and around the impact site. In certain instances such as for vessels D161, D225 and D163, secondary damage sites were located nearly 180 ° from the impact site, similar to the results found with the filled graphite/epoxy vessels (Section 3.3).

3.6 CONCLUSIONS (AU)

- The SWF formulated by the energy content of the frequency band between 750 and 1000 kHz can be used to locate critical zones in Kevlar/epoxy pressure vessels.
- The SWF increases drastically in the damage zone for the Kevlar/epoxy vessels.
- The SWF decreases only slightly in the impact zone for the graphite/epoxy vessels.
- The AURES has demonstrated the ability to determine the position were potential failure would occur in damaged and undamaged filament wound pressure vessels.

3.7 RECOMMENDATIONS (AU)

The AURES should be reconfigured to map the entire pressure vessel. The vessels tested in this report were designed to fail in the mid hoop region, but since the failure location may vary for vessels of a different geometry the AURES should be given the flexibility to search any portion of the vessel. This flexibility will most likely come from the use of two robots, instead of one, to independently control the positioning of the pulser and receiver.

The AU spectra and resulting energies should be analyzed for the potential to measure the residual vessel strength. The AU waveforms will have to be normalized so that the power spectra is not biased by the natural variation in attenuation resulting from contact pressure and local surface conditions.

4.0 CONCLUSIONS

The methods outlined in this report demonstrate that the quality of small FWPV can be determined nondestructively. Combining robotics and acousto-ultrasonics allows for vessel integrity to be checked without having to apply any form of loading other than the ultrasonic pulse. The automated technique works very well on the Kevlar vessels and to a lesser degree on graphite/epoxy with or without an inert propellant liner. Once the critical area of interest is found with AU, other NDE methods such as SDVIC or ES should be employed to map the zone and determine the type of damage present.

By recording, "active" flaw growth, and not just the size of a flaw, AE has shown the potential for quantitatively determining the quality of a pressure vessel. AE signal analysis, through back propagation neural networks, show the potential for developing burst pressure prediction models ijn both Kevlar/epoxy and graphite/epoxy vessels. The models can then be used to access the residual life of a vessel, at low proof loads, where fiber damage is at a minimum.

5.0 REFERENCES

1. Hoskin, B. C. and Baker, A. A., Editors, <u>Composite Materials for Aircraft Structures</u>, American Institute of Aeronautics and Astronautics, New York, NY, 1986.

2. Walker, J. L., Lansing, M. L., Russell, S. S., Workman, G. L. and Nettles A., "Materials Characterization of Damage in Filament Wound Composite Pressure Vessels.", Proceedings from the ASNT 1995 Spring Conference, Las Vegas, Nevada, March 20-24.

3. Caudill, M. and Butler C., <u>Understanding Neural Networks, Volume 1: Basic Networks</u>, Massachusetts Institute of Technology, Cambridge, MA, 1992.

4. Ely, T. E. and Hill, E. v. K., "Longitudinal Splitting and Fiber Breakage Characterization in Graphite Epoxy Using Acoustic Emission Data", Materials Evaluation, pp.288-294, February 1995, ASNT.

6.0 APPENDIX

6.1 AEHITS.BAS

```
    PRINT "THIS ROUTINE WILL SORT AN AE DATA FILE T0 FIND THE NUMBER OF HITS"
    PRINT "FOR A GIVEN AMPLITUDE."
    REM ***** AMPLITUDE SORTING ROUTINE *****
    PRINT " "
    CLEAR
    DIM AMP1(100), AMP3(100), AMP4(100), AMP5(100)
    PRINT "ENTER THE TEST FILE NAME AND PATHING INSTRUCTIONS"
     INPUT FILE$
    OPEN "I", 1, FILE$
    PRINT " "
    MINAMP = 60
    MAX1 = 0
    MAX3 = 0
    MAX4 = 0
    MAX5 = 0
    PRINT "ENTER THE CUT-OFF TIME LIMIT FOR THIS TEST"
    INPUT TCUT
150  INPUT #1, TIME, P1, CH, RISE, COUN, ENER, DUR, A
    IF TIME <= TCUT THEN
     IF A >= MINAMP THEN
      IF CH = 1 THEN
       AMP1(A) = AMP1(A) + 1
       IF A > MAX1 THEN MAX1 = A
       I1 = I1 + 1
       GOTO 150
      END IF
      IF CH = 3 THEN
       AMP3(A) = AMP3(A) + 1
       IF A > MAX3 THEN MAX3 = A
       I3 = I3 + 1
       GOTO 150
      END IF
      IF CH = 4 THEN
       AMP4(A) = AMP4(A) + 1
       IF A > MAX4 THEN MAX4 = A
       I4 = I4 + 1
       GOTO 150
      END IF
      IF CH = 5 THEN
       AMP5(A) = AMP5(A) + 1
       IF A > MAX5 THEN MAX5 = A
       I5 = I5 + 1
       GOTO 150
      END IF
     END IF
    END IF
```

```
    CLOSE #1
    REM ***** AMPLITDE OUTPUT ROUTINE *****
    PRINT "THIS ROUTINE WILL LIST THE HITS FOR A RANGE OF AMPLITUDES FROM 60 TO
100dB."
    PRINT " "
    PRINT " AMP EVENTS    AMP EVENTS    AMP EVENTS    AMP EVENTS"
    FOR Y = 1 TO 10
     PRINT USING " ### ####     ### ####     ### ####     ### ####"; Y + 60; AMP1(Y + 60); Y + 60;
AMP1(Y + 70); Y + 80; AMP1(Y + 80); Y + 90; AMP1(Y + 90)
    NEXT Y
    PRINT " "
    PRINT " AMP EVENTS    AMP EVENTS    AMP EVENTS    AMP EVENTS"
    FOR Y = 1 TO 10
     PRINT USING " ### ####     ### ####     ### ####     ### ####"; Y + 60; AMP3(Y + 60); Y + 70;
AMP3(Y + 70); Y + 80; AMP3(Y + 80); Y + 90; AMP3(Y + 90)
    NEXT Y
    PRINT " "
    PRINT " AMP EVENTS    AMP EVENTS    AMP EVENTS    AMP EVENTS"
    FOR Y = 1 TO 10
     PRINT USING " ### ####     ### ####     ### ####     ### ####"; Y + 60; AMP4(Y + 60); Y + 70;
AMP4(Y + 70); Y + 80; AMP4(Y + 80); Y + 90; AMP4(Y + 90)
    NEXT Y
    PRINT " "
    PRINT " AMP EVENTS    AMP EVENTS    AMP EVENTS    AMP EVENTS"
    FOR Y = 1 TO 10
     PRINT USING " ### ####     ### ####     ### ####     ### ####"; Y + 60; AMP5(Y + 60); Y + 70;
AMP5(Y + 70); Y + 80; AMP5(Y + 80); Y + 90; AMP5(Y + 90)
    NEXT Y
    PRINT " "
    PRINT "OUTPUT DATA TO A SPECIFIED DIRECTORY. Y/N"
    INPUT Q$
    IF Q$ = "N" OR Q$ = "n" THEN GOTO 301
    PRINT " "
    PRINT "ENTER THE OUPUT FILENAME AND EXTENSION"
    INPUT OUTFILE$
    PRINT " "
    PRINT "ENTER THE BURST PRESSURE OF THE BOTTLE IN PSI."
    INPUT ULTSTR
    OPEN "O", 2, OUTFILE$
    FOR Y = 60 TO 100
     PRINT #2, AMP1(Y),
    NEXT Y
     PRINT #2, ULTSTR
    FOR Y = 60 TO 100
     PRINT #2, AMP3(Y),
    NEXT Y
     PRINT #2, ULTSTR
    FOR Y = 60 TO 100
     PRINT #2, AMP4(Y),
    NEXT Y
     PRINT #2, ULTSTR
    FOR Y = 60 TO 100
     PRINT #2, AMP5(Y),
    NEXT Y
```

```
 PRINT #2, ULTSTR
 CLOSE #2
301  REM ***** WEIBULL ANALYSIS ROUTINE *****
 DIM R(100), XAXIS(100), YAXIS(100)
 PARSUMS = 0
 FOR Y = MINAMP TO MAXAMP
  PARSUMS = PARSUMS + AMP(Y) / I
  R(Y) = 1 - PARSUMS + AMP(Y) / (I * 2)
 NEXT Y
 PRINT USING "THE THRESHOLD AMPLITUDE IS SET TO ##."; MINAMP
 THRESHOLD = MINAMP
 PRINT " "
 FOR Y = MINAMP TO MAXAMP
  IF (Y - THRESHOLD) > 0 GOTO 350
   XAXIS(Y) = 0
   YAXIS(Y) = 0
   C = C + 1
  GOTO 360
350   XAXIS(Y) = LOG(Y - THRESHOLD)
  IF R(Y) > 0 THEN GOTO 355
   CC = CC + 1
   GOTO 360
355   YAXIS(Y) = LOG(LOG(1 / R(Y)))
360  NEXT Y
 REM ***** LINEAR REGRESSION ROUTINE *****
 N = 0
 SX = 0
 SY = 0
 SXY = 0
 SXS = 0
 SYS = 0
 SSXX = 0
 SSXY = 0
 SSYY = 0
 TMIN = MINAMP + C
 TMAX = MAXAMP - CC
 FOR Y = TMIN TO TMAX
  SX = SX + XAXIS(Y)
  SY = SY + YAXIS(Y)
  SXY = SXY + XAXIS(Y) * YAXIS(Y)
  SXS = SXS + XAXIS(Y) ^ 2
  SYS = SYS + YAXIS(Y) ^ 2
  N = N + 1
 NEXT Y
  SSXY = SSXY + SXY - (SX * SY) / N
  SSXX = SSXX + SXS - (SX ^ 2) / N
  SSYY = SSYY + SYS - (SY ^ 2) / N
  B1H = SSXY / SSXX
  B0H = SY / N - B1H * (SX / N)
  THETA = EXP(ABS(B0H / B1H)) + THRESHOLD
  REM ***** RESIDUAL ANALYSIS *****
  SUMRESID = 0
  SSE = 0
  FOR Y = TMIN TO TMAX
```

```
 SSE = SSE + (((XAXIS(Y) * B1H) + B0H) - YAXIS(Y)) ^ 2
NEXT Y
S = SQR(SSE / (N - 2))
SSR = SSYY - SSE
K = 2
DFR = K - 1
DFE = N - K
DFT = DFR + DFE
MSR = SSR / DFR
MSE = SSE / DFE
F = MSR / MSE
RSQ = 100 * (1 - (SSE / SSYY))
RSA = 100 * (1 - (SSE / DFE) / (SSYY / DFT))
REM ***** STATISTICAL OUTPUT *****
CLS
PRINT " "
PRINT USING " THE REGRESSION EQUATION IS Y = ####.#### + ####.####X."; B0H; B1H
PRINT " "
PRINT USING " AO = ###    b = ###.###    THETA = ###.###"; THRESHOLD; B1H; THETA
PRINT " "
PRINT "ANALYSIS OF VARIANCE"
PRINT " "
PRINT "SOURCE        DF        SS        MS        F"
PRINT USING " REGRESSION   ###    #####.####  #####.####  #####.####"; DFR; SSR; MSR; F
PRINT USING " ERROR        ###    #####.####  #####.####"; DFE; SSE; MSE
PRINT USING " TOTAL        ###    #####.####"; DFT; SST
PRINT " "
PRINT USING " S  = ####.####    R-SQ = ##.##%    R-SQa = ##.##%"; S; RSQ; RSA
PRINT " "
PRINT "CR TO RETURN TO MAIN MENU"
INPUT Q$
END
```

6.2 FILLED GR/EP VESSEL AMPLITUDE DISTRIBUTIONS (CHANNEL 1)

3501-6 RESIN CLASS

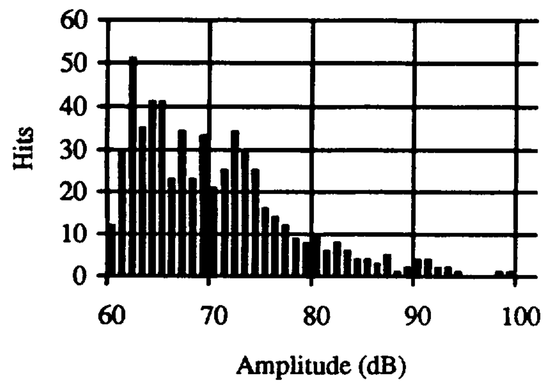

A003-004

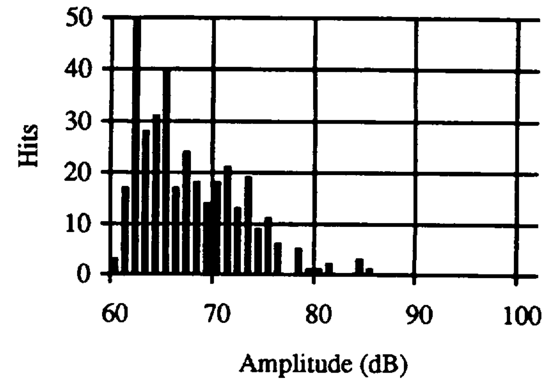

C069-070

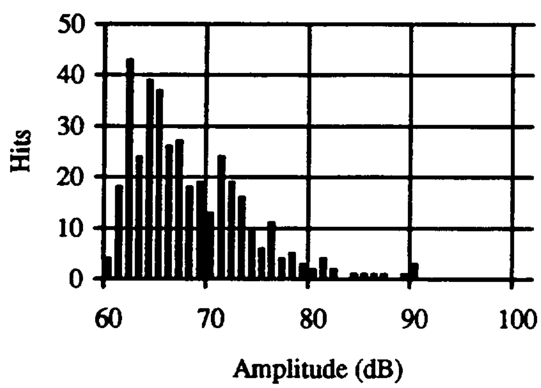

C077-078

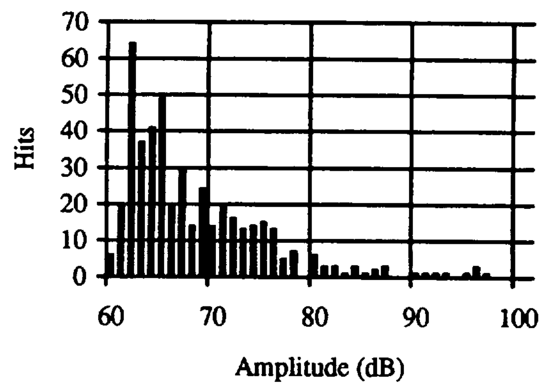

A013-014

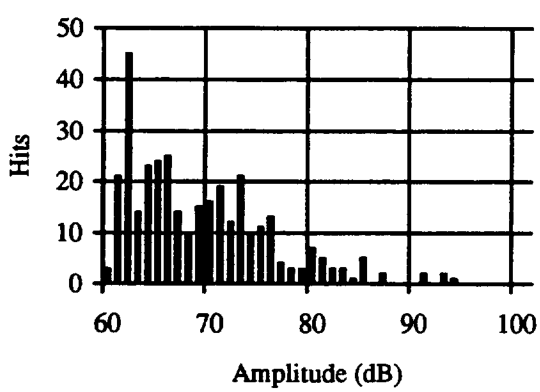

A017-018

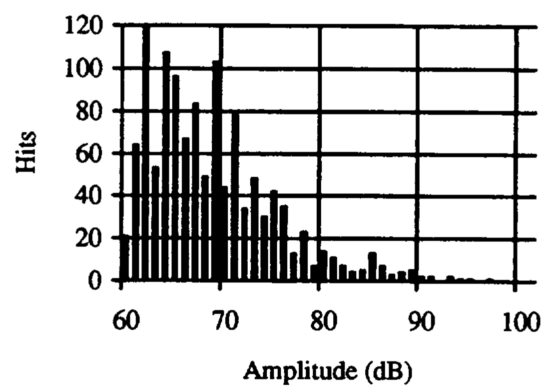

A023-024

977-2 RESIN CLASS

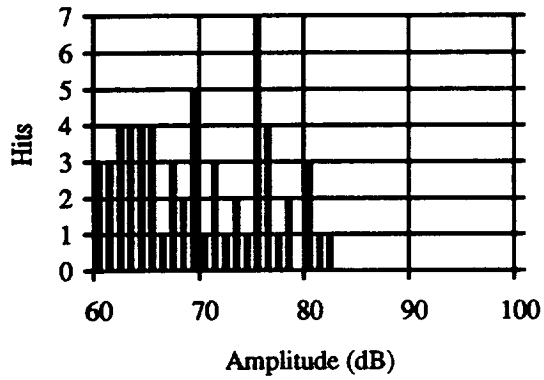

C115-116

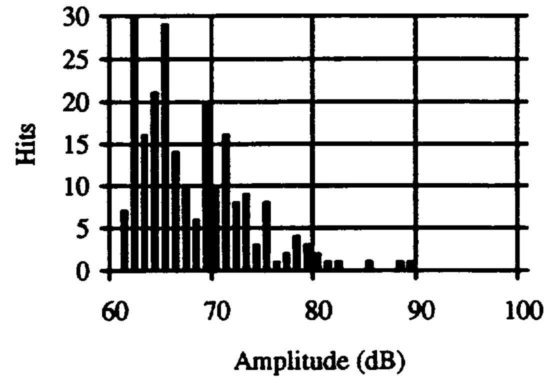

C139-140

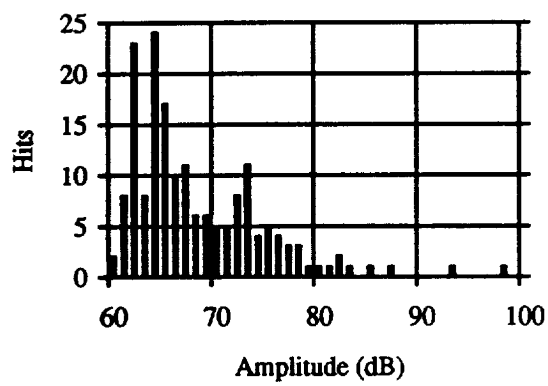

C141-142

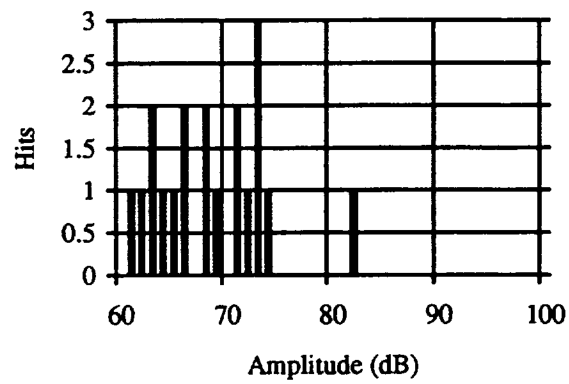

C117-118

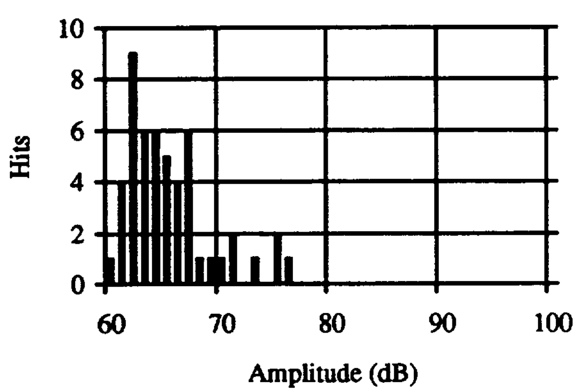

C131-132

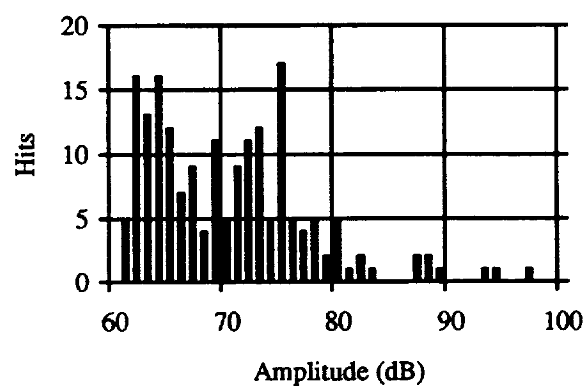

C155-156

8553-45 RESIN CLASS

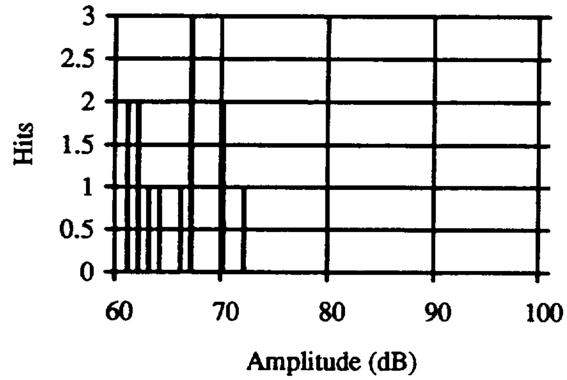

A025-026

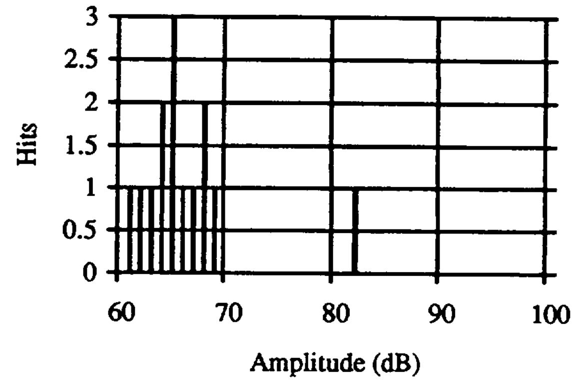

A029-030

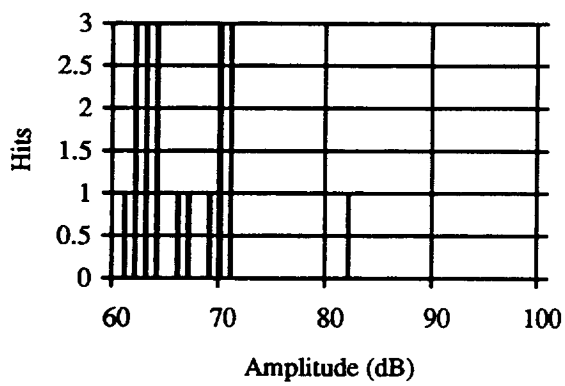

A047-048

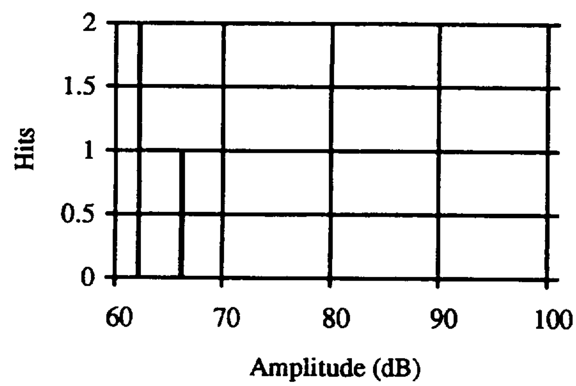

C087-088

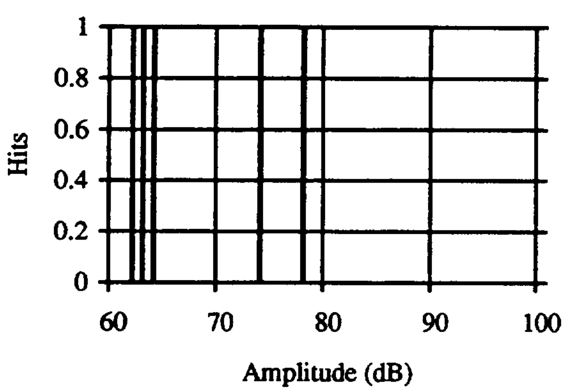

C093-094

6.3a NETWORK WEIGHTS FOR IM7/3501-6

	First middle layer processing elements												
	42	43	44	45	46	47	48	49	50	51	52	53	54
BIAS	.0174	.0592	.1333	-.0935	.0102	-.1016	-.1256	-.0073	.0845	-.0583	.0705	-.078	-.0608
1	.0224	.1047	-.0406	.0582	.055	.1475	-.1217	.0903	-.0441	-.1414	-.0596	.1078	-.0067
2	-.0692	.0505	.1406	.1529	.0941	.0773	.0826	-.0275	.1643	.1182	.0433	.0614	.1519
3	-.0635	-.0189	.1601	.0871	.1123	.1493	-.0283	-.1161	-.0211	.0269	.1188	.1232	-.0468
4	-.0008	-.0103	-.0161	-.117	-.0071	.0511	-.1343	.0186	-.0723	-.0746	-.144	.1836	-.0715
5	-.0635	.0316	.1557	.15	.118	.086	-.0669	.1084	-.0707	-.1403	-.0534	.1677	.0418
6	.0355	-.1494	-.0357	.0027	.0855	.1155	-.0115	.0165	-.093	-.1493	-.0925	.0262	-.0596
7	.0783	-.109	-.0549	.0314	.16	-.1089	.1215	-.0872	-.1184	.0777	-.026	-.0744	-.0719
8	.0456	.0889	.1573	-.1185	-.1724	.1513	-.0479	-.0133	.0465	-.1539	-.0387	-.0563	.1112
9	.1337	.0644	-.0369	.0942	.1207	.019	-.1468	.0617	.0443	.0165	-.1382	.1484	.0426
10	-.0962	.0288	-.0638	.0294	.1302	.0021	.0519	.1069	.102	-.0939	-.0386	.071	.0266
11	.1591	-.1016	-.0617	-.0977	-.1063	-.1164	-.0757	-.0793	-.0525	-.1434	-.0351	-.0892	.0758
12	.0333	-.063	-.0776	-.0677	.1214	-.0301	-.0851	.0088	.1111	-.1513	-.1387	.1246	-.1336
13	.0068	-.1113	.0724	-.1325	.0512	-.1229	.1594	.1516	.0898	-.0399	.139	.1978	.0961
14	.0158	-.0741	-.1142	-.0705	-.0982	-.0964	-.0285	.1384	.1551	-.083	.1151	.0788	.0287
15	.0806	.02	.1465	.0653	.0713	.1024	-.0167	-.1337	-.0247	-.1082	.0025	.189	.1059
16	.1231	.1105	-.0148	-.1303	-.0372	.069	.112	.1131	.0073	-.0333	.0717	-.128	-.1393
17	-.0394	.0661	.0842	-.0209	.0613	-.1271	-.1349	-.0789	.1279	.1152	.0475	.035	.0509
18	-.0959	-.0936	-.1387	-.011	-.073	-.1344	-.0905	.0308	.1407	-.1132	.1455	.0797	-.0535
19	.1125	.104	.0745	.0327	-.0615	.0191	-.1098	-.0037	.0299	.1017	-.1019	-.0766	-.1422
20	.0523	-.0165	-.1386	-.1427	.0621	.0887	.0831	-.0988	-.1228	.0715	.0238	.0993	-.0474
21	.0368	-.1032	-.1611	-.1037	.0204	-.1006	-.0334	.0606	-.127	-.0897	-.027	-.1315	-.0825
22	.1265	-.0763	.0422	.051	.0439	-.1485	.0895	.0301	.0644	.0879	-.0055	-.0631	.0288
23	-.1068	.0079	.1661	.1412	.0691	.137	-.0436	-.0014	-.0194	.0696	-.1256	-.1164	-.1114
24	.053	-.0512	-.0847	-.1194	.0559	-.1456	-.1449	.0611	-.0361	-.1051	-.0542	-.1724	.1357
25	.0013	-.0379	-.096	-.0235	-.0022	-.1066	-.0944	.0047	-.0292	-.031	.1012	.0113	-.1048
26	-.0641	.0762	-.0903	.0582	-.0478	-.1631	-.0684	-.0022	.0734	.1343	.1159	-.1565	.1488
27	.2161	-.1565	-.0443	-.0521	-.0576	-.0573	.0853	-.0542	.074	-.0629	-.0627	.2102	-.0205
28	-.0358	-.1411	-.0639	.0824	-.111	-.0786	.0681	.1345	.1519	.1349	-.1023	.0405	.0654
29	-.0471	-.1182	.1708	-.0175	-.147	.0912	-.0168	-.119	.158	-.0733	.1501	.1847	.0035
30	-.0261	-.0772	-.0109	-.074	-.0038	.1483	.0444	.0338	-.014	.0797	.0091	-.0232	-.0222
31	.0409	-.1853	.1508	-.0254	-.0342	-.072	-.1058	.1549	.0325	-.1235	.0751	.0983	-.0179
32	-.1137	.0914	-.1494	.0058	.0256	.0055	-.108	.0701	-.1609	-.0534	.0146	-.1428	-.0891
33	.0767	.0687	-.0694	-.0966	-.1558	-.0498	.0713	-.1048	.1248	-.0674	.0471	.1475	-.1133
34	-.0757	.1828	.1087	-.0207	-.0828	-.1317	.0114	-.0016	-.1931	.1747	.0828	.0222	.0365
35	-.0094	.1049	.1144	.0007	.0128	-.0037	.0868	-.0223	-.1128	.132	-.0488	-.1598	.0518
36	.0965	.0598	-.0272	.0621	.144	-.0128	.0574	.1229	.1174	-.0843	.0459	-.0154	-.1476
37	.0103	-.0171	.0591	-.1126	-.042	.049	-.1496	-.127	-.1205	.1333	-.1092	-.0401	-.0951
38	-.0458	-.131	-.0556	.1091	-.0798	-.034	.0611	-.0846	-.0073	-.1367	.0375	-.1402	.095
39	-.0194	.0955	.1005	.0255	.094	.0213	.0339	-.0695	-.0135	.049	-.0959	.1588	-.0143
40	.0422	-.1309	.0645	-.0994	.1264	.08	-.0332	.1312	.1183	-.1151	.0536	-.0582	.1358
41	-.0173	.0582	-.0781	.1159	-.1241	-.1275	-.1022	-.0366	.1269	-.0792	-.0629	-.0421	.1485

	Second middle layer processing elements												
	55	56	57	58	59	60	61	62	63	64	65	66	67
BIAS	.0726	-.1354	.0707	.2231	.0242	-.0885	.1719	.1547	.1153	.1456	-.2402	-.0235	.2248
42	-.1812	.1879	-.0738	-.1028	.0023	.1353	-.2275	.0677	.1688	-.2269	.1023	-.1062	-.1109
43	-.1283	.1152	-.0641	.2684	.1848	-.2702	.0986	-.1558	-.1941	.1436	.1235	.2815	.0401
44	.1977	.0734	-.265	.1715	-.1077	.0027	-.0932	-.0942	-.225	.2513	.1771	.0297	-.2747
45	-.1303	.0485	.088	-.0368	.0379	-.014	.1752	-.2838	-.2656	-.1677	.2233	-.0481	.1431
46	.0771	-.1872	.0903	.2746	-.1661	-.0304	.2572	.3047	.2506	.2349	.2222	.011	.2162
47	-.118	-.0083	-.2679	.0222	-.0743	.072	-.1914	.1693	.0395	-.0979	.0647	-.2085	.1484
48	-.0953	-.0762	.2631	-.2121	-.0985	-.2404	-.0091	-.0014	.2794	-.018	.2482	-.2137	-.1557
49	-.0656	.1253	-.2173	.066	.2257	.2866	-.1659	-.1636	-.2404	.0472	-.1329	-.0458	.0536
50	.0558	.0718	-.2412	-.226	-.2435	.0299	-.0474	.0534	-.0982	-.1814	.0736	-.2473	-.2813
51	-.1387	-.2598	.2833	.1916	.1772	-.1587	.1523	.0963	.2148	-.0305	-.2304	.0313	.2338
52	.1074	.2038	-.1836	.0405	.1181	-.273	.2528	-.0009	-.145	-.2038	.2081	-.1207	.2501
53	-.3393	.103	.0254	.0852	.1519	.3381	-.3212	.311	-.1814	-.2451	.1689	-.1026	-.2999
54	.2071	.1052	-.211	.0426	-.0097	-.1504	-.034	-.1902	-.2223	.1238	.1824	.2336	-.154

	Output layer processing element
Middle layer processing elements	68
BIAS	.0698:
55	-.2192
56	.1994:
57	-.2935
58	.0113:
59	-.1568
60	.4894:
61	-.2445
62	.2791:
63	-.0806
64	-.1633
65	.2309:
66	-.2203
67	-.3586

6.3b NETWORK WEIGHTS FOR IM7/977-2

	First middle layer processing elements												
	42	43	44	45	46	47	48	49	50	51	52	53	54
BIAS	.0519	.0352	.1431	-.0979	-.0341	-.0854	-.1196	.0048	.1185	-.0915	.068	-.0163	-.0666
1	.0937	.0797	-.0484	.0631	-.024	.1926	-.0989	.108	.0224	-.1614	-.044	.1599	-.03
2	-.1507	.0781	.1138	.1549	.1222	.0482	.0761	-.0528	.0852	.1548	.0396	.003	.1604
3	-.1557	.0135	.1349	.0898	.1522	.1164	-.0365	-.1472	-.1129	.0741	.1133	.0497	-.0337
4	-.1057	.0296	-.0552	-.1112	.0348	.0095	-.1408	-.0157	-.175	-.0174	-.1422	.0903	-.0634
5	-.2085	.0866	.0994	.1583	.1742	.0285	-.0762	.0605	-.2135	-.0571	-.0522	.0305	.0514
6	-.0732	-.1087	-.0769	.009	.125	.0754	-.0176	-.0207	-.2012	-.0859	-.0926	-.0747	-.0513
7	-.0058	-.0871	-.068	.0272	.2028	-.1517	.1048	-.1083	-.1975	.0992	-.0405	-.1216	-.0579
8	-.1046	.145	.1042	-.1105	-.1123	.0932	-.0575	-.0639	-.1019	-.0706	-.0382	-.1899	.1248
9	.0412	.1004	-.0826	.1014	.1449	-.0136	-.1493	.0307	-.0472	.0749	-.1346	.0543	.0432
10	-.0974	.0308	-.0846	.0336	.1059	.0082	.0596	.1059	.1009	-.0851	-.0305	.0611	.0152
11	.099	-.0821	-.0832	-.0971	-.0887	-.1371	-.0812	-.0963	-.1099	-.1193	-.0395	-.1296	.0807
12	-.0423	-.0328	-.1178	-.0612	.1422	-.0608	-.0871	-.0154	.0376	-.1042	-.1328	.045	-.1355
13	-.0816	-.0766	.0323	-.1267	.0805	-.1556	.1549	.1234	.0037	.0113	.1413	.1127	.0987
14	-.0289	-.0611	-.1313	-.0714	-.0868	-.1137	-.0345	.1283	.1141	-.0698	.1097	.0518	.0306
15	.0256	.0416	.116	.0696	.0806	.086	-.0173	-.1511	-.0782	-.0753	.005	.1367	.1047
16	.1763	.0874	-.0073	-.1333	-.0805	.0933	.1189	.1339	.0624	-.0701	.0737	-.0677	-.1514
17	.0706	.0175	.1039	-.0261	-.0261	-.0772	-.1201	-.0407	.237	.0494	.0498	.1474	.0286
18	-.1185	-.0869	-.1572	-.0098	-.0799	-.1406	-.09	.0256	.12	-.1032	.1462	.0622	-.0583
19	.0973	.1117	.0481	.038	-.0802	.0202	-.1026	-.0099	.0144	.1202	-.0934	-.1018	-.1525
20	-.0046	.0027	-.1602	-.1423	.084	.0628	.0759	-.1127	-.1752	.0924	.0209	.0569	-.0448
21	.1648	-.1553	-.1363	-.1092	-.0681	-.0447	-.0177	.1059	.0014	-.1653	-.0222	-.0058	-.1068
22	.284	-.1408	.0647	.0473	-.0808	-.0724	.1143	.0812	.2181	.0076	.0023	.0799	-.0049
23	-.0852	-.0023	.1554	.1421	.0294	.1542	-.0354	.0061	.0017	.0607	-.1224	-.0968	-.1241
24	-.0105	-.0313	-.1041	-.1206	.0805	-.1706	-.1542	.0455	-.0951	-.0845	-.0621	-.2128	.1419
25	-.0412	-.0212	-.1204	-.0187	-.0001	-.1168	-.0912	-.0109	-.0715	-.0047	.1071	-.0238	-.1053
26	-.0639	.0665	-.079	.0495	-.049	-.1661	-.0778	.0062	.0786	.1067	.1005	-.1222	.1527
27	.1625	-.1357	-.0737	-.0464	-.0512	-.0736	.0878	-.0737	.0206	-.0289	-.056	.1616	-.021
28	-.0844	-.1253	-.0816	.082	-.0924	-.1005	.0612	.1237	.1079	.1497	-.1059	.0084	.0679
29	-.098	-.0969	.1462	-.0143	-.1271	.0697	-.0201	-.1327	.1112	-.0483	.1537	.1389	.0037
30	-.0937	-.0497	-.0431	-.0695	.0226	.1177	.0402	.0142	-.0776	.1162	.0139	-.0891	-.022
31	-.0266	-.1593	.1151	-.0185	-.0224	-.0959	-.1041	.1306	-.0348	-.08	.0828	.0329	-.0185
32	-.1052	.0838	-.1492	.0038	.0069	.012	-.1057	.0752	-.1506	-.0689	.014	-.1147	-.0918
33	.0342	.0854	-.0938	-.0919	-.1537	-.06	.0744	-.1204	.0826	-.041	.053	.1124	-.1138
34	-.0881	.1784	.1139	-.0287	-.079	-.1401	.0012	.0034	-.1996	.1534	.0683	.0451	.0405
35	.0417	.0777	.1389	-.0097	-.0088	.0083	.0818	.0053	-.0547	.0732	-.0583	-.0791	.0476
36	.1049	.0552	-.0269	.0637	.1262	-.0016	.0638	.121	.122	-.0829	.0482	-.0047	-.1483
37	.0187	-.0217	.0594	-.1109	-.0598	.0602	-.1432	-.1289	-.1158	.1347	-.1069	-.0294	-.0958
38	-.0458	-.131	-.0556	.1091	-.0798	-.034	.0611	-.0846	-.0073	-.1367	.0375	-.1402	.095
39	-.1338	.1396	.0567	.0311	.1393	-.0204	.0254	-.1057	-.125	.1115	-.0973	.0552	-.0059
40	-.0003	-.1142	.0402	-.0946	.1285	.0698	-.0301	.1156	.0761	-.0887	.0594	-.0933	.1353
41	0	.0463	-.0733	.1137	-.1462	-.1194	-.0992	-.0305	.1439	-.0958	-.0641	-.0113	.1456

	Second middle layer processing elements												
	55	56	57	58	59	60	61	62	63	64	65	66	67
BIAS	.0452	-.1135	.0428	.2211	.0082	-.0472	.1564	.1843	.1114	.1134	-.2256	-.0544	.1841
42	-.2399	.2471	-.1487	-.1125	-.0376	.2246	-.2574	.1141	.1704	-.2799	.1431	-.1685	-.1852
43	-.1432	.128	-.0821	.2737	.1734	-.2437	.0866	-.1369	-.1995	.1337	.1406	.2674	.0159
44	.2128	.059	-.2464	.1709	-.0966	-.021	-.0825	-.1085	-.2228	.2624	.1625	.0448	-.2541
45	-.1378	.0557	.0797	-.0351	.032	-.0045	.1682	-.277	-.2676	-.1724	.2324	-.0558	.1321
46	.129	-.2388	.1582	.2736	-.1275	-.1156	.2875	.2553	.2551	.2723	.1747	.0603	.2869
47	-.1068	-.0172	-.2526	.0189	-.067	.0416	-.1814	.1491	.0455	-.0853	.056	-.1944	.1697
48	-.1109	-.0585	.2375	-.2063	-.1135	-.2064	-.0196	.0185	.2756	-.0212	.271	-.2249	-.1788
49	-.0831	.143	-.2385	.0574	.216	.3104	-.1737	-.1544	-.237	.0258	-.1274	-.068	.0347
50	.0047	.1236	-.306	-.238	-.2771	.1058	-.0724	.0906	-.0945	-.2305	.1054	-.3034	-.3435
51	-.1652	-.2335	.2433	.2043	.1536	-.0976	.1304	.1367	.2034	-.0414	-.1937	.0091	.1885
52	.0865	.2237	-.2121	.0445	.1021	-.2328	.2395	.0242	-.1496	-.2171	.2296	-.1394	.2187
53	-.2857	.0528	.0959	.0713	.1941	.2383	-.284	.2452	-.1672	-.2112	.1096	-.0534	-.2173
54	.2345	.0788	-.1814	.0508	.0075	-.179	-.0212	-.2046	-.226	.1511	.1663	.2635	-.1237

	Output layer processing element
Middle layer processing elements	68
BIAS	.1748
55	-.2768
56	.2806
57	-.3435
58	-.1035
59	-.1612
60	.42
61	-.2106
62	.1903
63	-.0098
64	-.305
65	.1618
66	-.3404
67	-.3499

6.3c NETWORK WEIGHTS FOR IM7/8553-45

	First middle layer processing elements												
	42	43	44	45	46	47	48	49	50	51	52	53	54
BIAS	.03	.0474	.1381	-.0969	.0042	-.1101	-.1147	.0033	.0919	-.0805	.0603	-.044	-.0664
1	-.0347	.1289	-.0691	.0637	.0777	.1228	-.1163	.0726	-.1033	-.107	-.0573	.0543	-.0071
2	.0254	.0095	.1841	.153	.0288	.1014	.1324	-.0064	.2659	.0514	.0664	.1592	.1784
3	-.0192	-.0376	.18	.0877	.0818	.1613	-.0048	-.1067	.025	-.0031	.1293	.1679	-.035
4	-.0672	.0173	-.0489	-.1113	.0199	.0216	-.1339	-.0015	-.1402	-.0352	-.1418	.1188	-.0733
5	-.1495	.0667	.1138	.1572	.1526	.0464	-.0677	.0818	-.1578	-.0883	-.0498	.0806	.04
6	-.0165	-.1284	-.0603	.0063	.1057	.0914	-.0147	.0011	-.1423	-.1204	-.0888	-.0259	-.0595
7	.2155	-.1724	.0095	.0254	.0777	-.076	.1683	-.0489	.0254	-.0234	-.0103	.0723	-.0493
8	.0907	.0695	.1775	-.1126	-.218	.1549	.0018	-.0113	.0978	-.1823	-.01	-.0198	.1393
9	.0623	.0933	-.0708	.0991	.1485	-.0137	-.1512	.0408	-.0232	.0557	-.1332	.0778	.0428
10	-.1562	.0535	-.0931	.0329	.1547	-.0241	.0454	.0911	.0447	-.0642	-.0367	.0163	.0243
11	.2205	-.1289	-.034	-.0988	-.1486	-.1021	-.0455	-.063	.0144	-.1929	-.022	-.0191	.0913
12	-.0511	-.0287	-.1182	-.0619	.1555	-.0684	-.0926	-.0159	.0291	-.104	-.1348	.0402	-.1357
13	.0649	-.1357	.0988	-.1276	.0002	-.1127	.2106	.1578	.1546	-.0769	.1674	.2493	.125
14	.0071	-.0733	-.1194	-.0715	-.0953	-.1057	-.0241	.1405	.1458	-.0888	.111	.0856	.026
15	-.0849	.0889	.067	.0708	.1638	.0438	-.0549	-.1733	-.1995	-.0071	-.0202	.037	.078
16	.1206	.109	-.0171	-.1318	-.0367	.0631	.1168	.1174	.0043	-.0434	.0672	-.1137	-.142
17	-.0245	.0542	.0908	-.0258	.0544	-.1318	-.132	-.0664	.1433	.088	.0396	.0715	.0465
18	-.1265	-.0829	-.1543	-.0094	-.0613	-.1519	-.0861	.0243	.1091	-.1016	.1439	.0594	-.0554
19	-.0684	.1793	-.0122	.0398	.0371	-.0464	-.1484	-.049	-.1605	.2142	-.1231	-.2474	-.1698
20	.0246	-.0073	-.1528	-.1415	.0727	.0718	.0874	-.1041	-.1515	.0805	.0218	.0827	-.0496
21	.0476	-.1114	-.1569	-.1072	.0154	-.1029	-.0291	.0704	-.1162	-.1112	-.0335	-.1006	-.0859
22	.1328	-.0837	.0446	.0475	.0405	-.1551	.0928	.0388	.0709	.0683	-.012	-.0373	.0249
23	-.1335	.0168	.1528	.1402	.0801	.1218	-.0506	-.0037	-.0425	.072	-.128	-.1298	-.1151
24	.0505	-.0527	-.087	-.1209	.0564	-.1514	-.1401	.0653	-.0391	-.1152	-.0587	-.1581	.133
25	-.0521	-.0152	-.1228	-.0183	.019	-.1292	-.0888	-.0117	-.0848	.0008	.1032	-.0377	-.1052
26	-.0029	.0451	-.062	.0491	-.0731	-.1469	-.0637	.0261	.1346	.0761	.1039	-.0675	.1438
27	.1515	-.1297	-.0762	-.0459	-.032	-.086	.0903	-.0745	.0073	-.0234	-.0599	.1478	-.021
28	-.0551	-.1352	-.0742	.0828	-.1037	-.0915	.0727	.1323	.1316	.1378	-.105	.0341	.0631
29	-.1006	-.0955	.144	-.0122	-.1257	.0686	-.0112	-.1353	.1025	-.0415	.1521	.1357	.003
30	-.0962	-.0483	-.0453	-.0674	.024	.1166	.0491	.0116	-.0862	.123	.0123	-.0923	-.0227
31	-.0376	-.1532	.1126	-.018	-.0032	-.1083	-.1016	.1298	-.0481	-.0745	.0789	.019	-.0184
32	-.1162	.0899	-.1517	.0042	.0261	-.0003	-.1032	.0744	-.1639	-.0634	.0101	-.1285	-.0917
33	.0233	.0915	-.0963	-.0914	-.1345	-.0724	.0769	-.1212	.0693	-.0355	.0491	.0986	-.1138
34	-.0271	.157	.1309	-.0291	-.1031	-.1209	.0153	.0233	-.1436	.1227	.0717	.0998	.0316
35	.0392	.0791	.1367	-.0076	-.0074	.0071	.0907	.0026	-.0633	.08	-.0598	-.0823	.0469
36	.094	.0613	-.0294	.0642	.1454	-.014	.0663	.1202	.1087	-.0775	.0443	-.0185	-.1482
37	.0077	-.0156	.0569	-.1105	-.0407	.0478	-.1407	-.1296	-.1291	.1401	-.1107	-.0433	-.0957
38	-.0483	-.1296	-.0579	.1112	-.0785	-.0351	.07	-.0872	-.0159	-.1299	.036	-.1433	.0944
39	-.0729	.1183	.0737	.0307	.1152	-.0013	.0395	-.0858	-.069	.0809	-.0939	.1099	-.0147
40	-.0112	-.1082	.0377	-.0942	.1477	.0574	-.0276	.1148	.0628	-.0832	.0556	-.1072	.1354
41	-.011	.0523	-.0758	.1141	-.127	-.1318	-.0967	-.0313	.1305	-.0903	-.068	-.0251	.1456

	Second middle layer processing elements												
	55	56	57	58	59	60	61	62	63	64	65	66	67
BIAS	.07	-.1314	.062	.2236	.0185	-.0535	.1651	.1734	.1117	.1361	-.2219	-.032	.2127
42	-.1999	.2154	-.1091	-.1082	-.0183	.174	-.2404	.0883	.1657	-.2495	.1321	-.1336	-.1508
43	-.1266	.1037	-.0525	.2775	.193	-.2737	.1004	-.1548	-.1951	.1554	.1089	.2936	.0545
44	.1897	.0887	-.2835	.1659	-.1191	.0202	-.0991	-.086	-.2259	.2375	.1951	.0139	-.2962
45	-.1325	.0464	.0905	-.0327	.0399	-.0187	.1753	-.2839	-.266	-.1628	.2154	-.0442	.1472
46	.1127	-.2248	.1391	.2733	-.1365	-.0891	.2824	.2685	.2574	.2643	.1811	.0498	.274
47	-.1003	-.026	-.241	.0195	-.0588	.021	-.1764	.1397	.0451	-.0806	.0378	-.1877	.1802
48	-.1472	-.0169	.1886	-.2146	-.1439	-.1608	-.0448	.0475	.2706	-.0642	.3092	-.2737	-.2431
49	-.0581	.1221	-.2132	.0618	.2286	.2805	-.1609	-.1699	-.2389	.0484	-.1353	-.0425	.0594
50	.0365	.1039	-.2815	-.2351	-.2675	.0716	-.0615	.0742	-.1011	-.2092	.11	-.2801	-.3274
51	-.175	-.2324	.2433	.2041	.1555	-.0993	.1297	.1371	.2067	-.0471	-.2075	.0051	.1896
52	.0688	.2473	-.2403	.0395	.0836	-.2013	.2242	.0415	-.1527	-.2404	.2597	-.167	.1822
53	-.2981	.0739	.069	.0692	.176	.2659	-.2944	.2617	-.1716	-.2263	.1409	-.0733	-.2504
54	.1679	.1523	-.2721	.0394	-.0461	-.0782	-.0619	-.148	-.2297	.0854	.2341	.1851	-.2251

	Output layer processing element
Middle layer processing elements	68
BIAS	.1029
55	-.1631
56	.2785
57	-.3448
58	-.1032
59	-.1985
60	.3107
61	-.1968
62	.1727
63	-.0575
64	-.2415
65	.3249
66	-.2983
67	-.4549

6.4 UN-FILLED KE/EP VESSEL AMPLITUDE DISTRIBUTIONS (CHANNEL 1)

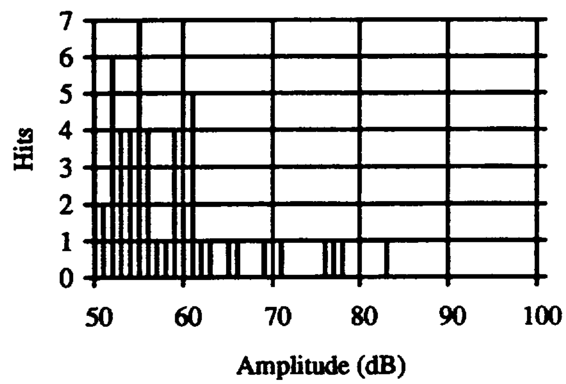

D249-250

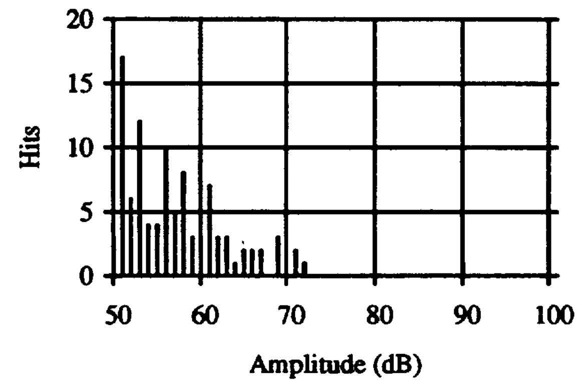

D205-206

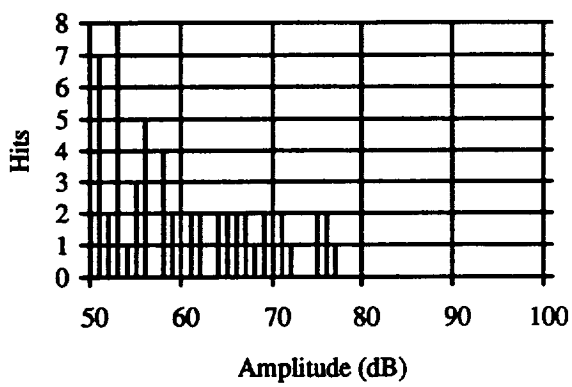

D191-192

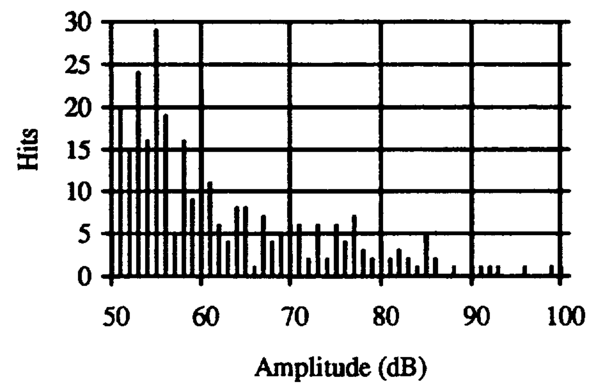

D243-244

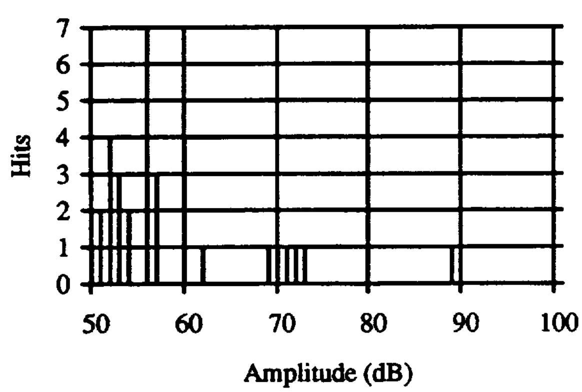

D245-246

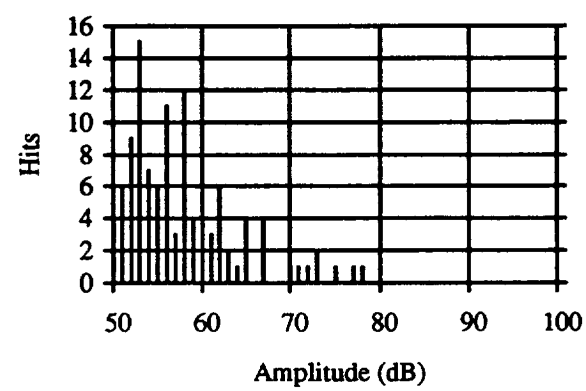

D231-232

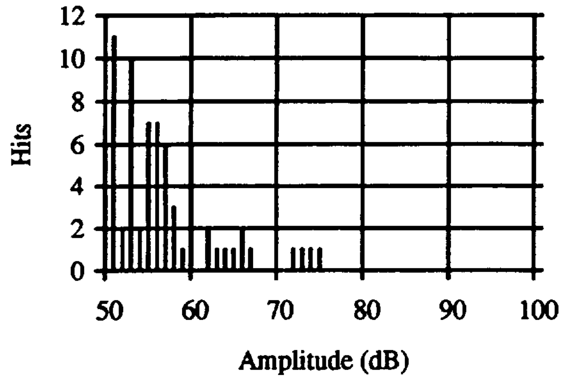

D181-182

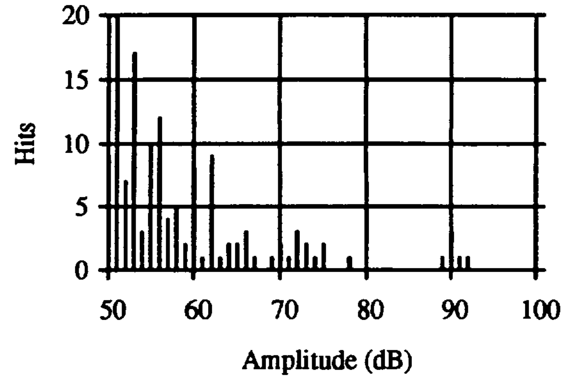

D223-224

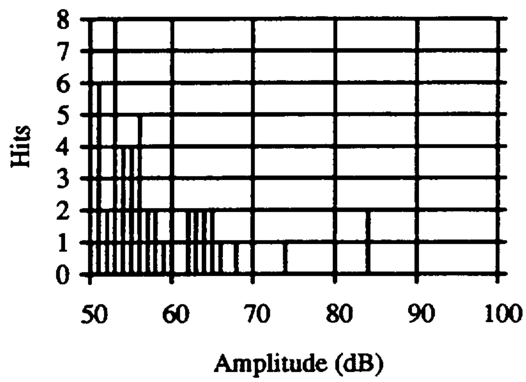

D185-186

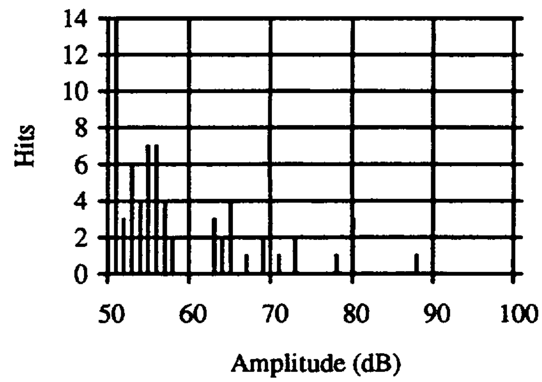

D175-176

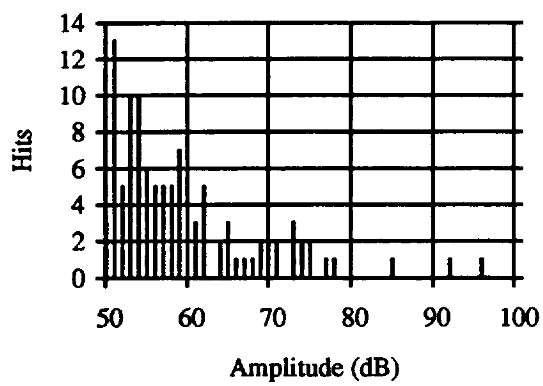

D255-256

6.5 NETWORK WEIGHTS FOR UN-FILLED KEVLAR VESSELS

	Middle layer processing elements																		
Input	52	53	54	55	56	57	58	59	60	61	62	63	64	65	66	67	68	69	70
BIAS	.0218	.0268	-.1175	-.0582	.1212	-.0332	.0431	.1257	-.1229	-.0092	-.1282	.0425	.1432	-.1076	.0338	-.1059	.1096	-.0044	-.0019
1	-.0407	-.1257	-.122	-.0143	-.136	-.114	.0041	.1074	.073	-.0018	.0348	.0812	.0321	.0944	-.1235	-.0114	-.1382	.0045	-.0692
2	-.0761	-.019	.0326	-.0006	-.0916	.0364	-.1009	-.0684	-.0802	-.1219	-.0485	.0159	-.0398	-.0337	.0969	.0221	-.032	.012	.0203
3	-.0581	-.0644	.1275	-.0871	.1182	-.0806	.0521	-.0342	-.0865	.0603	-.1264	-.0545	-.123	-.0047	-.0952	.0421	-.069	-.0165	-.0843
4	-.0654	-.0998	-.0618	-.0247	.0398	-.0619	.0572	-.1321	.0628	.0433	-.0505	-.0286	.1343	-.001	-.02	-.0358	-.112	-.0989	.0494
5	-.1295	.0273	-.1087	-.0091	.1251	.1427	-.0007	.0737	-.047	-.0728	-.079	-.1288	-.0565	-.0951	-.0654	-.1012	.0087	.0874	.0823
6	.0017	.1335	-.0792	.0493	.0417	-.0534	.0306	-.1236	.0358	.0131	.0282	.0076	.0663	.0018	.1662	-.0748	.0711	.0003	.0303
7	.1037	.0743	-.086	-.1059	.0584	-.0357	-.031	-.0503	.105	.1048	-.0976	.0403	-.1273	-.0845	-.0138	.1117	.0607	.0494	-.157
8	-.0392	-.121	-.0433	.1027	.0567	.1231	.0547	.1141	-.1177	.1131	.111	-.0937	.0674	-.1435	.0377	-.0195	-.1494	.0867	.1505
9	.068	.1463	.1137	.0213	-.0832	-.1446	-.0863	-.1116	-.0465	.1109	-.0886	.0981	-.0595	.086	.0207	.0092	.0177	-.1036	.0294
10	-.125	.013	-.0544	-.0904	.1175	-.099	.1028	-.0071	-.0807	-.1145	.1322	-.1199	.0739	-.0987	-.0567	-.1241	-.1069	.1016	-.1031
11	.1135	-.1518	.1292	.1066	-.0404	-.0717	-.0846	-.0454	-.022	.1044	-.0275	-.085	.1675	.0052	.0558	-.0929	.0582	.0511	.0593
12	-.0307	-.0563	-.1499	-.0028	-.009	.0569	-.0052	.0639	-.0308	.0413	.0596	.0918	-.1001	.0933	-.0657	.0151	-.03	.0368	-.0095
13	-.025	.0706	-.1208	.0594	-.0801	-.0703	.0742	.1189	-.1252	-.1647	.0124	-.1513	-.0432	.1399	-.0749	-.1204	-.0169	-.1039	-.0852
14	.0185	-.0303	.1033	.0874	-.0497	.0625	.0514	-.0838	-.0315	.0635	-.018	.0343	-.0863	.137	.1479	.0708	.1005	-.1095	-.091
15	.0173	-.0549	.1438	.1084	-.1569	-.0195	-.0803	-.0944	-.0262	-.0578	-.0236	-.0918	.0034	.0606	.0521	-.0613	.0716	-.0569	.0867
16	.1239	.0712	-.0442	.01	-.0759	-.1533	-.001	.1038	-.1228	-.0542	-.0766	.0894	.042	.0545	.1635	-.082	.1024	-.1134	-.1634
17	-.016	-.114	.0465	.1321	.0754	-.0909	-.0015	.0276	.1299	-.1146	-.1019	-.0588	.1198	.1415	.0806	.0185	.0853	-.0173	-.0005
18	-.1013	-.1043	-.0659	.0906	.0677	-.0778	.0924	-.0369	.101	-.1524	.0307	.1186	-.1481	-.057	-.0609	-.0539	.1255	.0904	.0674
19	.0648	-.0401	.0383	.1264	-.091	.0436	-.15	-.0898	.0002	-.0656	.05	.05	-.0463	.0769	.062	-.1051	-.0744	.1488	-.1862
20	.0067	-.0944	.0623	-.123	-.1629	.0872	-.0415	-.0996	.0687	-.0208	-.1413	.0151	.1166	-.137	-.1231	.1004	-.044	-.1511	.0297
21	.0205	-.2017	-.0279	.1423	-.0425	.0213	-.0275	.0466	.044	.182	-.0956	.1826	.0698	.056	-.0999	-.0968	.0862	-.1253	.1956
22	.1666	.1971	-.1577	.1193	.1311	-.0355	.0206	-.1181	.1157	-.0536	.1054	-.0728	-.1296	.1645	.0965	.0071	.1137	.037	-.2566
23	-.1173	.0739	.0608	-.0902	-.095	-.0942	-.0194	.0506	-.0873	.1296	-.0134	-.0989	-.0484	.0922	.1311	.0739	-.0198	-.0694	-.1319
24	.0921	.2541	.0703	.1202	-.0742	-.1704	.0148	-.0753	.0069	-.1646	.1414	-.0488	-.2001	.0924	.0182	-.0958	-.0414	.0075	-.0659
25	-.0375	.082	.0669	.0645	.1176	.0524	-.097	-.1336	-.0285	.0108	.1323	-.1274	.1338	-.0424	.0222	-.1274	.0178	-.0829	-.044
26	-.0127	.0257	-.081	-.0818	-.15	.0242	.1555	-.0941	-.0076	-.0917	.0299	.1247	.0849	.1041	-.1541	-.0201	-.0437	.1056	.0733
27	.1664	.0652	.1002	.0706	-.0698	.0265	-.0786	-.0206	-.126	.0318	-.0773	-.0275	-.0354	.0938	.0175	.002	-.1083	.1004	-.1876
28	-.0373	-.0992	-.0104	-.0383	-.1206	.0387	-.134	-.0851	-.0512	.0788	-.0745	.0195	-.098	-.0121	.1003	-.0934	.1222	-.0293	.0205
29	-.0732	.1373	-.0011	.0417	-.058	-.1552	-.159	-.08	.0916	-.095	.1086	-.0046	.0064	.0506	.0839	.1083	.1161	.033	-.1301
30	-.0612	-.0365	-.135	-.0643	-.0464	.0178	-.1705	-.0543	.0861	-.0594	-.0606	-.0322	.043	-.0387	.0782	-.1296	.125	.0345	-.2007

	Middle layer processing elements																		
Input	52	53	54	55	56	57	58	59	60	61	62	63	64	65	66	67	68	69	70
31	-.0167	.0782	.066	-.0392	.0806	.0064	-.1074	.0708	-.0546	-.06	.058	-.0272	-.0044	-.0881	-.1	.0973	.0147	-.0515	-.0823
32	-.0639	.2227	-.0281	.0498	.1584	-.0914	-.0908	-.1084	-.1033	-.1958	-.0353	.0149	.0707	.0739	.169	-.0772	.1449	-.1043	-.0412
33	-.0537	-.2612	.0254	.0402	-.2079	.028	.124	.1482	.163	.2502	-.0944	.0896	.0216	-.3096	-.1215	-.0891	-.0654	.0071	.3096
34	-.0209	.117	-.0568	.0347	.001	.0074	.0456	.067	.0126	-.0936	-.0256	.0136	.0564	-.0086	.0987	.1295	.0795	.0492	-.1224
35	-.0363	-.0576	-.0049	.0952	-.1734	.1872	.0863	-.0771	.0977	.1259	-.0017	.0626	.1933	-.256	-.1375	.0862	-.0771	-.1656	.2119
36	.0817	-.0499	-.0572	.0514	-.1124	-.0195	.042	.0551	.0103	-.0514	-.0966	-.0205	-.0964	-.0308	.0948	-.1083	.0469	.1238	-.0666
37	.0043	.096	.0695	.0179	.0024	-.0983	.0384	.0617	.0453	.0012	.0427	-.0485	-.1082	.1019	-.0333	.0695	.0255	.0603	-.0584
38	-.0312	-.0358	-.1361	-.0709	-.0014	-.0118	.1207	-.1088	.0657	.1217	-.1383	.1009	-.1433	.1246	-.0404	.0887	.1044	-.0113	.0943
39	-.0679	-.0479	-.0162	-.0279	.0389	.0826	-.0507	-.0055	-.0524	-.0353	.0968	-.1097	.1333	-.0676	.0248	.0363	-.0627	-.0477	-.0451
40	.0021	.1283	-.0263	-.0984	-.0204	-.0117	-.0062	.0627	.0411	-.0775	-.0624	.0514	.0146	.0212	.1352	-.0909	.1254	.0234	.0358
41	.0023	-.0453	.0169	-.1181	.01	-.0767	.1185	-.0265	-.0979	.0241	.0983	.033	.1309	-.1146	-.0885	.0567	-.1229	-.0148	.1003
42	.035	-.0899	-.1199	.0223	.0475	-.0241	.115	.1173	.0335	-.0463	.0681	.1103	-.1156	.0546	-.1284	-.0525	.052	-.0043	.0205
43	.1094	-.0703	-.0892	-.0021	-.1221	.0435	-.0157	-.0434	-.0829	-.061	.0326	-.0002	-.0439	.1211	.1125	.0743	-.1378	.1217	.0212
44	.0617	-.0847	.0247	.018	-.1087	.07	-.1458	.1048	.0512	.0863	.0317	-.0443	.0946	.1075	.1091	-.0628	-.0475	-.1269	-.1564
45	-.0187	.0291	.1342	-.1198	-.1172	-.0626	-.087	-.073	-.0597	.0454	-.1089	.0825	-.0712	-.1048	-.0414	.1338	-.0315	.0161	.0215
46	.0229	-.0868	-.1263	-.0978	.0806	-.0259	.0536	-.0624	-.0337	.0103	-.0114	-.135	-.0927	.0559	.0126	-.0501	-.1266	.0179	.0976
47	.0672	.1294	-.0343	-.0121	-.0166	.1076	-.0494	-.0374	.0516	.0532	-.0258	-.0235	-.1221	-.1181	.1109	-.1265	.1058	-.1201	-.1543
48	-.12	-.0227	.0509	.1311	-.1288	.1352	-.0179	.1038	.046	-.1127	.0556	.0097	.0751	.0705	.1131	-.0942	.0745	-.1396	.1126
49	-.1026	.1017	-.0591	-.0419	-.0544	-.1432	-.086	.0662	.1057	.0728	.0344	-.0572	-.1237	.1281	-.0917	-.026	.0893	.1026	-.1166
50	.1012	-.1457	.0811	-.0695	-.0182	.1146	.1379	-.0756	.1113	.0309	-.1077	.0217	.0686	-.1141	.1209	-.0199	.0449	.1175	-.0231
51	.0788	.0308	-.0041	.1041	.0989	-.0503	.0238	.1195	.077	.102	.1123	-.0958	.1342	-.0978	-.0249	-.03	-.1013	-.1404	.1135

	Output layer processing element
Middle layer processing elements	71
BIAS	-.1872
52	.1427
53	.4089
54	-.1559
55	-.0352
56	.2191
57	-.2196
58	-.2297
59	-.0755
60	-.0849
61	-.299
62	.0817
63	-.2048
64	-.2269
65	.3698
66	.292
67	-.0618
68	.1498
69	.1203
70	-.4523

6.6 FILLED KE/EP VESSEL AMPLITUDE DISTRIBUTIONS (CHANNEL 1)

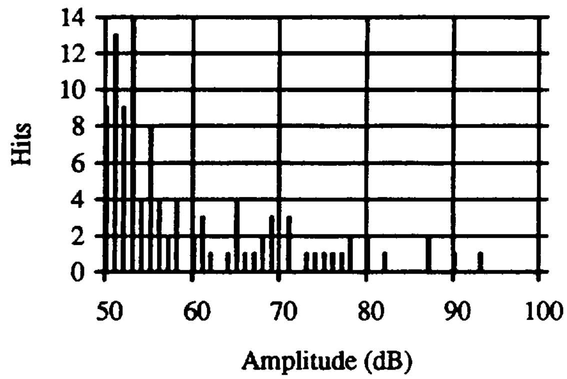

D254-255

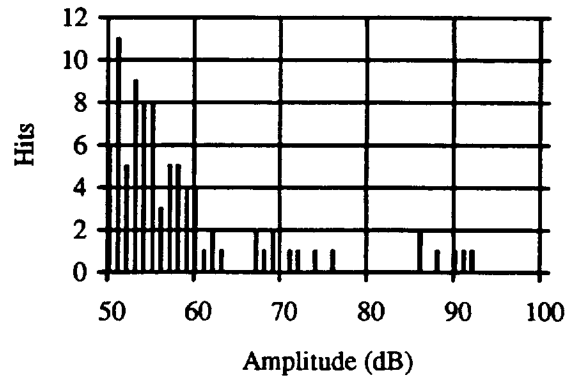

D213-214

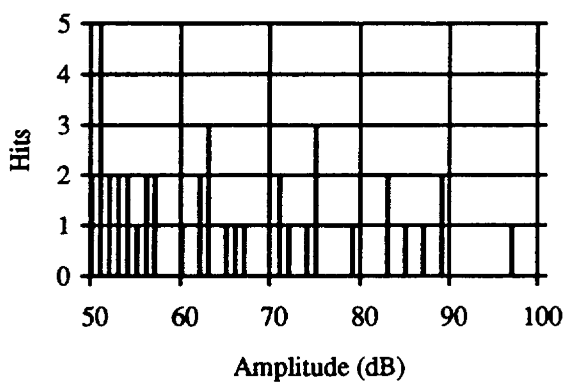

D169-170

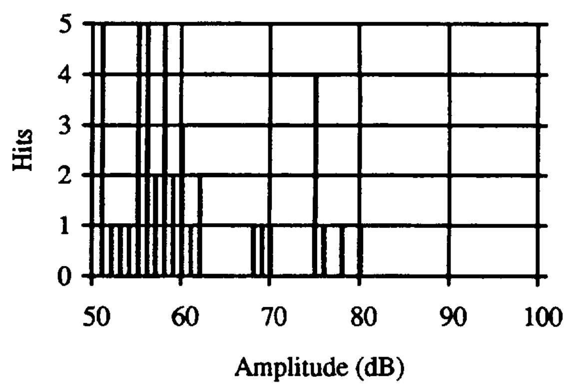

D187-188

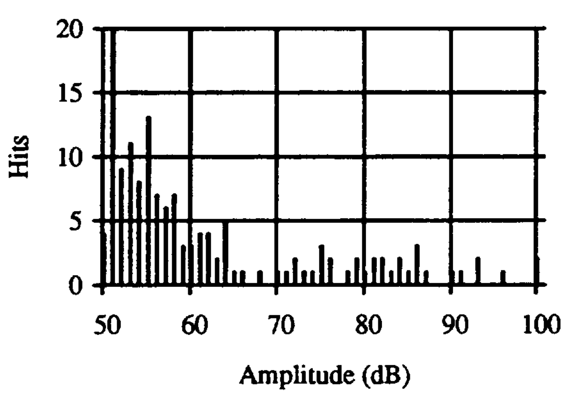

D239-240

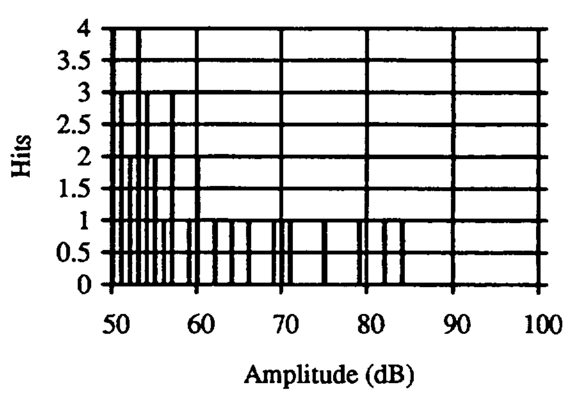

D235-236

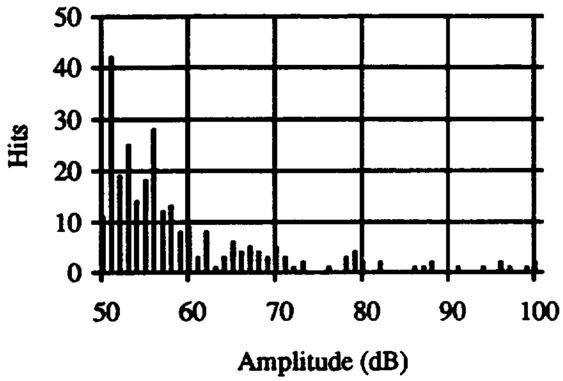

D241-242

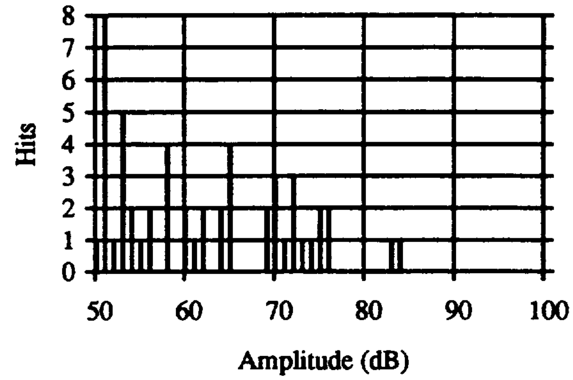

D177-178

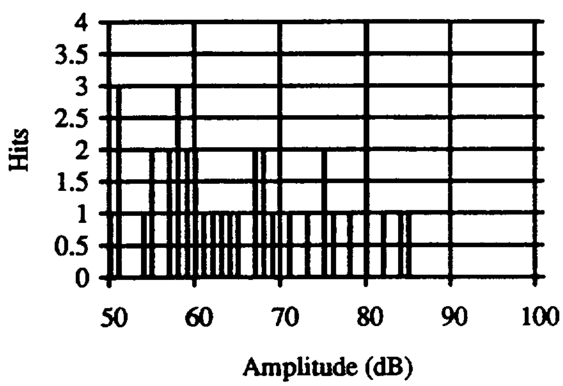

D225-226

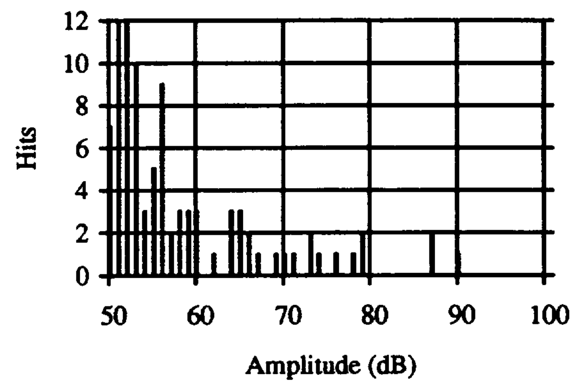

D201-202

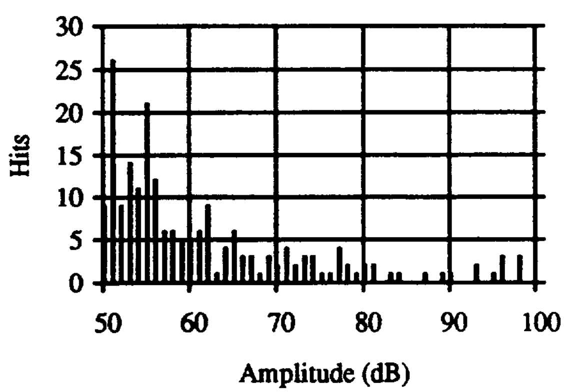

D233-234

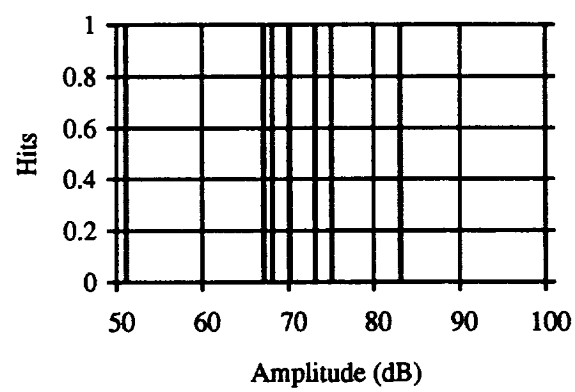

D237-238

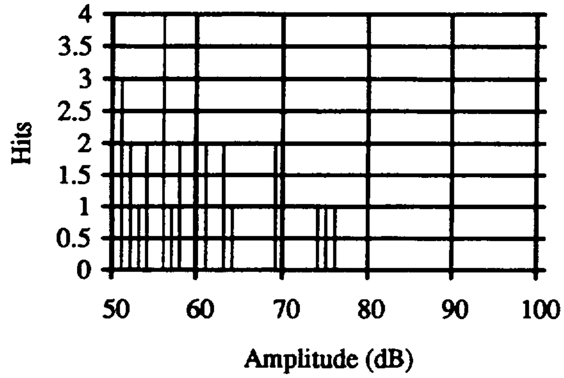

D161-162

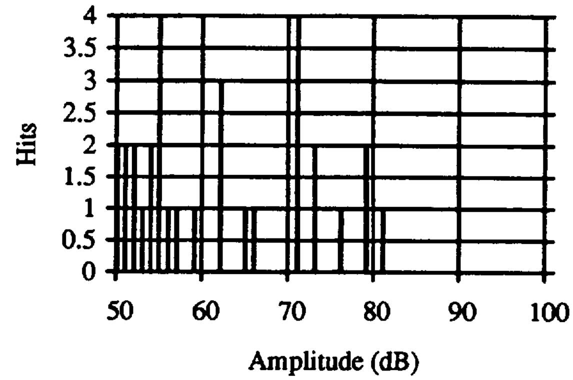

D221-222

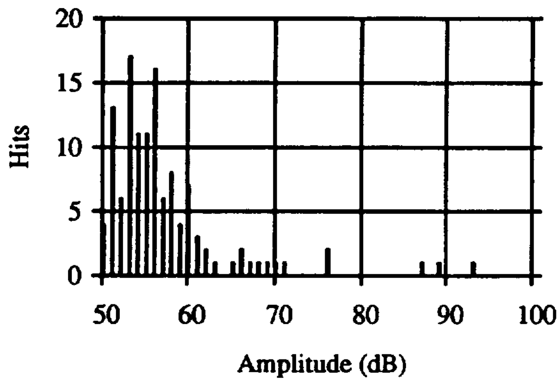

D215-216

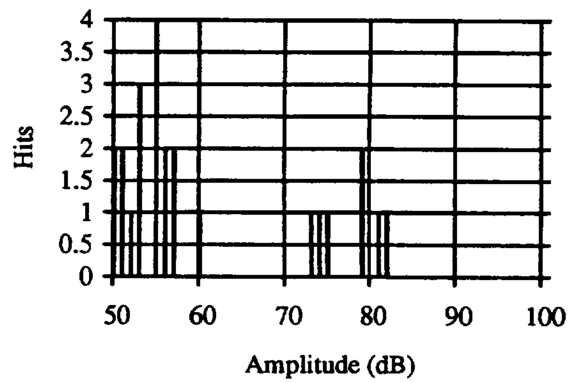

D163-164

6.7 NETWORK WEIGHTS FOR FILLED KEVLAR VESSELS

	Middle layer processing elements															
Input	52	53	54	55	56	57	58	59	60	61	62	63	64	65	66	67
BIAS	.0199	.0424	-.1429	-.0746	.133	-.0309	.032	.1082	-.1209	-.0378	-.1128	.0164	.1287	-.0727	.0673	-.0963
1	.0057	-.0728	-.1169	.0096	-.1192	-.1471	-.0334	.142	.0623	.0033	.0245	.0736	.0138	.1022	-.1232	-.0415
2	-.0887	-.0312	.0357	-.0067	-.0955	.0493	-.0863	-.0859	-.0793	-.1303	-.0399	.0207	-.0399	-.0307	.0969	.0321
3	-.0497	-.0693	.15	-.07	.109	-.0757	.0589	-.0142	-.0892	.0853	-.1352	-.0336	-.1166	-.0299	-.1237	.0332
4	-.0625	-.0684	-.0814	-.0324	.0585	-.0735	.0407	-.1463	.0575	.0118	-.0378	-.0499	.1125	.0361	.0094	-.0367
5	-.1203	.0397	-.1013	.0005	.1277	.1356	-.0063	.0847	-.0514	-.0682	-.0819	-.1246	-.0613	-.0968	-.0725	-.1116
6	-.0065	.1005	-.0468	.0639	.0196	-.034	.0573	-.108	.0375	.0493	.018	.0421	.0858	-.0409	.1228	-.0764
7	.1023	.0529	-.0595	-.0915	.0418	-.0204	-.0125	-.035	.1052	.1345	-.1059	.0678	-.1137	-.1182	-.049	.109
8	-.0127	-.071	-.0595	.1031	.0813	.0968	.0228	.1102	-.1259	.0818	.1195	-.1194	.0399	-.1035	.0695	-.0308
9	.0688	.123	.1383	.0371	-.1019	-.1276	-.0696	-.0909	-.0445	.1456	-.0993	.1247	-.0431	.048	-.0162	.006
10	-.1461	-.0109	-.0466	-.0939	.1068	-.0763	.1262	-.0187	-.0786	-.1105	.1379	-.1059	.0808	-.1085	-.0689	-.1122
11	.1169	-.106	.0938	.0906	-.0111	-.0939	-.1126	-.0694	-.0279	.0529	-.0089	-.1234	.1359	.0647	.1069	-.0941
12	-.0729	-.0886	-.1578	-.0247	-.0164	.09	.0277	.0213	-.0262	.0196	.08	.0954	-.0979	.1043	-.0572	.0442
13	-.0547	.0127	-.0893	.0654	-.112	-.0239	.122	.1208	-.1192	-.1261	.0093	-.1089	-.016	.0907	-.1231	-.1036
14	.0141	-.0464	.1226	.0942	-.0603	.0741	.0678	-.0822	-.0317	.0769	-.0196	.0533	-.0791	.1187	.1267	.0717
15	.0207	-.0182	.1197	.0977	-.134	-.0388	-.102	-.1112	-.0317	-.0964	-.01	-.1197	-.0216	.1057	.0892	-.0648
16	.157	.059	.0083	.0534	-.0996	-.1556	.003	.1674	-.125	.0169	-.1094	.1334	.0653	-.0149	.0948	-.1122
17	-.1421	-.1669	-.032	.0337	.0881	-.022	.06	-.1331	.1432	-.2412	-.0221	-.1054	.0982	.2465	.1808	.1135
18	-.0851	-.1106	-.0328	.1166	.0542	-.0743	.0992	-.0037	.0977	-.1131	.0149	.1482	-.1372	-.0959	-.1029	-.069
19	.0109	-.0999	.0467	.1086	-.1138	.0895	-.0989	-.1236	.0086	-.0637	.0632	.0725	-.0278	.0607	.0459	-.0746
20	.0136	-.049	.0275	-.1396	-.1338	.0646	-.07	-.1265	.0633	-.0746	-.122	-.0245	.0849	-.0766	-.0702	.1002
21	.0309	-.1433	-.074	.1242	-.0066	-.0107	-.0686	.0253	.0382	.1231	-.077	.1314	.033	.1266	-.0365	-.1022
22	.1179	.0785	-.0933	.1331	.0656	.0395	.1074	-.1072	.1309	.0276	.0893	.0074	-.0677	.0588	.0003	.031
23	-.1216	.0792	.0489	-.0965	-.0906	-.0913	-.022	.0407	-.0867	.1154	-.0057	-.109	-.055	.107	.1442	.0782
24	.0942	.1593	.169	.1748	-.1439	-.1226	.0776	.0002	.0153	-.0324	.0943	.0522	-.1317	-.0545	-.1197	-.1105
25	-.1043	.0465	.0402	.0221	.117	.0904	-.0587	-.2033	-.022	-.0373	.167	-.1384	.129	-.0051	.055	-.0849
26	.0026	.0558	-.0983	-.0823	-.1357	.0044	.1304	-.0889	-.01	-.1083	.0317	.1026	.0707	.1278	-.1325	-.0314
27	.1293	-.0182	.1347	.0749	-.1144	.077	-.0223	-.0149	-.1125	.0828	-.0875	.0189	.0079	.0262	-.0407	.0191
28	-.0459	-.116	.0075	-.0311	-.1314	.0508	-.117	-.0807	-.0517	.0946	-.0772	.0393	-.0901	-.0317	.0773	-.0935
29	-.0413	.1245	.0544	.0859	-.0819	-.1562	-.1523	-.0174	.0883	-.0234	.0764	.0427	.0295	-.0198	.0127	.0787
30	-.0928	-.1012	-.1066	-.0614	-.0806	.0584	-.1239	-.0531	.0954	-.0222	-.0666	.0059	.0752	-.0894	.0325	-.1153

	Middle layer processing elements															
Input	52	53	54	55	56	57	58	59	60	61	62	63	64	65	66	67
31	.006	.0608	.1169	-.0039	.0579	.0084	-.0962	.1201	-.0565	.0009	.032	.0158	.017	-.1493	-.1624	.0743
32	-.1107	.1249	.0244	.0587	.106	-.0291	-.0162	-.1053	-.0919	-.1341	-.0456	.0814	.1193	-.0087	.0916	-.056
33	.0143	-.0629	-.0942	.0074	-.0956	-.0911	-.0171	.1124	.1386	.093	-.0549	-.0545	-.0895	-.1135	.0535	-.1241
34	-.0309	.1136	-.0606	.0299	.0012	.0113	.0502	.058	.0132	-.1016	-.0204	.0115	.0542	-.0021	.1028	.1325
35	-.069	.0973	-.1835	-.0142	-.052	.121	-.007	-.2315	.0842	-.1216	.0965	-.1157	.068	.0171	.112	.124
36	.0777	-.0434	-.0708	.0441	-.107	-.0228	.0362	.0471	.0113	-.0668	-.0907	-.0337	-.1026	-.0144	.1103	-.1077
37	.0004	.1025	.0559	.0106	.0078	-.1016	.0326	.0537	.0462	-.0142	.0486	-.0617	-.1144	.1183	-.0179	.0701
38	-.0468	-.0556	-.124	-.0729	-.0106	.009	.1423	-.1182	.0665	.1279	-.1331	.1165	-.138	.1147	-.0534	.1
39	.0238	-.0038	.036	.038	.0338	.0319	-.0973	.1009	-.062	.0423	.0467	-.0842	.1419	-.1289	-.0363	-.0311
40	-.0136	.1085	-.0142	-.1004	-.0296	.009	.0155	.0533	.042	-.0713	-.0572	.067	.0199	.0113	.1222	-.0797
41	-.0833	-.0941	-.0215	-.1766	.009	-.0224	.1708	-.1289	-.0886	-.047	.1477	.0166	.1242	-.0625	-.04	.1195
42	.031	-.0834	-.1335	.0151	.0529	-.0274	.1092	.1093	.0345	-.0617	.074	.0971	-.1218	.071	-.1129	-.0519
43	.1054	-.0638	-.1028	-.0093	-.1167	.0402	-.0215	-.0514	-.082	-.0764	.0385	-.0134	-.0501	.1375	.128	.0749
44	.043	-.1059	.0359	.0169	-.1184	.0864	-.1245	.0961	.052	.0914	.035	-.029	.101	.0965	.0948	-.0557
45	-.0196	.0369	.1215	-.128	-.1113	-.0614	-.0926	-.0817	-.0587	.0311	-.1012	.0695	-.0785	-.0874	-.0246	.1386
46	.0072	-.1066	-.1142	-.0998	.0714	-.0051	.0752	-.0718	-.0329	.0165	-.0062	-.1194	-.0874	.046	-.0004	-.0389
47	.0485	.1083	-.0231	-.0131	-.0262	.1239	-.028	-.0461	.0524	.0583	-.0225	-.0081	-.1157	-.129	.0965	-.1194
48	-.1209	-.0149	.0382	.123	-.1229	.1364	-.0234	.0951	.047	-.127	.0633	-.0034	.0679	.0879	.1299	-.0894
49	-.1182	.0818	-.047	-.0438	-.0635	-.1224	-.0644	.0568	.1065	.079	.0396	-.0417	-.1184	.1182	-.1047	-.0148
50	.0972	-.1392	.0675	-.0768	-.0128	.1113	.1321	-.0836	.1122	.0155	-.1018	.0084	.0624	-.0977	.1364	-.0193
51	.0748	.0373	-.0177	.0969	.1043	-.0535	.018	.1115	.078	.0866	.1182	-.1091	.1279	-.0814	-.0094	-.0294

Middle layer processing elements	Output layer processing element 68
BIAS	.2545
52	-.2573
53	-.1216
54	-.1844
55	-.1859
56	.0413
57	.1447
58	.1127
59	-.3383
60	.0497
61	-.255
62	.143
63	-.1253
64	.0021
65	.2272
66	.2258
67	.1835

Table 9. Middle layer to output weights.

6.8 RBTBOT.M

```
% Program RBTBOT.M
% This program automates the acousto-ultrasonic pressure vessel inspection
% process by controlling the robot and A/D data acquisition board.
% Make sure that the sampling rate and size are the correct size for the A/D.
!cls
clear
 h=4096;                    % Sample size
 s=32;                      % Sampling rate (Mhz)
q=input('Enter the output filename. ','s'); % Enter an output filename
disp(' ')
n=input('Enter the sample size. ');       % Enter a samples                    % Number of samples to read
disp(' ')
tt=input('Press enter when ready to start.');% Confirm program start
disp(' ')
ptime=input('Enter the time to pause during data display. '); % Pause time              % Number of
samples to read
disp(' ')
uf=input('Enter upper frequency limit (1 = 1Mhz, 2 = 2Mhz, 3 = 3Mhz).');
disp(' ')
if uf==1
 uf = 128;                  % 4096/32
end
if uf==2
 uf = 256;
end
if uf==3
```

```
  uf = 384;
 end
 lb=1;                          % File number counter
 for ps=1:40                      % Position index
 for k=1:n                       % Sample index
 !downrbtn                      % execute DOWNRBTN.EXE (Quickbasic)
 fprintf('Collecting data from buffer for signal %.0f at position %.0f .\n',k,ps)
 disp(' ')
 fprintf('Total samples taken %.0f.\n',lb)
 disp(' ')
  !p2>data.m;                 % Store data from buffer in a Matlab File
 disp('Moving data into Matlab.')
  data;                         % Transfer data to Matlab.
 disp(' ')
 !uprbt                         % execute UPRBT.EXE (Quickbasic)
  qout =[q,int2str(lb),'.bas'];          % Define signal filename
  a=1.28-(a*.01);                  % Scale data (Original size 0-255)
  eval(['save  ',qout,' a',' -ascii'])     % Save signal
 y = fft(a,h);                    % Calculate the FFT
  x=1:h;                         % X axis points
  t=x*.03125;                      % Scale time axis
  Pyy = y.*conj(y)/h;                 % Compute power spectrum
  fname=[q,'P',int2str(lb),'.bas'];        % Construct an output filename
  power=Pyy(5:uf);                % Group the first 2 MHz worth of points
  eval(['save ',fname,' power ','-ascii'])  % Save the grouping to fname
  f=s*(0:uf)/h;                    % Compute frequency axis
  et=sum(Pyy(5:uf));                  % Compute total energy
!cls;
  subplot(211),plot(t(1:h-1),a(1:h-1))        % Plot signal versus time
   xlabel('time microseconds');
   title(['Signal ',qout,' .']);
   ylabel('volts');
   grid;
  subplot(212),semilogy(f(5:uf),Pyy(5:uf)); % Plot power spectrum
   xlabel('frequency MHz');
   title(['Power spectrum ',fname,' has a total energy of ',num2str(et),'.']);
pause(ptime);
clg;
lb=lb+1;                          % Increment file counter
end
!spinbt                         % execute SPINBT.EXE (Quickbasic)
end
disp(' Do you wish to calculate energy values or combine spectral values?');
qe=input('Yes=1 No=2 ');
 if qe==1
  !enrgydta
 end
q=input('Do you wish to take more data? Yes=1 No=2 ');
 if q==1
  rbtbot
 end
end
```

6.9 UPRBT.EXE

```
' This program moves the SCARA robot arm up.
1 CLS
10 OPEN "com2:9600,e,7,2,cs,ds,cd" FOR RANDOM AS #1
160 FOR I = 1 TO 5
170 PRINT #1, "C+20"
180 PRINT #1, "C?"; : GOSUB 220
190 IF W > 45 THEN 180
200 NEXT
210 END
220 IF LOC(1) = 0 THEN 220 ELSE W$ = INPUT$(LOC(1), #1)
230 W = ASC(W$) - 32
240 RETURN
```

6.10 SPINBT.EXE

```
' This program spins the pressure vessels 40/1600 of a turn.
1 CLS
10 OPEN "com2:9600,e,7,2,cs,ds,cd" FOR RANDOM AS #1
170 PRINT #1, "H+40"
180 PRINT #1, "H?"; : GOSUB 220
190 IF W > 45 THEN 180
200 END
220 IF LOC(1) = 0 THEN 220 ELSE W$ = INPUT$(LOC(1), #1)
230 W = ASC(W$) - 32
240 RETURN
```

6.11 DOWNRBT.EXE

```
' This program lowers the SCARA robot head after a request.
2 CLS
3 PRINT "PRESS ENTER TO LOWER SENSOR."
4 INPUT Q$
10 OPEN "com2:9600,e,7,2,cs,ds,cd" FOR RANDOM AS #1
20 PRINT #1, "C-1"
30 PRINT #1, "J"; : GOSUB 110
40 GOSUB 140
50 IF I(0) = 1 THEN 90
60 PRINT #1, "C?"; : GOSUB 110
70 IF W > 45 THEN 30
80 GOTO 20
90 PRINT #1, "CX";
100 END
110 IF LOC(1) = 0 THEN 110 ELSE W$ = INPUT$(LOC(1), #1)
120 W = ASC(W$) - 32
130 RETURN
140   IF W AND (2 ^ 0) THEN I(0) = 1 ELSE I(0) = 0
150 RETURN
```

6.12 CALIBRATION PROCEDURE FOR ROBOT LOAD CELL

1. Calculate force required for sensor pressure
2. Measure voltage across CD (Box 9 - 2) with no load (CDNL)
3. Measure voltage across CD with load (CDL)
4. Subtract CDL - CDNL to get X
5. Measure voltage across BD (Box 4 - 2)
6. Adjust potentiometer until voltage across BD is equal to voltage across CD (no load) minus X/2 [BD = CDNL +X/2] (Clockwise decreases BD output voltage)
7. Measure voltage across ED. No load should equal 5 volts; Load should equal 0 volts. (External connections not installed)

1.157 kg/volt with offset 2.908 volt

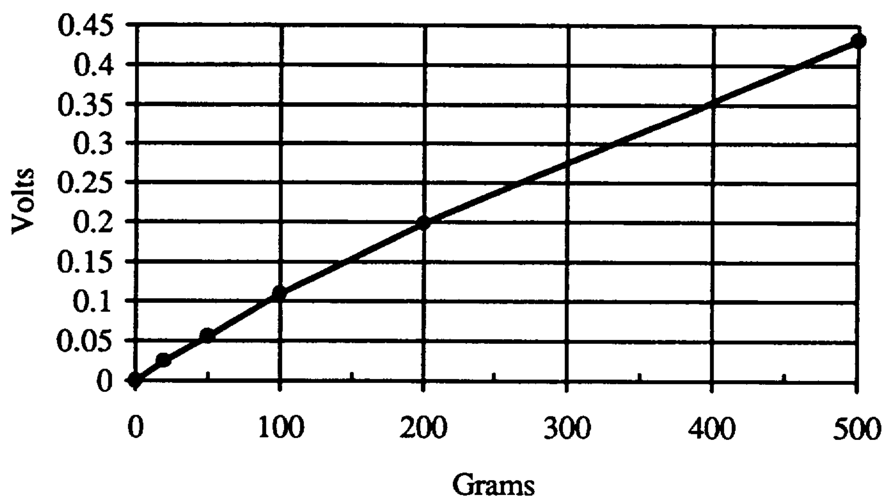

6.13 LOAD CELL CIRCUIT

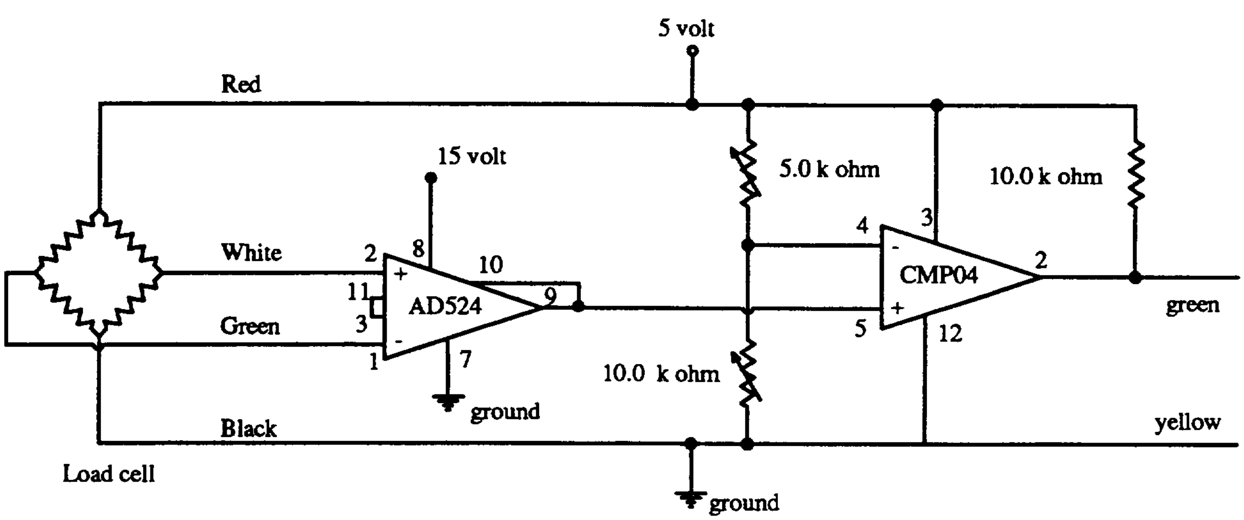

6.14 ROBOT OPERATIONS

1. Plug in power supply for PA2040G (receiver) preamplifier
2. Turn on pulser (set rep rate = EXT., Energy = 4, Damping = 0)
3. Turn on RHINO Controller (set Mode select to Teach Pendant)
4. Turn on power supply for load cell.
5. Calibrate load cell circuit.
6. Mount pressure vessel in fixture (Bottle ID letter on side opposite motor and label up).
7. While spinning bottle with teach pendant, apply a small bead of Soundsafe couplant
8. Confirm proper send/receive by;
   lower sensor => C:\MATLAB\BIN\SPECTRUM\ Type **DOWNRBT**
   activate A/D => C:\MATLAB\BIN\SPECTRUM\ Type **SCOPE**
   Press "esc" to exit SCOPE
   raise sensor => C:\MATLAB\BIN\SPECTRUM\ Type **UPRBT**
9. Taking AU data.
   C:\MATLAB\BIN\SPECTRUM\ Type **MATLAB**
   >> Type **RBTBOT**
   Output Filename => **RB** (Enter a 1 to 5 character filename)
   Sample Size => **3** (Enter a number up to 999)
   To lower sensor press **ENTER**
   To exit MATLAB type **exit**

6.15 PRESSURE VESSEL CRADLE.

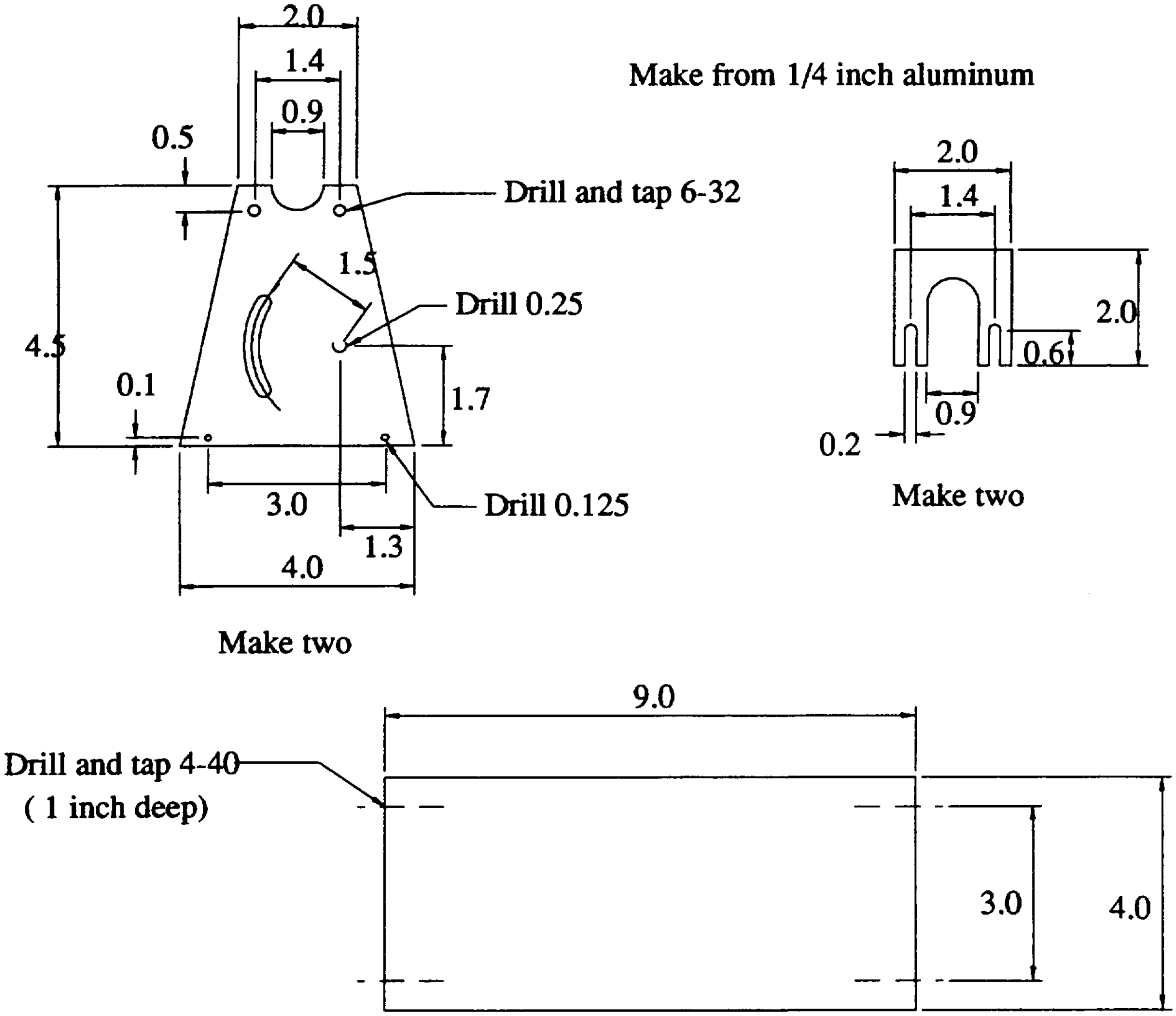

6.16 BROADBAND RECEIVER HOLDER

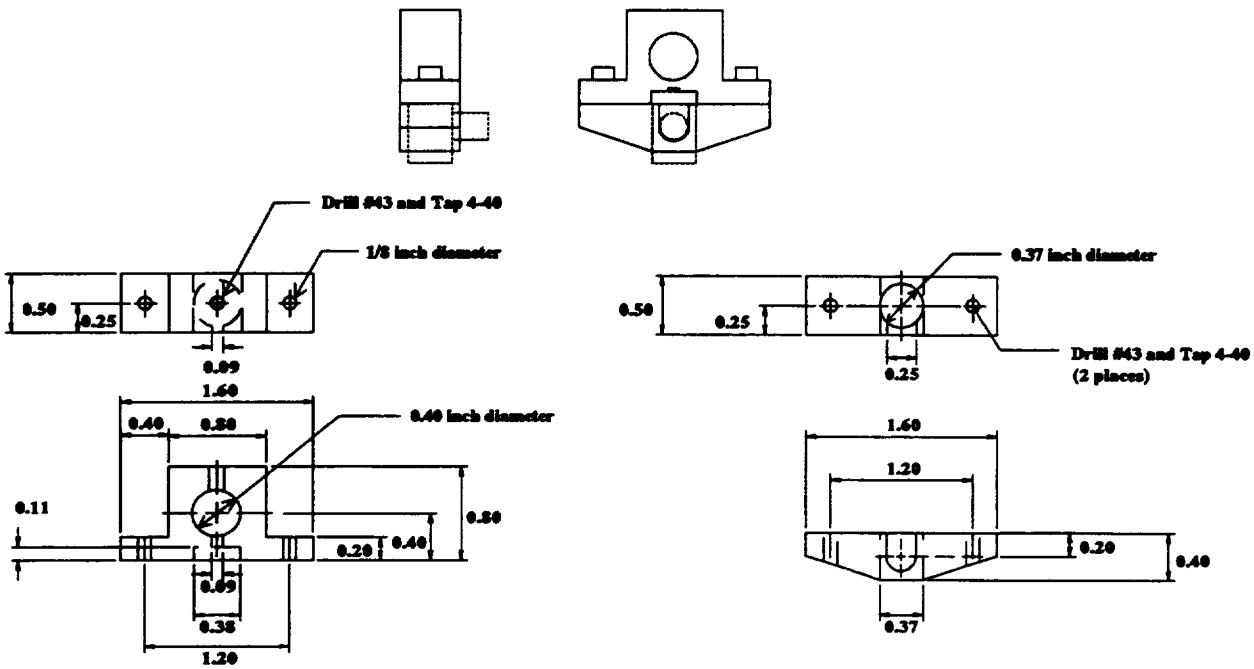

6.17 SENSOR ARM FOR AURES

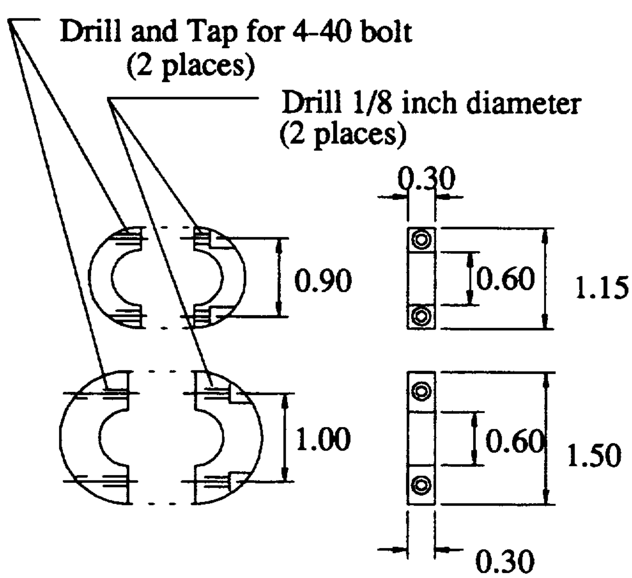

Sensor lock rings

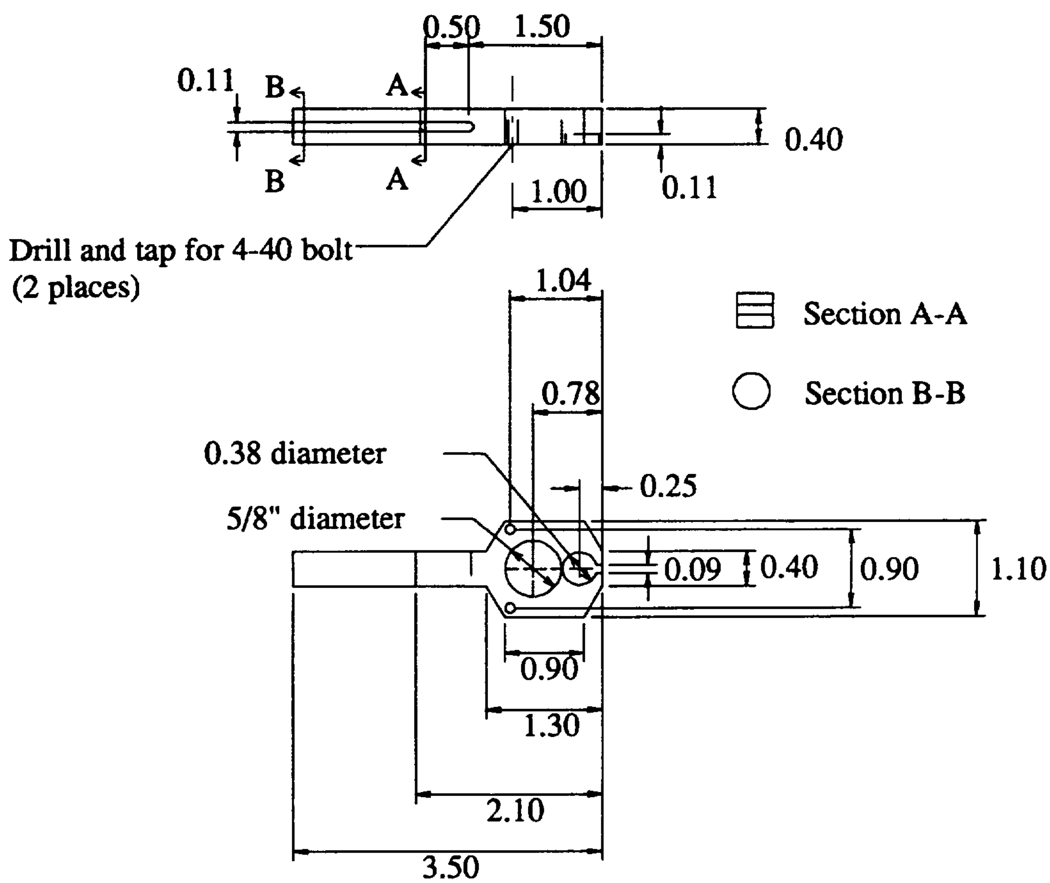

Pivot arm

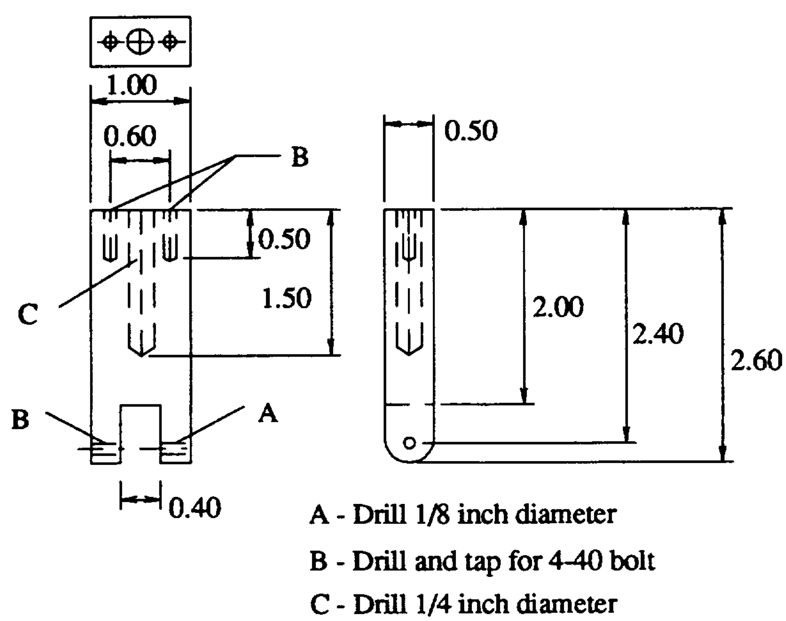

Pivot support

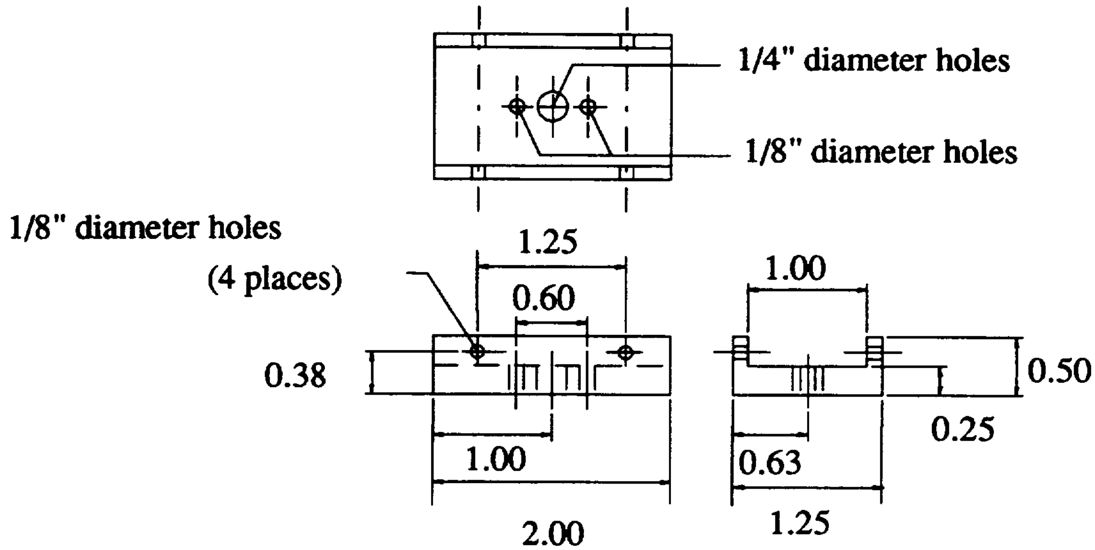

Pivot support attachment plate

6.18 TRA2MLAB.BAS

```
' This program converts a file from the TRA format to a MATLAB format.
' The user should specify the upper limit on the loop before executing the program.
FOR r = 0 TO 20
 IF r < 10 THEN
  w$ = "ch.00" + LTRIM$(STR$(r))
 END IF
 IF r > 9 AND r < 100 THEN
  w$ = "ch.0" + LTRIM$(STR$(r))
 END IF
 IF r > 99 THEN
  w$ = "ch." + LTRIM$(STR$(r))
 END IF
  ww$ = "ch" + LTRIM$(STR$(r)) + ".m"
  PRINT w$, ww$
  OPEN "i", 1, w$
  OPEN "o", 2, ww$
FOR y = 1 TO 9
LINE INPUT #1, q$
NEXT y
 PRINT #2, "a=[",
 FOR y = 1 TO 8191
  INPUT #1, z
  PRINT #2, z
 NEXT y
  INPUT #1, z
  PRINT #2, z,
  PRINT #2, "];"
CLOSE #1
CLOSE #2
NEXT r
END
```

6.19 ENGYDATA.M

```
% This program computes the energy content as measured by the area under
% the power spectral density curve for a series of user defined PAC TRA
% files. The input files should first be organized into sequentially
% numbered ".m" files befor running this program. The program "TRA2MLAB.BAS"
% can be used to create the ".m" files.
!cls
clear                    % Clear all variables.
for k=0:20,               % The range of "m" files.
eval(['ch',int2str(k)]);     % Load the file into MATLAB.
k                        % Indicate the current file number.
a=a*.01;                  % Scale the signal amplitude to volts.
y = fft(a,8192);            % Calculate the FFT for the signal.
Pyy = y.*conj(y)/8192;        % Calculate the power spectral density.
low(k+1)=sum(Pyy(25:192));     % Low energy for file (k+1).
high(k+1)=sum(Pyy(193:359));   % High energy for file (k+1).
end
save low.bas low -ascii      % Save energy data in an ASCII file.
save high.bas high -ascii
```

6.20 OUTPUT.BAS

```
' This program is used to organize the energy files from MATLAB.
' The input files "low.bas" and "high.bas" are created in MATLAB for a given
' TRA file. The user needs to supply an output filename for files 3 and 4
' and the upper limit on the loop.
OPEN "i", 1, "low.bas"
OPEN "i", 2, "high.bas"
OPEN "o", 3, "a029hl.bas"
OPEN "o", 4, "a029hh.bas"
FOR x = 1 TO 21 STEP 3
  INPUT #1, l, l2, l3
  INPUT #2, h, h2, h3
  avgl = (l + l2 + l3) / 3
  avgh = (h + h2 + h3) / 3
  WRITE #3, l, l2, l3, avgl
  WRITE #4, h, h2, h3, avgh
NEXT x
CLOSE
END
```

NASA
National Aeronautics and Space Agency

Report Document Page

1. Report No.	2. Government Accession No.	3. Recipient's Catalog No.

4. Title and Subtitle STUDY OF ACOUSTIC EMISSION NDE METHODS	5. Report Due
	6. Performing Organization Code University of Alabama in Huntsville
7. Author(s) Gary L. Workman James Walker	8. Performing Organization Report No.
	10. Work Unit No.
9. Performing Organization Name and Address University of Alabama in Huntsville Huntsville, Alabama 35899	11. Contract or Grant No. NAS8-38609 D.O. 122
12. Sponsoring Agency Name and Address National Aeronautics and Space Administration Washington, D.C. 20546-001 Marshall Space Flight Center, AL 35812	13. Type of report and Period covered Quarterly
	14. Sponsoring Agency Code MSFC

15. Supplementary Notes

16. Abstract

The use of acoustic emission to characterize impact damge in composite structures is being performed on composite bottles wrapped with graphite epoxy and kevlar bottles. Further development of the acoustic emission methodology will include neural net analysis and/or other multivariate techniques to enhance the capability of the technique to identify dominant failure mechanisms during fracture. The acousto-ultrasonics technique will also continue to be investigated to determine it ability to predict regions prone to failure prior to the burst tests. Characterization of the stress wave factor before and after impact damage will be useful for inspection purposes in manufacturing processes. The combination of the two methods will also allow for simple nondestructive tests to be capable of predicting the performance of a composite structure prior to being placed in service and during service.

17. Key Words (Suggested by Author(s))	18. Distribution Statement
Acoustic Emission Acoustic Ultrasonics Nondestructive Testing, Composites Damage Assessment	cc. CN22D (3) AT-01 (1) EM-13/L. Smith (1) ONRR (1) Russell/EH-13 (1 + reprol) Sci. & Tech. Inf. Fac. (1+ reprol) Vaughan/UAH (1)

19. Security Class. (of this report)	20. Security Class. (of this page)	21. No. of pages	22. Price
Unclassified	Unclassified		

NASA FORM 1626 OCT 86